KWAME NKRUMAH UNIVERSITY OF SCIENCE AND TECHNOLOGY

KUMASI, GHANA

ASSESSMENT OF REHABILITATED SURFACE MINE LANDS USING GEOSPATIAL TECHNOLOGY

A CASE STUDY:

ANGLOGOLD ASHANTI IDUAPRIEM MINE, TARKWA, W/R - GHANA

SUBMITTED BY:

OSEI, PATRICK DARKO

A Thesis submitted to

The Department of Geomatic Engineering

Kwame Nkrumah University of Science and Technology, Kumasi, Ghana

In partial fulfilment of the requirements for the Degree

of

MASTER OF PHILOSOPHY IN GEOMATIC ENGINEERING

Department of Geomatic Engineering

College of Engineering

SUPERVISORS:

DR. EDWARD M. OSEI JNR. AND

REV. JOHN AYER

OCTOBER 2016

DECLARATION

I hereby declare that this project is my own research except for the reference of others' materials which have been duly acknowledged.

Signed …….. Date ……

Osei Patrick Darko (PG9742013)

We hereby declare that we have supervised this student in the undertaking of his project and confirm that he has our permission to present it for assessment.

Signed ……. Date ……

Dr. E. M. Osei Jnr. (Supervisor)

Signed …….... Date……..... Rev.

John Ayer (Supervisor)

Signed …….... Date……..... Dr.

Isaac Dadzie (Head of Department)

DEDICATION

This research is dedicated to my parents, Mr. Osei Kwame and Madam Florence Serwaah for their encouragement and support and also to my wife – Mrs. Cecilia Osei Darko and my son – Gad Kwame Osei Darko for their love and support.

ACKNOWLEDGMENTS

I thank the Management and staff of the AngloGold Ashanti Iduapriem Mine Health, Safety and Environmental Department for assisting with data and materials used in this thesis.

ABSTRACT

Increased awareness of the importance of environmental sustainability has put pressure on mine reclamation projects, as stakeholders demand close monitoring and detailed reporting. Non-compliance with standard acceptable practices and regulatory requirements can result in the levying of huge fines and loss of social license and legal right to operate a mine. Existing ground-based monitoring techniques such as the Ecological Function Analysis (EFA) and Landscape Function Analysis (LFA) are time and labor intensive when utilized for monitoring vegetation change with periodic assessments. Airborne Light Detection and Ranging (LIDAR) and Landsat spaceborne remote sensing technologies offer a quick, less demanding alternative in monitoring post-mining reclamation projects. To demonstrate the utility and effectiveness of LIDAR and Landsat in reclamation monitoring, the technologies were applied in the assessment and monitoring of reclaimed disturbed mine-lands at the AngloGold Ashanti Iduapriem mine in the Tarkwa area of the Western Region of Ghana. Digital surface and elevation models were extracted from LiDAR dataset and used to estimate vegetation canopy height as well as percentage canopy cover. Derived canopy heights were validated with field measurements. Stepwise regression analysis yielded a linear model with a strong correlation of R^2 = 0.913 with RMSE = 1.961. The study also utilized Landsat 4 Thematic Mapper (TM), Landsat 7 Enhanced Thematic Mapper (ETM+) and Landsat 8 Operational Land Imager (OLI) Imagery for the monitoring of land reclamation projects within the study area, using vegetation cover as proxy for ecosystem health. Spectral vegetation indices were employed to monitor temporal changes of vegetation productivity from 1991 to 2014 of the ecosystem. LiDAR analysis shows mean tree height of 11.59 meters for 10 years old reclaimed site, which compares well with 17.88 metres mean height recorded for adjacent undisturbed natural forest. A Canopy cover percentage, nearing 100% depicting a dense canopy for the reclaimed sites was also recorded. Normalized difference vegetation indices computed shows an average of 0.473 in 1991, -0.005 in 2000 and 0.681 in 2014 with a standard deviation of 0.054, 0.154 and 0.057 respectively. It is demonstrated that LIDAR and Landsat can be effective and relatively precise for monitoring and assessment of reclaimed mined out lands to help take up remedial measures required for environmental sustainability.

GLOSSARY

Closure - is the period of time when the exploration or production activities of a site or part thereof have ceased and final decommissioning and/or rehabilitation are carried out.

Closure plan - is a generic term and means the conceptual, intermediate or final closure Plan, as appropriate.

Completion criteria - are specific to each mining operation and reflect its unique set of environmental, social and economic circumstances. Where possible, they should be quantitative and capable of objective verification.

DTM - Acronym for digital terrain model. The representation of continuous elevation values over a topographic surface by a regular array of z-values, referenced to a common vertical datum. DTMs are typically used to represent the bareearth terrain, void of vegetation and manmade features.

DSM - Acronym for digital surface model. The representation of continuous elevation values over a topographic surface, including vegetation and man-made features, by a regular array of z-values, referenced to a common datum. DSMs are typically used to represent terrain relief that includes the elevations of the top surfaces of buildings, trees, towers, and other features elevated above the bare earth. The DSM is also known as the "First Return Surface"

Height - The vertical distance between two points, or above a specified datum

Land cover - The classification of land according to the vegetation or material that covers of its surface; for example, pine forest, grassland, ice, water, or sand.

Light Intensity - The strength of LiDAR returns varies with the composition of the surface object reflecting the return. The reflective percentages are referred to as LiDAR intensity

Operation - refers to a producing mine.

Project - refers to an exploration project or a new mine expansion.

Rehabilitation - is understood to mean the return of disturbed land to a safe, stable and

self-sustaining condition. "**Reclamation**" and "**restoration**" are also used interchangeably.

Site – Is used when referring collectively to operations and projects.

Spaceborne - Operating in or involving equipment operating in outer space

Stakeholder - A person, group or organization with the potential to be affected by or to affect the process, or outcome, of closure of the site. They include shareholders; employees, their families and employer representatives; communities in which we operate; business partners; and governments.

Many stakeholders will be impacted by the outcome of the site's closure to a greater extent than those planning it.

TABLE OF CONTENTS

LIST OF FIGURES

LIST OF TABLES

APPENDICES

CHAPTER ONE GENERAL INTRODUCTION

1.1 Background

Mining inevitably disturbs land, making the economic gains associated with it sometimes achieved at an environmental cost (Obiri *et al*., 2006). Reclamation of disturbed lands is required by regulators during and after mining is completed to minimize these impacts, restore the land and establish a stable, safe and a selfsustaining ecosystem capable of triggering the establishment of pre-mining landuse capability.

Post-mining reclamation is done to restore the disturbed land to its prior mining use, or to a better and sustainable use to support the livelihoods of the landholders. Some of the methods and reasons for reclaiming mine lands into useful post-mining landuse are reported in the literature (Sopper, 1992; Pichtel *et al*., 1994; Barnhisel *et al*., 2000; Sheoran *et al*., 2010; Mborah *et al*., 2015). To achieve multiple landuse options that enhance post-mining investment opportunities, reclamation of disturbed mine lands are synchronized with the mining operations. This allows the growth of the vegetation to compete well with that of adjacent vegetation after the mine life, and also increase the success of reclamation effort.

Additionally, Reclamation Security Agreement (RSA) Criteria signed between Environmental Protection Agency (EPA) Ghana and mining company's states among other requirements that mining companies should carry out quantitative monitoring and assessment of biophysical and structural attributes of the reclaimed sites including vegetation productivity or health, to help take up remedial measures, required for environmental sustainability.

1.2 Statement of the Problem

Successful reclamation projects require monitoring and evaluation of the plants and soil ecosystems. Traditional methods as well as modern technologies have been utilised to quantitatively assess and inventorise the biophysical and structural attributes of reclamation forest. One biophysical variable fundamental to quantitative assessments of biomass growth and productivity is tree height and canopy closure.

Existing conventional monitoring techniques such as the Ecological Function Analysis (EFA) and Landscape Function Analysis (LFA) can be time and labor intensive when used for monitoring vegetation changes with periodic assessments. Airborne Light

Detection and Ranging (LIDAR), an active remote sensing technology, offers a quick and less demanding alternative in monitoring post-mining reclamation. LiDAR systems can record information starting from the top of the canopy through the canopy all the way to the ground. This makes LiDAR highly valuable for understanding forest structure and shape of the trees.

On the other hand, Landsat satellite imagery usually acquired in digital forms has provided a repetitive and cost-effective approach to ensure regular measurement, monitoring and mapping of periodic changes of vegetation productivity.

This study demonstrates the utility and effectiveness of LIDAR and Landsat in the assessment and monitoring of reclaimed disturbed mine-lands at the AngloGold Ashanti Iduapriem mine in the Tarkwa area of the Western Region of Ghana.

1.3 Aim

The main aim of the research is to demonstrate the utility and effectiveness of geospatial technology for the assessment of biophysical and structural attributes of reclaimed forest and vegetation productivity, within the leasehold area of AngloGold Ashanti Iduapriem Mine, Tarkwa, and recommend remedial measures, required for environmental protection.

1.4 Objectives of Research

This study explores ways in which geospatial technology can support mined land reclamation monitoring and assessment. It also assesses the changing pattern of vegetation cover by incorporating the temporal dependence of multi- temporal image data and consequently enhances the interpretations capability thereof.

The objectives therefore are:

[1] Assess land cover change from 1991, 2000 and 2014 using multi-temporal Landsat data

[2] Monitor Spatio-Temporal changes of vegetation productivity of the reclaimed sites using vegetation cover as proxy for ecosystem health.

[3] Map structural attribute (canopy heights and canopy closure) of reclaimed forests using LiDAR optical remote sensing technique.

[4] Assess tree height estimation error using regression analysis

1.5 Research Questions

[1] What was the pre-mining Land cover type of the study area?

[2] How much of the pre-mining Land cover changed during mining phase and how much has been reclaimed?

[3] How does the reclaimed forest productivity compared with the pre-mining conditions?

[4] How does the structural attribute of the reclaimed forest compared with adjacent natural undisturbed forest?

1.6 Organization of Report

This report is organized into five chapters. Chapter 1 gives an introduction of the research topic and general information about the study area. Chapter 2 looks at the literature review. Chapter 3 Materials and Methods used for reclamation assessment. Chapter 4 discusses the results, Chapter 5, is made up of conclusions and recommendations.

1.7 General Information about AngloGold Ashanti Iduapriem Mine

1.7.1 The Company

AngloGold Ashanti Iduapriem Limited (AAIL) is one of two mining operations managed by AngloGold Ashanti Limited in the Republic of Ghana. The other operation is AngloGold Ashanti Obuasi Limited (AGA). Since 1 September 2007, Iduapriem has been 90% owned by AngloGold Ashanti Limited and the Government of Ghana holding the remaining 10%. AAIL concessions include Iduapriem, Teberebie and Ajopa covering approximately 107 km^2 total Land size. The concessions are adjacent to the Gold Fields Ghana Limited mining leases in the Tarkwa Nsuaem Municipal Area (Figure 1.1). As at the end of 2013, the total mineral resource was reported around 103Mt at 1.49 g/t with 220.657Moz of gold.

Open cast mining with a carbon-in-pulp (CIP) processing plant is the adopted mining techniques at Iduapriem near Tarkwa. Three-year (2011-2013) performance assessment depict annual averages strip ratio of 5.48:1 yielding about 5.5 Mt of ore. In 2013 AAIL CIL plant achieved its best production with 220,687 oz gold production as against a budget of 193,385 oz. This production was based on a head grade of 1.50g/t and a recovery factor of about 95.6%. Before then, the best production was 219, 063 oz. achieved in 2003. The plant also achieved record tonnes crushed and treated in 2013.

AAIL workforce comprise of approximately 2,283 (AAIL employees and contractors) multinational and indirectly provides people in the Tarkwa and Iduapriem catchment communities significant supports in various disciplines.

1.7.2 Location of the Mine

AAIL is situated in the Iduapriem Township of the Tarkwa Nsuaem Municipal Area of the Western Region of Ghana. The mine site is about 70 km north of Takoradi and 10 km south-west of Tarkwa on grid-point reference 5º 17'N and 2º 00' W. The largely forested region has a general elevation of approximately 180 m above sea level. The mine is accessible by road from Accra through Takoradi or from Kumasi via Tarkwa. The Location Map of the Iduapriem mine and selected sites for the study are provided in Figure 1.1

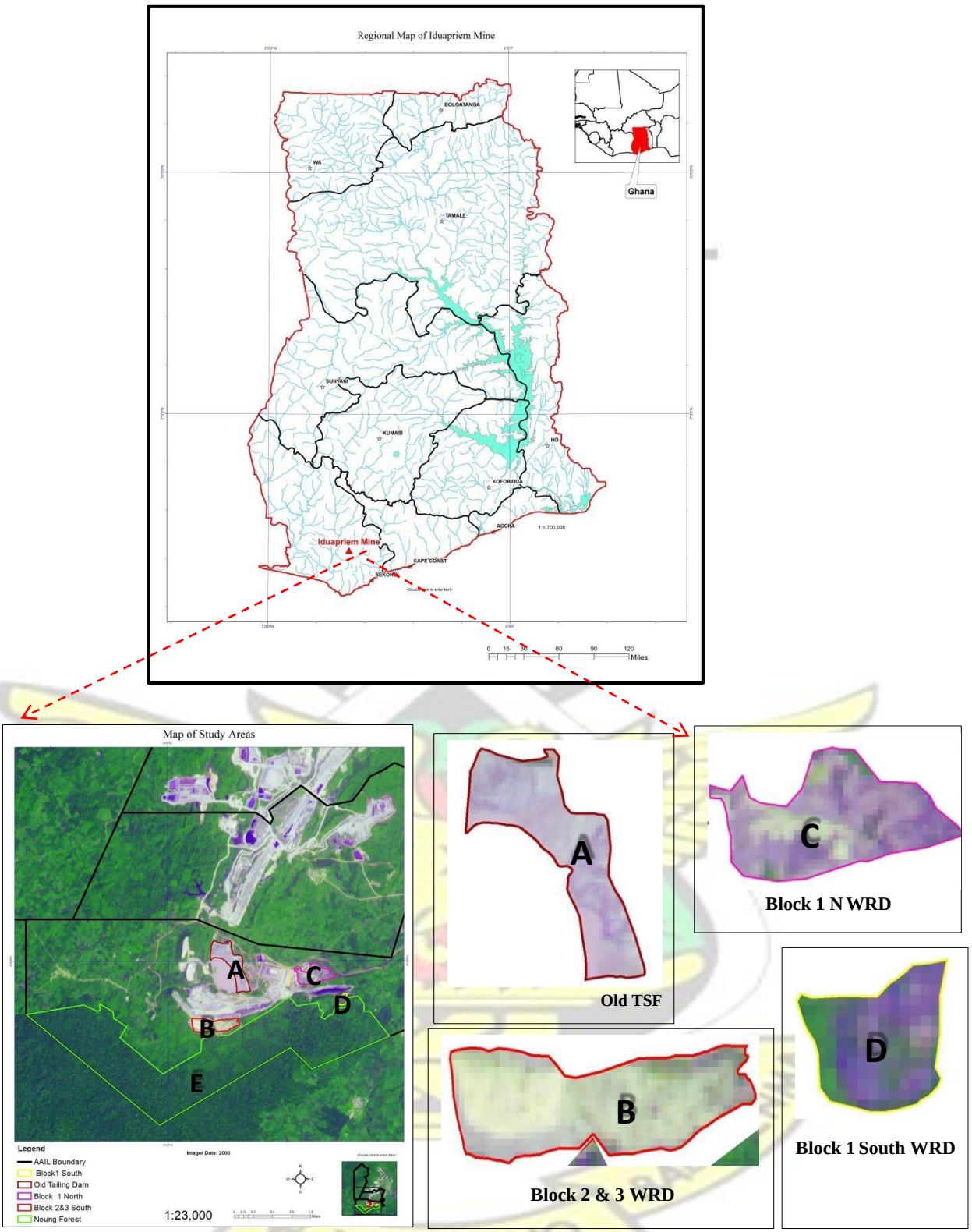

1.7.3 Physiography Figure 1. 1: SPOT Satellite Imagery of the Study Areas in the Year 2000 prior to Reclamation

The relief of the area is characterized by a series of undulating landscapes with prominent ridges that are about 60 to 80 meters above mean sea level. The ridges which

form the main specific areas are Blocks 1 to 6 (Ajopa), Block 7 (Teberebe) and Block 8 (Awunabeng).

1.7.4 Climate and Vegetation

The study area has two rainfall seasons per year with the main raining season being from April to July with the peak in May and June. The minor raining season occurs between September and October and reaches its peak by the end of September. The minor raining season is characterized by low rainfall and showers while torrential rains are experienced in the major seasons. Temperatures are usually high with the highest daily temperature recorded during March (26ºC) and the lowest during September (20.5ºC). Humidity values are relatively high with the highest during March (94%). The heavy rainfall coupled with high temperature and humidity promotes the relatively deep residual soil profiles over the rocks in this region.

The vegetation within study area comprises of tropical rain forest with rich undergrowth of shrubs and climbers of different heights. Generally trees height within the study area ranges between 15 m and 45 m, are distributed mostly at undisturbed areas of the mine. There has been a rapid reduction in the density of trees in areas affected by mining activities. Akabzaa and Darimani, (2001) attributed Lack of protection from mining and lumber activities as the primary responsibility for the poor vegetation in the area for example in areas where mining has taken place, the vegetation mainly comprise of ferns and other shrubs which grow copiously on the hilly slopes.

1.7.5 Drainage

The relief of the area provides a good drainage pattern, which serves as catchments for the streams that flow along adjacent lowlands. Prior to the commencement of mining activities the drainage system was quite uniform. A large proportion of the land was used for commercial farming activities for the provision of food crops for the people within Tarkwa and its environs. As a result of the mining activities the river courses have been disturbed to a great extent. These are the results of unidentifiable sources of water ingress into the mining pits.

1.7.6 Geology Mineralization and Resources

The ore body found on the AAIL concessions forms part of south western margin of the Tarkwa syncline, and it is the Banket Series of rocks within the Tarkwaian system. The

geology is composed of stacked fluvial sedimentary rocks developed from a river system deposited simultaneously with gold about two billion years ago**.**

The Banket Series of rocks in the study area mainly form prominent ridges extending southwards from Tarkwa, westwards through Iduapriem and northwards through Teberebie. There are eight major ridge segments (Block 1-5, Teberebie, Awunabeng and Ajopa) within the mining lease and the Banket Series rocks. These extend over a total strike length of 13 km.

Dykes and sills of doleritic affinity intrude the sedimentary sequences and frequently occur adjacent to complex structural zones. Pyritisation is known to be associated with the complex zones within the hanging wall quartzite and the mineralogically matured (silicified) breccia conglomerate, which marks the end of the Banket reef zone. All known pyrite on the mine is therefore found within the siliceous quartzite (hanging wall quartzite) and the breccia conglomerate close to dolerite intrusions and quartz veins. It is also not uncommon to find pyrite within the dolerite and the quartz veins.

The rocks generally dip at moderately angles ($30\text{-}75^0$) to the southeast and the grade of metamorphism is generally low. Intrusives in the Tarkwaian System include, dolerite aplite felsite and quartz porphyry, which form dykes and sills. These rocks are moderately to highly jointed.

Aquifer systems of the Tarkwa area have been influenced greatly by geological parameters and as such groundwater occurs, mainly in discontinuous aquifers. Even though much of the primary porosity of the bedrock has been destroyed due to consolidation, cementation and recrystallization, the rocks have acquired secondary and variable permeabilities through fracturing and weathering.

CHAPTER TWO ENVIRONMENTAL IMPACTS OF MINING, RECLAMATION AND MONITORING

2.1 Surface mining

Surface mining techniques also known as opencast mining mainly involve excavation and extraction of minerals near the soil surface. This technique began in the midsixteenth century and has increased rapidly since its inception due to advancement in technology which makes mineral extractions from low mineralogy feasible (MontrieChad, 2003; Miller *et al*., 1996). Surface mining involves clearing of vegetation cover, removal of top soil by earth movers, blasting, loading and hauling of ore to the processing plant with heavy mining equipment's (HME) such as dozers,

excavators, and the likes. The increase in surface mining in many mining countries has been attributed to the under listed factors by Yirenkyire (2008):

[1] Operational cost and safety considerations as compared to underground operations.

[2] Mining of mainly low grade ore which requires processing of massive quantities

[3] Ore body location

[4] Investor competition among gold producers.

2.2 The environmental impacts of surface mining

Although mining is regarded as a global activity with significant economic benefits, mining also impacts adversely on the environment (Balkau, 1993). Due to its operations, especially opencast mining certainly leads to severe dilapidation on ecological and aesthetic values of the landscape.

Mining industry often exhibited lack of respects for the environment in the past particularly with regards to disposal of mine waste rocks and the likes. This resulted in unpleasant spoil heaps being left to damage the landscape, and to the contamination of surface and groundwater. Recent development today has led to increased awareness of the prominence of the environmental sustainability which has consequently led to imposition of tighter regulations by many countries to lessen the impact associated with mining and its related activities.

In Ghana for example, mining operations in most cases result in the loss of farmlands due to the large surface of lands mining companies acquire. (Aryee *et al*., 2003) indicates that surface mining pervade about 13% of the total forest land of 240,000km^2. Also Tetteh, (2010) indicated that surface mining is the greatest agent of land degradation. In recent years there have been clashes between mining catchment communities and mining companies due to loss of farmlands which the communities depend on for their living and this has been reported by Gyimah, (2004).

Some consequences associated with surface mining are permanent changes of topography and geological structures and disturbs both surface and subsurface hydrologic systems, destroying the natural ecosystems such that it requires some form of human mediation to restore it back to sustainable use (Bradshaw, 1996). The earthwork and other decommissioning activities during rehabilitation (e.g., Cutting and

shaping, spreading topsoil, cross ripping, mulching etc) also affects in a way soil compaction and alter physical and structural characteristics and restrict root development due to high bulk densities and low infiltration rates.

Land cover change is also a prominent environmental impact particularly associated with open cast or surface mining. Time, commodity and method of extraction have been attributed to the extent of land cover change. Coal mining, for instance, is often a surface activity and causes significant land cover changes according to (Markus, 1997).

Potential environmental, pollution and occupational/health impacts associated with mining and related activities have been reported adequately by Balkau, (1993). Some of these impacts according this literature are mainly natural habitat destruction at both mining and mine waste disposal sites and as results of emissions and discharges as well as influx of settlers.

Changes in landform and land degradation due to lack of proper rehabilitation practices being implemented at various mining sites have been identified as some of the key environmental impacts of mining. These practices have proven to pose various degrees of pollution related issues spanning from mine acid drainage, soil contamination from chemical spillages and other health related instances for example exposure to mine emissions (Balkau, 1993)

2.3 Environmental protection

Ghana Environmental Protection Agency (EPA) is mainly responsible for the enforcement of environmental regulations and other related legislations. It was under the Environmental Protection Agency Act, 1994 (Act 490) that establishment of the body was realized. In accordance with Act 703 section 18 and the L.I. 1652 (Environmental Assessment Regulations) 1999 of the EPA, a holder of a mineral right is required to secure an environmental permit from the EPA in order to commence any mineral operations.

During surface mining the vegetation and the soil disturbed are required to be rehabilitated through a variety of treatments in accordance with the Legislative Instrument 1652 and Act 490.

Several terms are used interchangeably to indicate post-mining measures to counteract the impacts of surface mining. Terms such as restoration, rehabilitation, and

reclamation are commonly used in scientific and non - scientific literature to describe practices that help re-establish the structural and functional characteristics of a disturbed ecosystem to its natural or near natural state. (Mustapha, 2013)

Rehabilitation process involves systematic steps focused at restoring system to, or very close to its original state of active life, good condition and usefulness, again. This practice forms a major aspect of every successful mining operation. The reclamation is done to restore the disturbed land to its prior mining use, or to a better and sustainable use to support the livelihoods of the landholders. To achieve multiple landuse options that enhance post-mining investment opportunities, reclamation of disturbed mine lands are synchronised with the mining operations. This allows the growth of the vegetation to compete well with that of adjacent vegetation after the mine life, and also increase the success of reclamation effort.

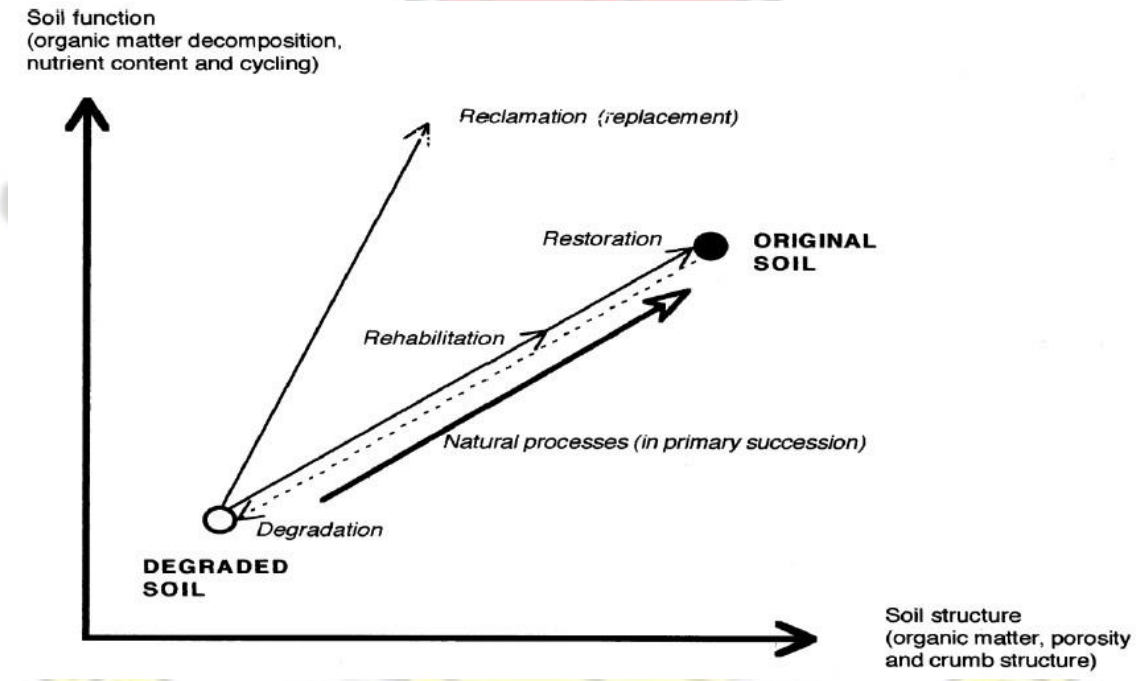

Figure 2. 1: Contrasting approaches to the restoration of soils of degraded land by surface mining

(Source: Bradshaw, 1992)

2.4 Rehabilitation Practices in Ghana

Mining companies in Ghana embarks on progressive land rehabilitation programme, with the objective of achieving multiple land-use options that will enhance after mining investment prospects. In accordance with the above, areas mined-out and related waste rock dumps are re-vegetated in stages, rather than awaiting final closure of the mine.

Appropriate rehabilitation strategies are utilized. These include but not limited to: cutting, shaping of the waste rock dump slopes to an angle of repose as outlined in the reclamation security agreement. This is followed by the loading, hauling and application of topsoil from designated stockpile normally to a standard requirement of 0.5 m minimum thickness and seedlings transplanting followed with routine assessment as well as care and maintenance programmes which enhances undergrowth and general plant growth. Where topsoil availability is a concern, combination of laterite with humus in dug-out holes is ensured and spreading poultry droppings with sawdust, this is consequently trailed with mulching.

The organic matter and soil nutrient is enriched by allowing the decomposition of plant biomass in-situ. The selection of plant species for use in the reclamation has also proved to be very key step in reclamation projects. The species selected is normally required to have the ability to thrive on open lands as well as withstand harsh conditions, and also be capable of adding nitrogen to the soil to help boost soil nutrients and hence serve the needs of catchment communities.

The land reclamation projects are typically intended to prevent soil erosion (part of primary completion criteria) and restore disturbed land surfaces to conditions that could be used by catchment communities for productive farming or agro-forestry purposes. Key objectives are to ensure agro-diversity (which enhances biodiversity and ecological stability).

2.5 Rehabilitation Monitoring and Assessment

Over the years traditional as well as modern techniques have been used for quantitative assessment and inventory of the biophysical and structural attributes of reclamation forest. Some of the biophysical variables fundamental to quantitative assessments of biomass growth and productivity are tree height and canopy characteristics such as closure. Example of conventional monitoring techniques are the Ecological Function Analysis (EFA) and Landscape Function Analysis (LFA) which can be time and labour intensive when utilised for monitoring vegetation change and periodic assessments. Mustapha, 2013 used Landscape Function Analysis developed by the CSIRO as a monitoring tool to assess two surface mine sites which were 1 and 20 year/s old respectively and compared with their natural ecotypes to determine their extent of success in AngloGold Ashanti, Obuasi.

Geospatial technology comprising of range of optical remote sensing technologies such as Light Detection and Ranging (LiDAR) and Landsat Multi-spectral satellite imagery, offers a better alternative in monitoring post-mining reclamation.

LiDAR for example have been utilised in the measurement of the three-dimensional forest structure and have proven to produce a model of the underlying terrain. The technology has proven to be very successful in estimating tree heights. Tree height estimated from LiDAR by Wulder and Seemann, (2003) greatly approximated the measurements obtained by field surveys. Rosette *et al.*, (2012) supported the fact that LiDAR remote sensing tree height measurements complement traditional field measurements

2.6 Overview of Geospatial Technologies in reclamation forest Assessment and Periodic Change Monitoring

Geospatial technologies involve a number of sub-disciplines, including mapping and surveying systems such as Geographical Information Systems (GIS) and remote sensing, photogrammetry and Global Positioning Systems (GPS). Each of the specific sub-disciplines within geospatial technologies plays a distinctive role, but they are inter-reliant and most effectively used in an integrated fashion. (Wes and Leslie, 2006).

Geospatial technology has a key strength in integration/ analysis of geographically referenced spatial dataset and its acquisition. In recent years the technology has been accepted as an effective decision making tool globally. This ability stretches from data acquisition to data storage, manipulation, image analysis, geo-visualization /display and data output (Tsou and Yanow, 2010).

2.6.1 Remote Sensing (RS)

Remote sensing geospatial technique is the science and art of gathering data about an object, area, or phenomenon through the analysis of data acquired by a device that is not in in contact with the object, area, or phenomenon under investigation. (Lillesand *et al.*, 2004)

All matter with a temperature above zero (K) radiates electromagnetic waves of various wavelengths. The total range of wavelengths is commonly referred to as the electromagnetic spectrum and extends from gamma rays to radio waves. Remote sensing operates in several regions of the electromagnetic spectrum as shown in the Figure 2.2.

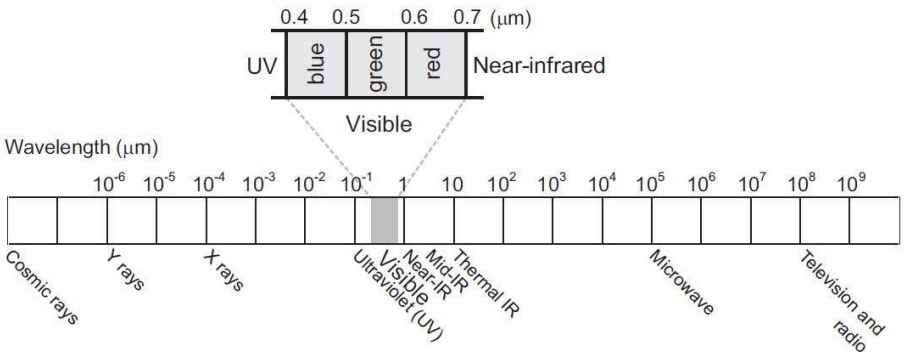

Figure 2.2: Range of wavelengths within the electromagnetic spectrum

(Source: Lillesand *et al*., 2004)

Active and passive remote sensing are the two main types of remote sensing technology. The differences between these types are mainly their energy sources. Passive sensors measure energy that is naturally available for example radiation from the sun, whilst Active sensors provide their own energy source for illumination. The sensor emits radiation which is directed towards the mapping surface and the radiation reflected from that surface detected and measured by the Active sensor (Lillesand *et al*., 2004).

2.6.2 Airborne remote sensing

Airborne remote sensing is carried out using different types of aircraft depending on the operational requirements and other factors. The speed of the aircraft can vary between 150 km/h and 750 km/h and must and is carefully chosen in relation to the mounted sensor system. The selected altitude influences the scale and resolution of the recorded image. Example is Airborne LiDAR mapping

2.6.3 Principles of Light Detection and Ranging (LIDAR) and Laser scanning

Basically LiDAR system is referred to as a distance technology. Light energy known as pulse is sent by an airborne LiDAR system actively to the mapping surface (ground). The reflected light referred to as return is measured by the sensor. In a nutshell, pulses of light is sent to a mapping surface, they are reflected (return) and are measured by the sensor giving the range (Distance variable) to the surface of the earth. This is how the name Light Detection and Ranging was derived.

Normally the aircraft floor opening is fitted with laser range finder of high accuracy. The rangefinder scan underneath the aircraft, a wide swath is produced over which the

distance (d) to the mapping surface/ground is measured as well as the angle(θ) at which the laser is scanned. Lewis and Handcock, (2007) indicated that given the return signal timing (t) provides measurement of the distance between the LiDAR instrument and the target (d)):

$$t = \frac{2d}{c}$$

The constant (c) represent the speed of light = 299.79 x10^6 m/s.

LiDAR systems have been useful in mapping forest structure and have been reported extensively in several literatures (Magnussen and Boudewyn, 1998; Magnussen, 1999; Zimble, 2003; Chen *et al.,* 2005; Goodwin, 2006 and Wulder *et al*., 2012). The benefits of LiDAR measurements compared with other forms of remote sensing mapping techniques are attributed to the fact that LiDAR is measurements relatively direct or as a function of height. LiDAR systems capable of recording forest structural attributes beginning from the canopy top through the canopy and to the ground (Figure 2.3). This makes LiDAR highly valued for investigating forest structure and shape of the trees.

Typical characteristics of Airborne Laser Terrain mapping (ALTM) techniques can be summarized below;

[1] Compared to aerial photography ALTM have Higher resistance to adverse meteorological conditions than aerial photography [2] Vegetation penetration capability.

[3] Discrimination first and last pulse

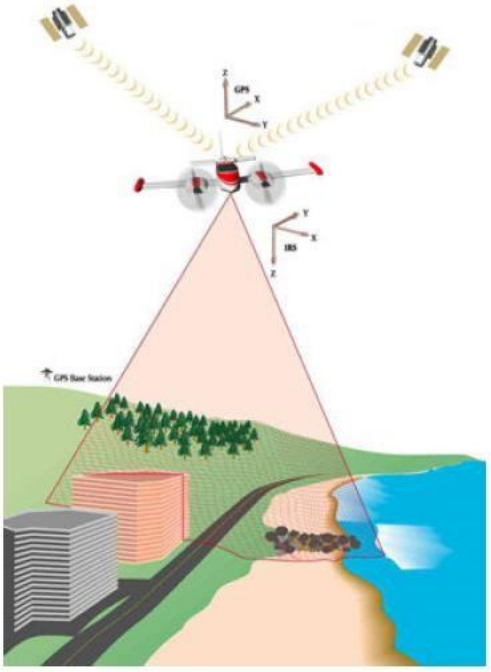

Figure 2.3: Typical Airborne Laser scanning system

(Source: Hansa Luftbild Group, 2011)

2.6.5 LiDAR Systems Types Available

[1] **Profiling LiDAR**: First type of Lidar system used in the eighty's mainly for mapping Single line features for example power lines by sending in one line individual pulse whilst measuring height along a transect with a fixed Nadir angle.

[2] **Small and Large Footprint LiDAR:** Small foot print LiDAR system is in use today. It scans at about 20 degrees scan angle if this is exceeded, the instrument may realize the sides of trees instead of top to down.

Mainly two types can be distinguished namely topographic and bathymetric. Topographic type of LIDAR system maps the land typically using nearinfrared light whilst Bathymetric type uses water-penetrating green light to measure seafloor and riverbed elevations.

Large Footprint type on the other hand uses full waveforms and averages LiDAR returns in 20m footprints. With this type because pulse return are based on larger target area it becomes difficult to get terrain from it since it could be sloping

[3] **Ground based LiDAR:** This type has a wide application in geology, forestry construction and other applications. It normally mounted on a tripod and scans the hemisphere.

Optech's ALTM and Leica's ALS series (small footprint discrete type of return systems) is mostly regarded as the commonly used type of commercial LiDAR sensors with the capability to record two(2) to four(4) returns for individual laser pulse emitted (Ussyshkin and Theriault, 2010)

2.6.6 Storage of LiDAR return

LiDAR return pulses are stored in two ways namely Discrete LiDAR and Full waveform.

The major dissimilarities between discrete LiDAR and full waveform systems can be explained with this scenario, In a typical forest LiDAR survey, pulse being sent hit branches multiple times, comes back as 1st, 2nd, 3rd returns then last return (large pulse by the bare ground return) Figure 2.7.

When the data is separated into returns, it is known as discrete return LiDAR.
Discrete takes each peak and separates each return.

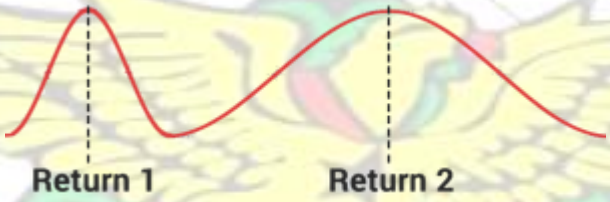

Figure 2.4: LiDAR Discrete return pulses storage form

(Source: http://gisgeography.com/lidar-light-detection-and-ranging)

When the whole return is stored as one continuous wave, it is referred to as fullwaveform LiDAR. Full waveform data is more complicated. What makes it discrete is the ability to count the peaks.

Figure 2.5: LiDAR Full Waveform return pulses storage

(Source: http://gisgeography.com/lidar-light-detection-and-ranging)

2.6.7 Areas of Application of LiDAR Technology

[4] Open cast mines and waste rock dump volume control.

[5] Overhead power lines (High tension) surveillance and monitoring

[6] Topographic mapping including forested areas

[7] Mapping of vegetation height

[8] Surveying of coastlines and erosion monitoring of coastal areas

[9] Mapping and simulation of floods (Flood plain)

[10] Subsidence and degradation Monitoring

[11] Modeling city in 3D for telecommunication network planning and control of noise

[12] Railway, road, pipeline and cable rout planning

2.6.8 Modelling Canopy Height (CHM)

LiDAR has been widely accepted as very precise way of gathering spatial information about the ground surface (Ussyshkin and Theriault, 2010).

A Canopy Height Models also referred to as Normalized Digital Surface Model (nDSM) represents true height of topological features on the earth surface (Gordon, 2010). It is computed by subtracting LiDAR ground returns which are normally the last return (bare Earth) from first return including topology (tree, building).

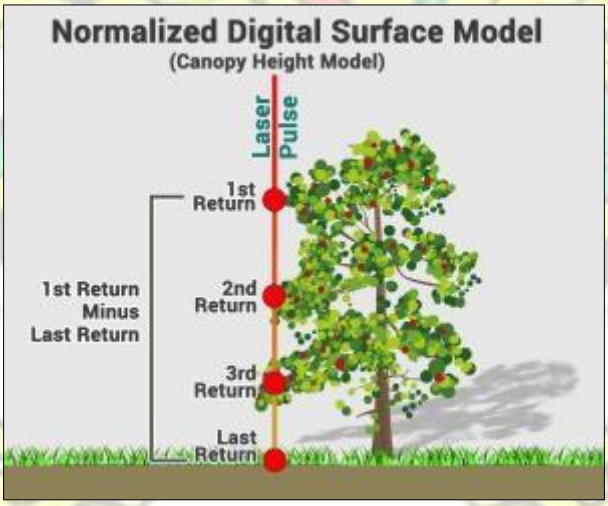

Figure 2.6: Normalized Digital Surface Model

(Source: http://gisgeography.com/lidar-light-detection-and-ranging)

2.6.9 Field Validation of LiDAR Canopy Heights

A tape measure and a Clinometer + Bubble level application installed on smart device can be used to measure tree height (Hemery, 2011). The clinometer application is

designed to be as accurate as possible (normally in the range of ±0.1 degrees, although this might depend on the device).

The angle of elevation are measured with the clinometer bubble application phone device from the eye level and sighted along the phone edge to the canopy level of the tree, whilst the distance to the tree also measured with a tape measure (Hemery, 2011).. The height of the tree is computed from simple trigonometric computations.

$H_t = H_{eye} + Tan\sigma \times D$

Where H_t = Height of tree

H_{eye} = Height of eye above ground level σ = Angle of elevation measured from the clinometer

D = Distance to tree from the point of sighting.

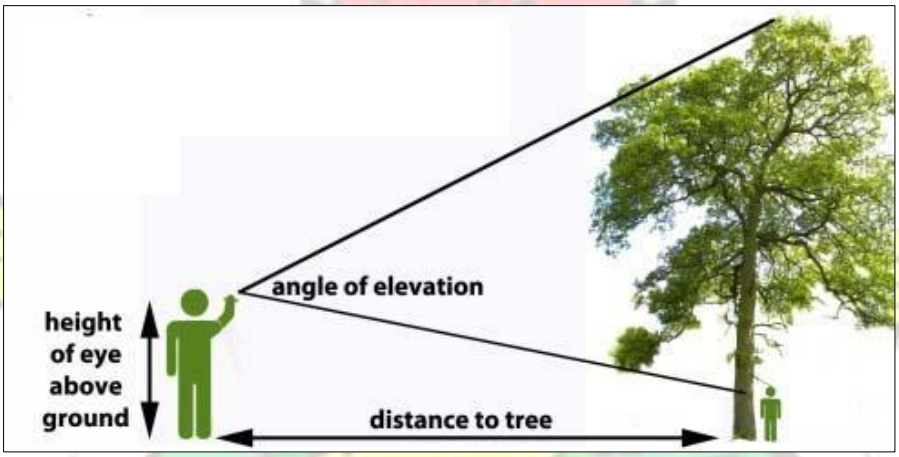

Figure 2.7: Tree height measurement with Clinometer + Bubble level android application.

2.6.10 Computation of LiDAR Height Metrics

Canopy height metrics can be computed from the LIDAR point cloud data with Grid metrics command in Fusion software specifying (lowest height), and (highest height) parameters set as an outlier for the target area. A large number of statistics are produced for describing canopy height at specified grid cell size. The metrics produced includes basic distribution statistics such as the mean, mode, variance, maximum height values, and height values of a range of percentiles. The metrics also includes statistics describing the shape of the point cloud height distributions including measurements of skewness, kurtosis, and linear (L) moments (McCallum *et al*., 2014).

2.6.11 Canopy Cover Metrics

Cover metrics are generally computed as ratios of first LIDAR returns above specified height threshold to the total first returns as described in equation 1.0 below:

$$Cover = \left(\frac{\#returns > Specified\ threshold}{Total\ Returns}\right) * 100 \quad \text{Equation 1}$$

Different cover differ according to the type of LIDAR returns (just first returns or all returns) used in the numerator and/or denominator of the expression above, as well as the cutoff height threshold value which determines the number of returns in the numerator. In general, metrics calculated using only the first returns from each LIDAR pulse represent measures of canopy cover, while those considering all returns represent the overall density of the canopy (McCallum *et al*., 2014).

US Forest Service suggest a point density of ≥4 pts/m2 for LIDAR application in forests (Laes *et al*., 2008). (Zhang and Qui, 2011) suggests relatively lower density would not significantly influence the results of tree height measurements where most of the trees have bigger canopies

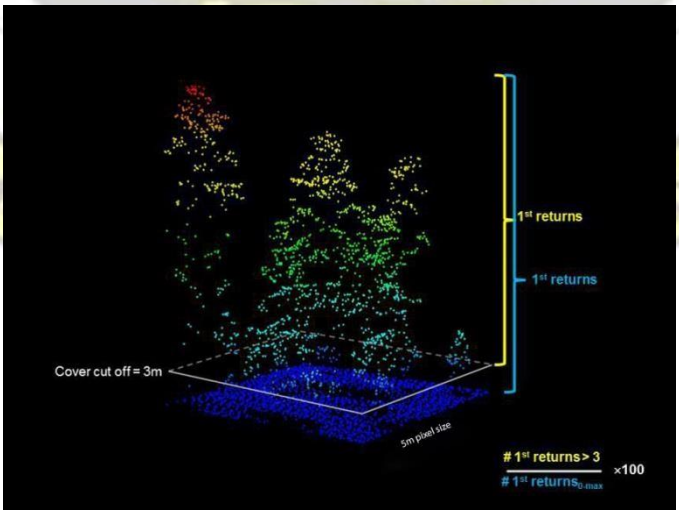

Figure 2.8: Cover metrics illustration at 3m cut-off threshold

(Source: McCallum et al., 2014)

2.6.12 Spaceborne remote sensing

Spaceborne remote sensing is carried out using sensors that are mounted on satellites, space vehicles and space stations. The monitoring capabilities of the sensors are to a larger extent determined by the parameters of the satellite's orbit. In general, an orbit is a circular path described by the satellite in its revolution about the earth. Different types of orbits are required to achieve constant assessments and monitoring, global or selective imaging. Example of Spaceborne technologies is Landsat series of satellites.

2.6.13 Landsat Satellite

Landsat series of satellite constitutes a very important resource for observing global change and it is also a primary source of medium spatial resolution remotely sensed observations used in planning (Chander *et al*., 2009) since Landsat succession of satellites delivers the lengthiest continuous record of satellite-based measurements. To meet observation requirements at a scale enlightening landscape changes, Landsat provides the only catalog of the worldwide land surface over time on a regular basis (Spanning from 1984 - 2016) (Chander *et al*., 2009).

Landsat satellites can be categorized into groups of three (Group 1 2 and 3), based on sensor and platform features. Landsat sensor, spatial resolutions, and band characteristics are reported by Chander *et al*., 2009.

Table 2. 1: Summary Characteristics of Landsat TM, Landsat ETM+ and Landsat 8 sensors (United States Geological Survey (USGS) Global Visualization Viewer (Source: glovis.usgs.gov))

	Thematic Mapper (TM)	**Thematic Mapper (TM) Enhanced Thematic Mapper Plus (ETM+)**	**Landsat 8 Operational Land Imager (OLI) and Thermal Infrared Sensor (TIRS)**
Platform	Landsat 4 (launched 16 July 1982) Landsat 5 (launched 1 March 1984)	Landsat 6 (failed on launch) Landsat 7 (launched 15 April 1999)	Landsat 8 (Launched on February 11, 2013)
Orbit	16 day/705 km	16 day/705 km	16 day/705 km

Inclination	98.2°	98.2°	98.11°
Equatorial crossing time	10:00 am	10:00 am	10:00 am
Swath width	185 km	185 km	185 km
Bands	1 (0.450.52µm) 2 (0.520.60µm) 3 (0.630.69µm) 4 (0.760.90µm) 5 (1.551.75µm) 6 (10.412.5µm) 7 (2.082.35µm)	1 (0.45-0.52µm) 2 (0.52-0.60µm) 3 (0.63-0.69µm) 4 (0.76-0.90µm) 5 (1.55-1.75µm) 6 (10.4-12.5µm) 7 (2.08-2.35µm) panchromatic band 8 (0.500.90µm)	1 (0.43 - 0.45 µm) 2 (0.45 - 0.51 µm) 3 (0.53 - 0.59 µm) 4 (0.64 - 0.67 µm) 5 (0.85 - 0.88 µm) 6 (1.57 - 1.65 µm) 7 (2.11 - 2.29 µm) panchromatic band 8 8 (0.50 - 0.68 µm) 9 (1.36 - 1.38 µm) 10 (10.60 - 11.19 µm) 11 (11.50 - 12.51 µm)
Ground pixel size	30 m (bands 15,7) 120 m (band 6)	30 m (bands 15,7) 60 m (band 6) 15 m/18 m (band 8)	30 m (bands 1-7,9) 15 m (band 8) 100m (band 10-11)
Quantization	8 bits	best 8 of 9 bits	12 bits

The Landsat multi-temporal data archive at the Geological Survey of the U.S (USGS) Earth Resources Observation and Science (EROS) Center stores record surface of the Earth's and it is readily available at no fee to users using the web (Woodcock *et al.*, 2008).

2.6.14 Landsat Image Processing for Periodic Assessment

Before processing and analyzing Landsat image dataset, numerous pre-processing routines, suitable for the assessment are applied to the imagery. These includes but not limited to geometric and radiometric corrections to improve the quality of the image data by decreasing or eliminating various errors associated with radiometric and geometric caused by both internal and external conditions

There has been numerous application of Digital Number (DN) conversion to Top of Atmosphere (TOA) in many research (e.g. Collet et al., undated; Furby undated), and Guyot and Gu (1994) confirms that it is the most important step in the production of 'accurate' Normalized Difference Vegetation Index (NDVI) results. Else a relatively constant error attributed to the sensor affects the computed spectral index.

Numerous remotely sensed spectral indices for vegetation applications have been developed to characterize vegetation canopy structure. Huete, (1988) assessment reveals a strong correlation between the indices and various vegetation parameters for example green leaf area, biomass, percent green cover, productivity, and photosynthetic activity.

2.7 Environmental Based Vegetation Indices (VI)

Fundamentally vegetation Indices (VIs) combines surface reflectance at different wavelengths (two or more) to retrieve information of value pertaining to state of vegetation cover, photosynthetic capacity, vegetation structure, leaf density and distribution, mineral deficiencies and evidence of parasitic shocks or attacks as well as water content in leaves (Jensen, 2007; Liang, 2005).

The fundamental concept behind the development and usage of these spectral indices is that some algebraic combination spectral bands must consequently be sensitive to not less than one of the factors mentioned above. Contrariwise, a relatively better vegetation index should have less sensitivity to dynamics that impact on spectral reflectance such as atmospheric conditions, soil characteristics, sensor viewing geometry and solar illumination (Liang, 2005, Jensen; 2007, Yengoh, 2014).

2.7.1 Vegetation Reflectance

The structure of leaves, developed for photosynthesis, regulates how flora relates with sunlight. There are two main processes that occur within leaves namely absorption and scattering of sunlight.

Plant pigments for example chlorophyll and carotenoids, and liquid water absorb specific wavelengths of light. Scattering is triggered by the internal structure of leaves (where the leaf interior which is a labyrinth of air spaces and irregularly shaped waterfilled cells). Internal scattering of light is instigated by variances in the refractive index between air and water-filled cells, and internal reflections from irregularly shaped cells.

Jensen, (2007) indicated that green leaves absorb sturdily in the blue and red regions, and a smaller amount so in the green region, hence their green color. No absorption happens from the upper limit of our vision at 700nm out to beyond 1300nm where liquid water begins to absorb strongly (Figure 2.9). Tucker and Garratt, (1977) reported that no absorption means higher levels of reflectance from green vegetation. NIR is reflectance in the near-infrared band and RED is reflectance in the visible red band.

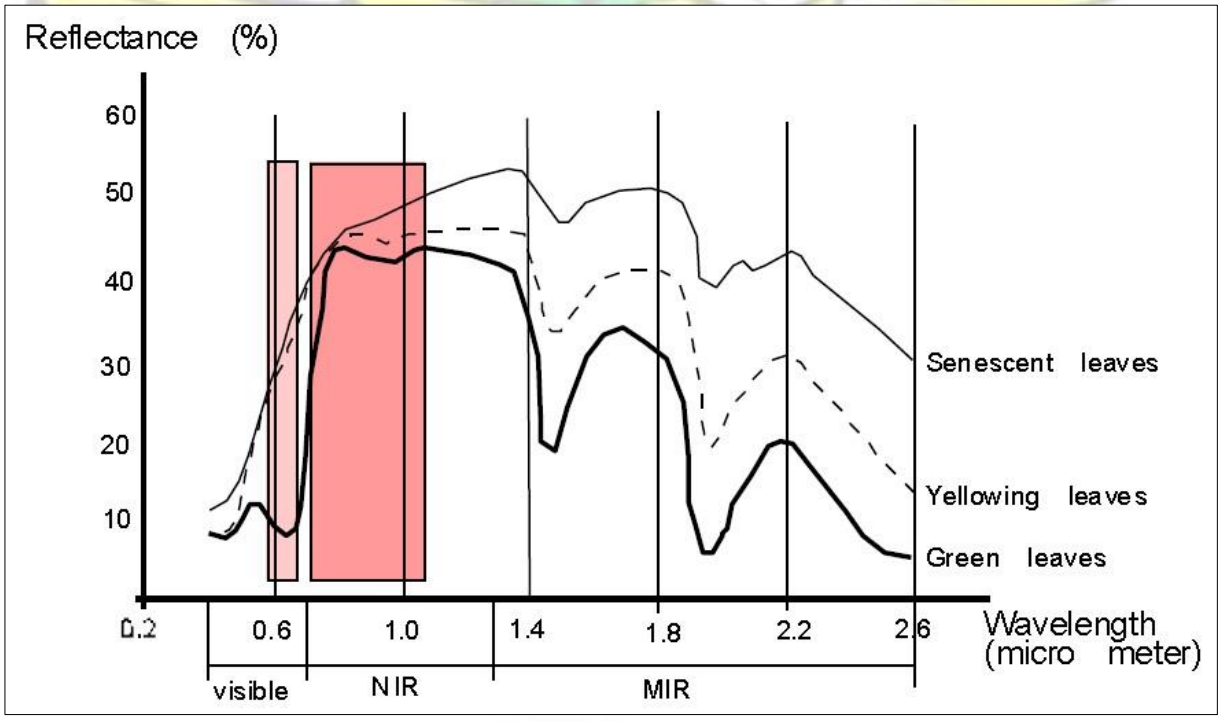

Figure 2. 9: Characteristics of spectral response of vegetation at three different stages of development (Source: Yengoh *et al*, 2014)

2.7.2 Broadband Greenness Vegetation Indices (VI)

In general measurement of vegetation quantity and vigor, the broadband greenness VIs are among the simplest measurement approach. They are combinations of reflectance measurements that are sensitive to the combined effects of foliage chlorophyll concentration, canopy leaf area, foliage clumping, and canopy architecture. These VIs are designed to provide a measure of the overall amount and quality of photosynthetic material in vegetation, which is essential for understanding the state of vegetation for any purpose. Table 2. 2: Broadband Greenness Indices

Index	Description	Equation
Normalized Difference Vegetation Index	Normalized difference of green leaf scattering (in near-infrared, chlorophyll absorption in RED)	$NDVI = \frac{NIR - R}{NIR + R}$
Simple Ratio Index	Ratio of green leaf scattering (in near-infrared, chlorophyll	$\frac{NIR}{NDVI} = \frac{}{R}$
	absorption in RED)	
Enhanced Vegetation Index	NDVI enhancement (to account for soil background and atmospheric aerosol effects)	$EVI = \frac{NIR - R}{NIR + C_1R - C_2B + L}$
Atmospherically Resistant Vegetation Index	NDVI enhancement (to account better for atmospheric scattering)	$ARVI = \frac{(NIR - RB)}{NIR + RB}$
Sum Green Index	Integral of scattered light (in the GREEN spectral range is sensitive to gaps in vegetation canopy)	$SGI = \sqrt{0.5 + \frac{NIR - R}{NIR + R}}$

(Source: ENVI 4.7 Help)

2.7.3 Normalized Difference Vegetation Index

Landscape productivity measures for example NDVI can be used to characterize vegetation community, differentiate healthy vegetation from others or from nonvegetated areas (Manandhar *et al.*, 2009).

Comparisons of NDVI values between vegetation populations can be used to understand the structure and distribution of vegetation within focus area.

From table 2.2 NDVI is defined by equation below:

$$NDVI = \frac{NIR-R}{NIR+R} \quad \text{Equation 2}$$

From -1 to 1 is the ranges value of this index. Green vegetation reflects less amount of visible light and more Near Infra-Red, while scant vegetation reflects a larger portion of the visible and less Near Infra-Red. Fundamentally the NDVI algorithm is based on this concept.

NDVI associates the reflectance characteristics in a ratio; hence it is an index simultaneous to photosynthetic composition. NDVI values greater than zero compares with vegetated areas; the higher the spectral index, the more the chlorophyll composition of the target.

In the evaluation of land cover type change; NDVI has been very useful (Lunetta *et al*., 2006, Gilabert, 2009 and Deyong *et al.*, 2009) and also useful in assessing responses to ecological factors in environmental change assessments (Pettorelli *et al*., 2005). The researchers listed above found NDVI to be effective indicator for monitoring environmental degradation and other ecological impacts due to climatic disasters.

Wang *et al*., (2000) reported that there is a strong relationship between the pattern of mean annual rainfall and the general spatial distribution of NDVI values while the effect of temperature on NDVI values was mainly observed in the initial and later parts of the growing season

In a study conducted by Xu and Guo, 2014, NDVI values derived from Landsat 8 (L8) images was compared with values derived from Landsat 7 (L7) and ground measurement data from hyperspectral sensor. The result proved that NDVI computed from Landsat 8 is generally higher than NDVI from Landsat 7 in sparsely vegetated zones and the variation becomes lesser as the value of NDVI rises. Xu and Guo , 2014 Further indicated that NDVI of L8 and L7 is consistent when dealing with highly vegetated areas (e.g. forested area) since when the NDVI is high the difference between L8 and L7 NDVI is near zero.

2.7.4 The Use of NDVI for Landuse Landcover (LULC) mapping

A good amount of research effort has been devoted in the use of NDVI to assess and analyzed extent of land use and land cover change (Yuan and Elvidge, 1998; Mas, 1999; Diouf and Lambin, 2001; Veldkamp and Lambin, 2001; Stow *et al*., 2004; Martínez, 2009).

NDVI applications range from global studies of land cover classification and mapping according to these literatures (DeFries and Townshend, 1994; Turner and Meyer, 1994; Hansen *et al.,* 2000; Friedl *et al.,* 2002), at varying scales (Lambin and Ehrlich, 1997; Stow *et al.*, 2004) to specific case studies (Shalaby and Tateishi, 2007; Sternberg *et al.*, 2011; Yuan and Elvidge, 1998; Lunetta *et al.*, 2006).

Research conducted by Horion *et al.,* (2014) revealed that during dry season minimum NDVI was found to be uncorrelated with dry grass residues; hence the NDVI parameter can be used as a proxy for assessing changes in tree cover in such ecosystems.

2.7.5 Limitations to the use of NDVI in LULC assessment

In spite of the advantages of satellite derived dataset for example supply of spatially continuous data and the ability to yield time-series signatures from which temporal patterns, trends, variations and relationships may be derived (Jacquin *et al.,* 2010). Users of NDVI scientific methodology are advised to tread cautiously with regards to its usage so as to avoid misusage of the NDVI (*Yengoh et al*., 2014)

The under listed key limitations are raised by Yengoh *et al*., 2014 with regards to the use of NDVI for LULC Assessments.

[1] Difficulty in separating the effects of climate from the effects of land degradation.

[2] Difficulty in dealing with cloud cover.

[3] Underestimation of land degradation when utilized for mapping trends.

CHAPTER THREE MATERIALS AND METHODS

3.1 Study Area

Four reclaimed mined land namely Old Tailing storage facility (TSF) Block 1 North, Block 1 South and Block 2 & 3 Waste Rock Dump (WRD) within the catchment area of AngloGold Ashanti Iduapriem mine were selected for the purpose of this research (Figure 3.1). These sites represented difference in years after rehabilitation.

The ages of the study areas at the time of LiDAR mapping in 2010 were; Block 2/3 WRD age was 10 years, followed by Old TSF rehabilitated site 9 years, Block 1 North; 4 years, and Block 1 south 3 years in the respective order.

Block 1 North and South as well as Block 2 & 3 WRD are mine waste rock dump site whilst Old TSF represented a typical decommissioned tailing storage facility (Appendix 5 and 6).

Also portion of adjacent natural undisturbed forest reserve known as Neung Forest which have an intact ecologies and higher functionality than the ecosystem of the rehabilitated sites was selected as a benchmark or reference site for the study areas.

3.2 Materials used

The methods used in this research include:

[1] Review of relevant literature.

[2] Collation of LiDAR data

[3] Obtaining Landsat historic data form USGS archives [4] Field data collection and validation.

[5] Image processing and analysis

3.3 Software Used for Research

[1] GIS and Remote Sensing software such as ENVI, ERDAS IMAGINE, ArcGIS, Fusion LDV

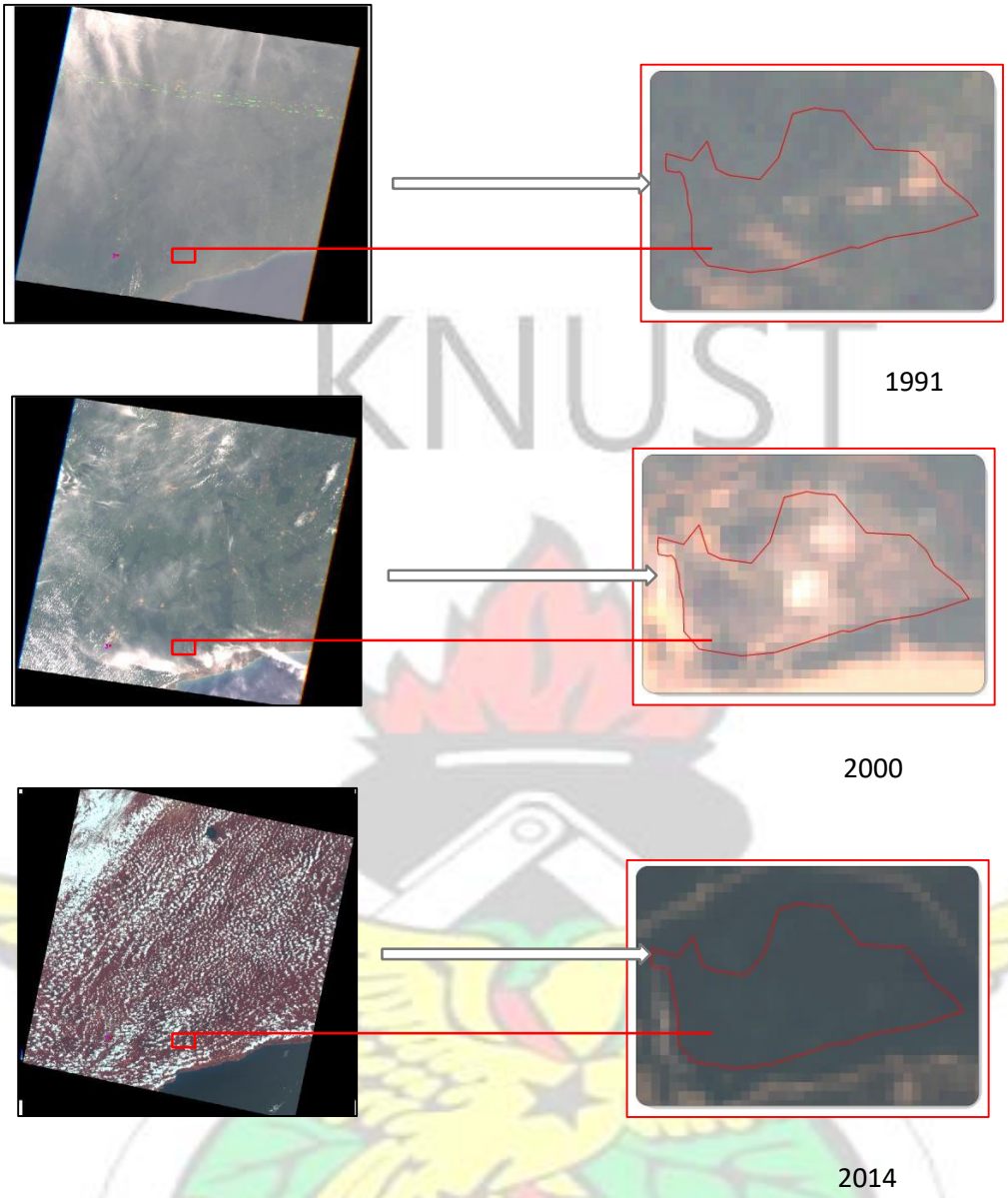

Figure 3.1: Study area (Block 1 North WRD) plotted on Landsat Imagery obtained from USGS

3.3 Flow chart of task

The study uses remotely sensed satellite image data and Airborne LiDAR data of the study area to assess reclaimed lands within the catchment areas of AAIL. The steps used for the study is organized in figure 3.2

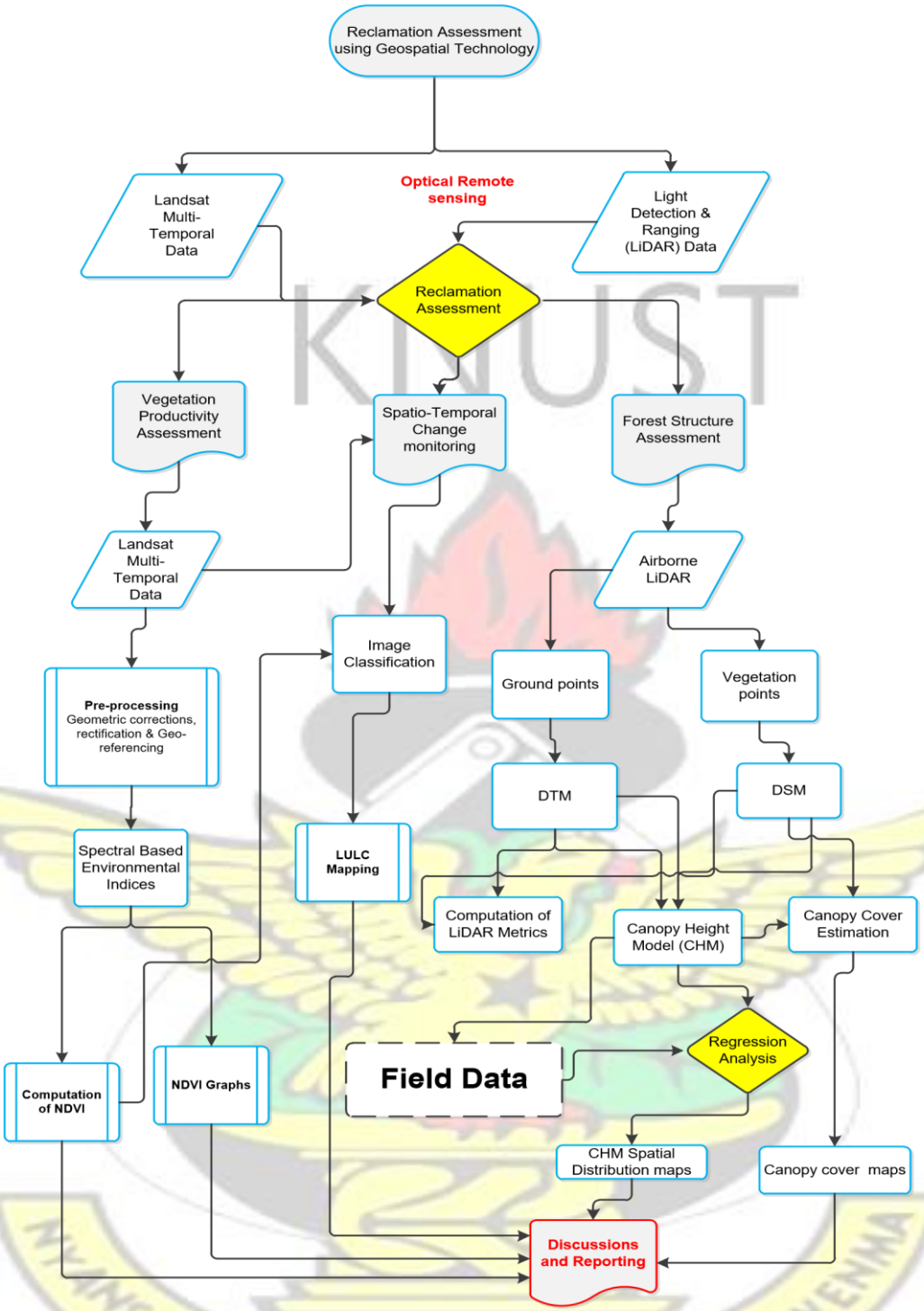

Figure 3.2: Methodology for the studies arranged in a Systematic flow diagram

3.1 Vegetation Productivity Assessment

3.1.1 Landsat Multi-Spectral Data

The type of remotely sensed data selected for this Assessment was Landsat TM (Bands 1-7), Landsat 7 ETM+ (Bands 1-7), and Landsat 8 OLI imagery (Bands 1-11) all acquired within the early half of the benchmark period.

Cloud free Landsat data for the year 1991, 2000, and 2014 were obtained for the study area from the USGS (United States Geological Survey) Earth explorer directory (earthexplorer.usgs.gov), from Thematic Mapper (TM) sensor on Landsat 4, Enhanced Thematic Mapper (ETM+) sensor on Landsat 7, and Landsat 8 Operational Land Imager (OLI) on Path 194 and Row 056. Table 3.1 list the dataset and some characteristics of data used in this study.

Table 3.1: List of Landsat Dataset utilised for land cover change assessment

DATE ACQUIRED	SPACECRAFT	SENSOR	PIXEL SIZE
01/01/1991	Landsat 4	TM	30m
17/05/2000	Landsat 7	ETM	30m
13/03/2014	Landsat 8	OLI	30m

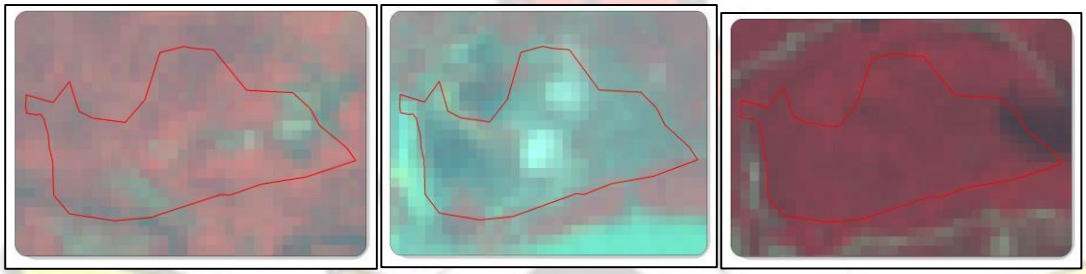

Figure 3.3: False color composite map of Block 1 North WD 1991, 2000, and 2014

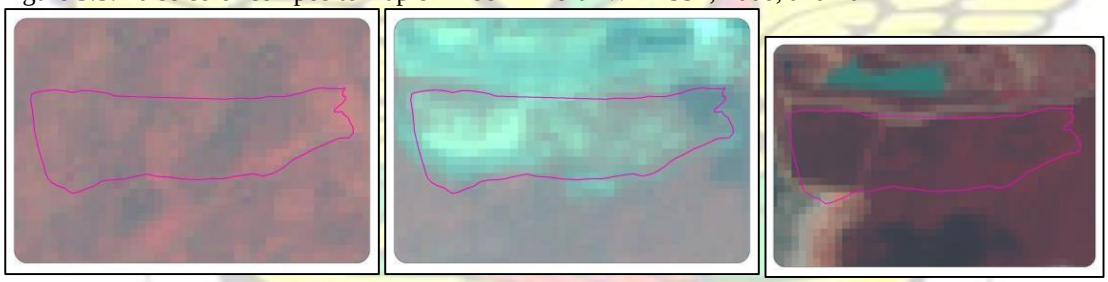

Figure 3. 4: False color composite map of Block 2/3 WD 1991, 2000, and 2014

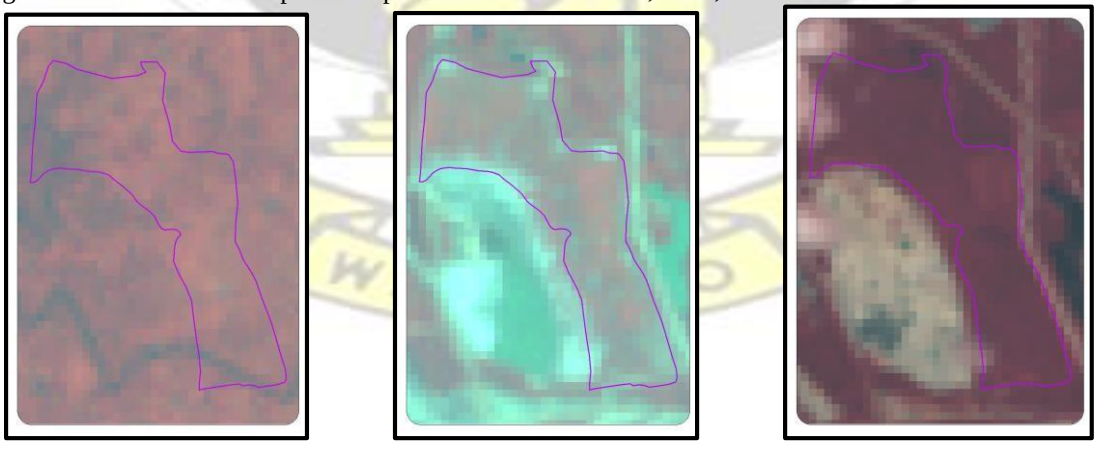

Figure 3. 5: False color composite map of Old Tailing Dam 1991, 2000, and 2014

3.1.2 Landsat Pre-processing

The data obtained from USGS directory had already been processed and geometric correction applied to the image datasets with the appropriate projection also assigned in UTM (Universal Transverse Mercator), zone 30N NAD 1983 horizontal coordinate system.

Radiometric correction were applied for the TM, ETM+ and OLI satellite imageries which mainly necessitated the conversion of the multispectral brightness measured values to top of atmosphere (TOA) reflectance values.

Landsat calibration function for atmospheric correction in Environment for Visualizing Images (ENVI) image processing software package version 4.7 was used to implement the analysis of the radiometric correction to all multi-temporal Landsat dataset for the benchmark periods (1991, 2000, and 2014) of the study areas.

The radiometric correction function undertaken can be broken into two main steps namely conversion of measured Digital Number (DN) to radiance using (inflight sensor) calibration parameters provided with the imagery obtained from USGS directory.

The equation used for converting each band DN to radiance is expressed in Equation 3.

$$\mathbf{L = DN \times Gain + Bias} \quad \text{Equation 3}$$

Where:

L = Measured spectral radiance (over spectral bandwidth of a channel)

DN = Recorded digital number value

$$\mathbf{Gain = L_{max} - L_{min} = \textit{Slope response function}} \quad \text{Equation 4}$$

$$\textbf{Bias} = \mathbf{L_{min}} = \boldsymbol{intercept\ of\ response\ function} \quad \text{Equation 5}$$

L_{max} = Measured radiance at detector saturation (mWcm-2sr^{-1})

L_{min} = Measured lowest radiance by detector (mWcm-2sr-^{1})

Secondly top of atmosphere (TOA) reflectance computation which corrects illumination variations (Earth-sun distance and sun angle) both within and between scenes for individual band was achieved with Equation 6.

The correction algorithm was implemented using the conversion parameters supplied in the image metadata.

The exoatmospheric irradiance an earth sun distance for Landsat 4 and 7 were retrieved from literature by Chander *et al*., 2009.

$$\boldsymbol{\rho_\lambda = \frac{\pi d^2 L_\lambda}{E_{0\lambda} cos\emptyset_s}} \quad \text{Equation 6}$$

Description of parameters used in Equation 6 is as follows: P_λ

= Reflectance (As a function of bandwidth) d

= Correction for Earth-sun distance

L_λ = Radiance (As a function of bandwidth) $E_{0\lambda}$

= Exoatmospheric irradiance

θ_s = solar zenith angle

Landsat 8 (OLI_TIRS) band data were converted to TOA spectral radiance using the radiance rescaling parameters supplied in the metadata file as follows:

$$\boldsymbol{L_\lambda = MLQ_{cal} + AL} \quad \text{Equation 7}$$

Where:

L_λ = TOA (spectral radiance in Watts/(m^2 * srad * μm))

ML = Multiplicative rescaling factor (Band specific)

AL = Additive rescaling factor (Band-specific)

Q_{cal} = DN value (Quantized and calibrated standard product pixel values)

TOA planetary reflectance conversion was undertaken in ArcGIS environment with Raster calculator tool using reflectance rescaling parameters supplied in metadata file (MTL file) that comes with the imagery obtained from USGS directory.

$$\rho\lambda = M\rho Q_{cal} + A\rho \quad \text{Equation 8}$$

Where:

ρ_λ = TOA planetary reflectance (without correction for solar angle)

M_ρ = Multiplicative rescaling factor (Band specific)

A_ρ = Additive rescaling factor (Band specific)

Q_{cal} = DN value (Quantized and calibrated standard product pixel values)

TOA reflectance (with a correction for the sun angle) was computed as follows:

$$\rho_\lambda = \frac{\rho\lambda'}{\cos(\theta_{SZ})} = \frac{\rho\lambda'}{\sin(\theta_{SE})} \quad \text{Equation 9}$$

Where:

ρ_λ = TOA planetary reflectance θ_{SE} = Sun elevation angle (Local) θ_{SZ} = solar zenith angle (Local)

$$\theta_{SZ} = 90^0 - \theta_{SE} \quad \text{Equation 10}$$

3.1.3 Calculating Environmental based Spectral Indices

The NDVI (normalized difference vegetation index) was considered as spectral vegetation index for assessing vegetation productivity and landcover type of the study area. This index was assessed from the multi-temporal Landsat imagery in ERDAS Imagine remote processing software.

The NDVI was estimated using near infrared and red bands as per the equation below in ERDAS Imagine environment.

$$NDVI = \frac{NIR-R}{NIR+R}$$ **Equation 11**

Where:

NDVI = Value of Normalized difference vegetation index

NIR = Near infrared band

R = Red band

The Equation yields values between -1.0 to 1.0. Higher NDVI values correspond to a greater abundance of chlorophyll, an indicator for vegetation productivity.

NDVI was calculated for all usable data products in each of the reclaimed sites. The study areas were sub-divided 30m X 30m plots and center point of the plot selected for monitoring change in NDVI form 1991 – 2014. Descriptive statistics were obtained in the study areas to observe NDVI change on the three aforementioned benchmark periods.

3.2 Spatio-Temporal Change Monitoring

3.2.1 Land Cover Classifications

The study areas were visually inspected and classified using spatial analyst Reclassify tool in ArcGIS; NDVI values below 0.2 were classified as Bare land , NDVI values ranging between 0.2 - 0.4 classified as Grasslands and Shrubs whilst values greater than 0.4 classified as Vegetation or Forest (Figure 3.8) for NDVI change analysis.

Table 3. 2: Reclassified land cover schemes

Land cover Types	Description
Bare Earth and Rocks	Barren Land (Waste rock dumps, Open

	Pits, Heap leach pad etc.)
Shrubs and Grasslands	Sparse Vegetation (Herbaceous land mainly shrubs and grass)
Forest and Vegetation	Dense Vegetation (Forested Land)

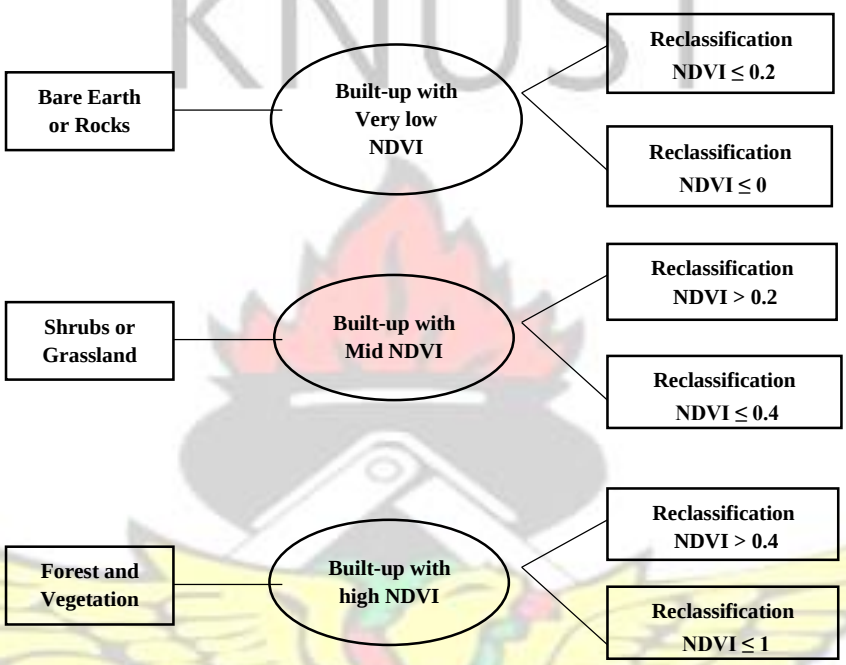

Figure 3. 6: Reclassification of NDVI values for land use land cover mapping

3.3 Forest Structure Assessment with LiDAR

3.3.1 Airborne LIDAR Survey

The LiDAR survey was conducted with an Airborne Laser Terrain Mapping technique (ALTM) fitted with a high accuracy rangefinder which scanned beneath the coverage of the aircraft and producing a wide swath over which the distance to the mapping surface measured as well as the scan angle. To correct for the aircraft's movements, the motions of the aircraft were recorded by an inertial reference system for later post-processing.

A Global Positioning System (GPS) receiver fitted in the ALTM records the aircraft's location at fixed intervals. A second, ground-based receiver was used to assess the differential correction for more accurate position estimation.

Summary of accuracy report of the Lidar survey utilized for this study are presented in Table 3.3

3.2.2 LiDAR Data Acquisition

Airborne LIDAR surveys were conducted on rehabilitated waste rock dumps and a tailings dam at the AngloGold Ashanti Iduapriem Limited (AAIL) site (Figure. 1.1) located in the Tarkwa Nsuaem Municipal Area of the Western Region of Ghana to assess tree height and the reclamation success. The study site comprises of mixed species such as; family of Leguminous, comprising of Acacia auriculiformis, and Cacia siamea, Acacia mangium, Gliricidia sepium, Cacia nodosa, Leuceana leucocephala and indigenous species such as Ceiba pentandra, Terminalia superb, and Tarrietia utilis as well as other species.

Airborne data acquisition was conducted with a fixed wing aircraft fitted with Airborne Laser Terrain Mapping System at a point density of 1.6 points per square meter (pts/m^2) in December 2010 over the study area.

Table 3. 3: Achieved Accuracy of Ground Control Points (All coordinates in GHTM. All data in meters.)

Point	Ground Control Point Terrestrial			Measured Position		Measured elevation		Deviations			
	Easting	**Northing**	**Elev.**	Easting	Northing	Photogrammetrical	Laser data	dX	dY	dZ	dZ(L)
PP01	162787.63	65863.96	69.91	*1)	*1)	*1)	*1)	*1)	*1)	*1)	*1)
PP02	160886.07	60553.03	57.85	*1)	*1)	*1)	*1)	*1)	*1)	*1)	*1)
PP03	155554.52	63292.79	53.45	155554.50	63292.80	53.68	53.49	-0.023	0.015	0.237	0.043
PP04	155455.65	69805.51	54.40	155455.67	69805.41	54.67	54.39	0.022	-0.106	0.270	-0.011
PP05	151826.38	73410.94	43.40	151826.35	73411.04	43.46	43.38	-0.034	0.103	0.060	-0.022
PP06	151339.80	65407.19	59.28	*1)	*1)	*2)	*2)	*2)	*2)	*2)	*2)
PP07	157178.56	75415.78	188.59	157178.61	75415.73	188.60	188.69	0.053	-0.046	0.007	0.096
PP08	158752.91	63242.57	68.18	158752.80	63242.56	*1)	*1)	-0.111	-0.007	*1)	*1)
PP09	150861.52	62677.07	19.19	150861.27	62676.96	19.39	19.11	0.028	-0.110	0.201	-0.079
PP10	158115.64	66461.28	129.96	158115.63	66461.45	*2)	*2)	-0.011	0.175	*2)	*2)
PP11	167717.55	66420.54	130.63	161717.52	66420.60	130.56	130.65	-0.026	0.058	-0.062	0.025
PP12	159198.32	68223.75	141.83	159198.37	68223.64	141.90	141.88	0.058	-0.104	0.078	0.054
Relative (inner) accuracy of imagery after aerotriangulation:					0.116	Minimum:		-0.111	-0.110	-0.062	-0.079
						Maximum:		0.058	0.175	0.270	0.096
						Standard Deviation:		0.053	0.101	0.125	0.058

3.2.3 Data Processing

Post-flight data processing were conducted by combining the laser range, GPS data and inertial measurement data to determine the accurate position of a point on the earth's surface and generate a geocoded point cloud.

The acquired data was processed using Terrasolid software; and subsequently data exported into a 1m resolution ASCII xyzit file format (xyz intensity format) (Table 3.3).

Digital terrain model and digital surface model were subsequently derived from the dataset and used for estimating reclamation vegetation heights and canopy closure.

3.2.4 Building Digital Terrain Models (DTM) and Digital Surface Models (DSM) from LIDAR

LIDAR Surface and ground multipoints in ASCII format covering the study area were imported into Fusion/LDV software with AsciiImport command into a LAS (LASer) file format; a binary format developed primarily for exchange 3D of LiDAR point cloud. (McGaughey, 2013; McCallum, 2014)

3.2.5 Estimation of Canopy Heights (CHM) of Reclaimed Sites

Further processing and analysis were carried out in FUSION/LDV and ArcGIS environment to generate canopy height model from the DSM and DTM with Fusion/LDV tools.

Reclamation heights were modelled from the LIDAR dataset by analysing the difference between the canopy surface (interpolated surface-classified altitudes) and ground surface (interpolated ground-classified hits) in Fusion software with the 'canopymodel' command. Output from 'canopymodel' is PLANS format DTM files that use floating point elevation values as well as coordinate projection information, which can then be exported as an Esri Grid file to be used for mapping the canopy heights in ArcGIS environment.

CanopyModel assigns the elevation of the highest return within each grid cell to the grid cell center. When used with a bare-earth model, CanopyModel subtracts the ground elevations from the return elevations to produce a canopy height model.

(McGaughey, 2013)

3.2.6 Computation of LIDAR Metrics

3.2.7 Height Metrics

Canopy height metrics were computed from the LIDAR point cloud data with Gridmetrics command in Fusion software with 2 m (lowest height) , 60 m (highest

height) parameters set as an outlier for the reclamation forest as well as the control undisturbed forest.

Generally all LIDAR returns below 2 m were assumed to be outliers in the estimation of Canopy Heights. In other words all trees below a 2 m height threshold were considered as shrubs and those above considered as trees.

A large number of statistics were produced for describing canopy height at 5m grid cell size. The metrics produced included basic distribution statistics such as the mean, mode, variance, maximum height values, and height values of a range of percentiles. The metrics also includes statistics describing the shape of the point cloud height distributions including measurements of skewness, kurtosis, and linear (L) moments.

3.2.8 Canopy Cover Metrics

Cover metrics were computed as ratios of first LIDAR returns above 3m height threshold to the total first returns as described in the generic equation expressed below:

$$Cover = \left(\frac{\#returns > 3m\ threshold}{Total\ Returns}\right) * 100 \quad \text{Equation 12}$$

3.3 Ground Truthing of LiDAR CHM

3.3.1 Field data Collection

The individual tree heights were randomly sampled and measured on the Old TSF reclaimed site using Clinometer + Bubble level smart phone application and tape measure method as described by (Hemery, 2011). Tree height were measured and recorded twice from different positions separated by at least right angle to ensure independence between the two measurements.

Trees for which the two heights measured differ by more than 1 meter or by more than 5% were discarded so that errors in comparing heights extracted from LIDAR CHM to actual heights measured from the field can mostly be ascribed to the LIDAR. The two field measured heights for all well measured trees were later used to assess the accuracy of the height predicted from LiDAR CHM.

The measurement was done on mixed species: Acacia mangium, Oil Palm and Cocoa trees located at the Old TSF rehabilitated site. After measurement, error filtering was

done and 17 trees remained. These trees were plotted on the LIDAR dataset by using coordinates derived from a 3m accuracy handheld GPS of the tree measured and performing zonal statistics with the GPS coordinates on the LIDAR derived canopy height model (Table 3.4).

Table 3. 4: Field data Collected and Corresponding LiDAR CHM height

POINT ID	Northern (Y)	Eastern (X)	Field Height	Model Height - Top Height mean
T101	64395.71	157911.4	4.05	3
T102	64391.3	157902.3	5.02	1
T103	64384.33	157905.7	6.01	3
T104	64367.62	157913.6	5.3	4
T105	64317.71	157875.1	4.3	3
T106	64288.42	157867	5.8	3
T107	64275.76	157900.4	3.9	2
T108	64246.32	157913.6	5.2	2
T109	64200.33	157911.7	5.4	2
T110	64170.55	157928.5	4.4	1
T111	64173.15	157894.8	5	5
T112	64197.07	157871.9	5.02	2
T113	64282.13	157791.8	5	1
T114	64319.96	157781.8	5.2	2
T115	64315.37	157816.8	5.7	2
T116	64369.45	157880.7	6.3	2
T117	64375.23	157924.5	31.5	17

CHAPTER FOUR RESULTS AND DISCUSSION

4.1 Vegetation Productivity Assessment using NDVI index

In each reclaimed sites the center points of the 30m x 30m transect selected and localized on the NDVI maps and extraction of corresponding NDVI values yielded a statistical output (Table 4.1) which reveals an NDVI spatial pattern of 0.473 in 1991, 0.005 in 2000 and 0.681 in 2014. Statistical analysis and comparison of mean supported the rejection of the null hypothesis with a p-value of <0.001 for pairwise ttest.

Table 4.1: Summary of NDVI values for pre-mining (1991), after mining (2000) and after reclamation (2014) of the study areas

	N	Minimum	Maximum	Mean	Std. Deviation
1991.	1283	.1664	.5671	.473159	.0537119
2000.	1283	-.2415	.5652	-.005329	.1536376
2014.	1283	.3101	.7676	.680817	.0574263
Valid N (listwise)	1283				

Descriptive statistics (Table 4.2) performed on Normalized difference vegetation indices extracted shows an average of 0.448 in 1991, 0.085 in 2000 and 0.677 in 2014 with a standard deviation of 0.085, 0.099 and 0.041 respectively for block 1 North (Figure 4.1 and 12). The study reveals in general that the reclaimed area is regaining its initial biomass after a decrease that occurred in 2000 due to intensive mining activities and disturbances

Table 4.2: Summary of NDVI values recorded for Block 1 North pre-mining (1991), after mining (2000) and after reclamation (2014).

	N	Minimum	Maximum	Mean	Std. Deviation
1991	332	.1664	.5671	.448021	.0850192
2000	332	-.0830	.4801	.085001	.0985589
2014	332	.4581	.7268	.677068	.0411214
Valid N	332 (listwise)				

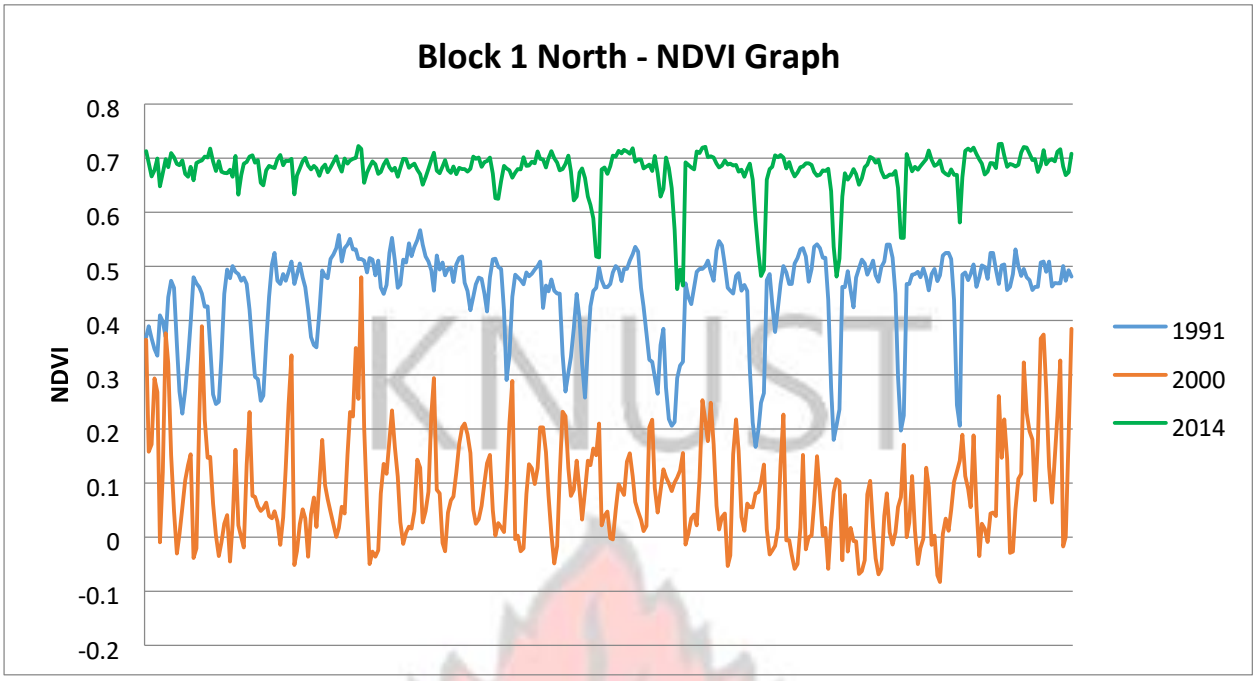

Figure 4. 1: Comparison of NDVI values for pre-mining (1991), after mining (2000) and after reclamation (2014) of Block 1 North WRD

Vegetation productivity at Block 1 south using the NDVI index reveals that average NDVI was 0.475 in 1991 whilst the year 2000 saw a remarkable reduction in the vegetation productivity to 0.256 (Table 4.3). This reduction saw very significant change in 2014 to 0.653 (Figure 4.2) which suggests that drastic decline recorded in 2000 as a result of mine waste dumping has been remediated.

Table 4.3: Summary of NDVI values recorded for Block 1 South pre-mining (1991), after mining (2000) and after reclamation (2014).

	N	Minimum	Maximum	Mean	Std. Deviation
1991	42	.4369	.4984	.475007	.0120023
2000	42	.0810	.3901	.255829	.0857169
2014	42	.5550	.7264	.653488	.0386735
Valid N (listwise)	42				

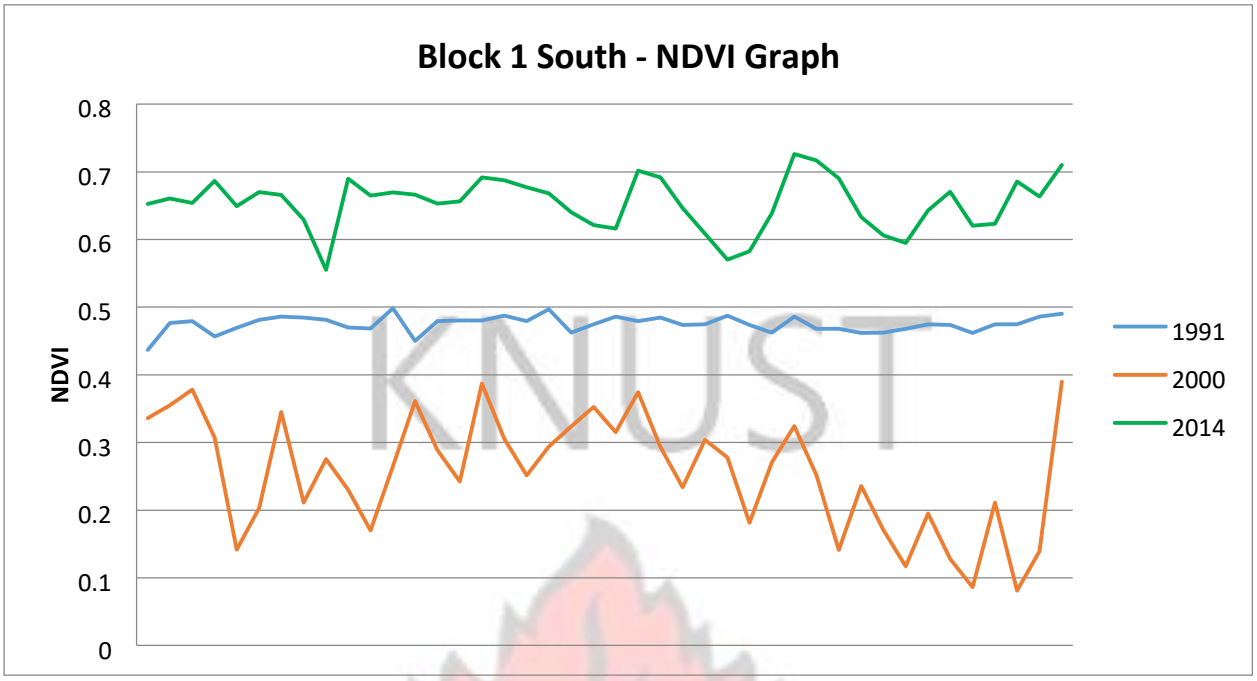

Figure 4. 2: Comparison of NDVI values for pre-mining (1991), after mining (2000) and after reclamation (2014) of Block 1 South WRD

Block 2 & 3 WRD recorded the highest average NDVI index which suggests healthy vegetation cover in 2014 (Table 4.4) with an NDVI of 0.678 contrary to the lowest average NDVI of 0.055 recorded in 2000. The pre-mining NDVI value of 0.477 was recorded in 1991. Comparison of NDVI changes within the benchmark period are presented in figure 4.3

Table 4.4: Summary of NDVI values recorded for Block 2 & 3 WRD pre-mining (1991), after mining (2000) and after reclamation (2014).

	N	Minimum	Maximum	Mean	Std. Deviation
1991	353	.3916	.5671	.476584	.0317461
2000	353	-.1791	.5652	.054946	.1546640
2014	353	.4221	.7676	.678109	.0533135
Valid N (listwise)	353				

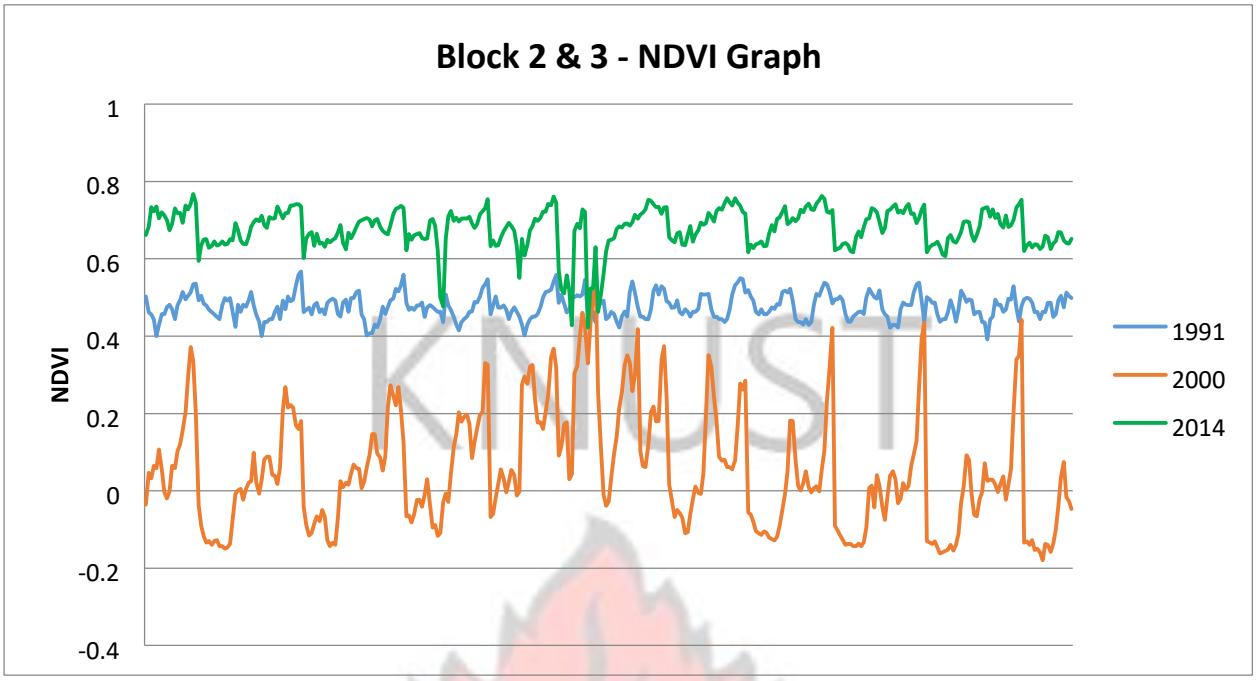

Figure 4. 3: Comparison of NDVI values for pre-mining (1991), after mining (2000) and after reclamation (2014) of Block 2 & 3 WRD

Similarly Old TSF also recorded an average NDVI index of 0.687 in 2014 (Table 4.5) which is an indication that disturbance which resulted in in a decline of the 1991 NDVI value of 0.486 to -0.117 in 2000 is regaining its initial biomass. Figure 4.4 shows a comparison of NDVI indicators recorded from 1991 – 2014. Mean NDVI value recorded in 2014 was 0.687, a good indication of healthy vegetation.

Table 4.5: Comparison of NDVI values for pre-mining (1991), after mining (2000) and after reclamation (2014) of Block 2 & 3 WRD

	N	Minimum	Maximum	Mean	Std. Deviation
1991	556	.3482	.5427	.485856	.0340010
2000	556	-.2415	.4087	-.117264	.0900642
2014	556	.3101	.7502	.686840	.0677492
Valid N (listwise)	556				

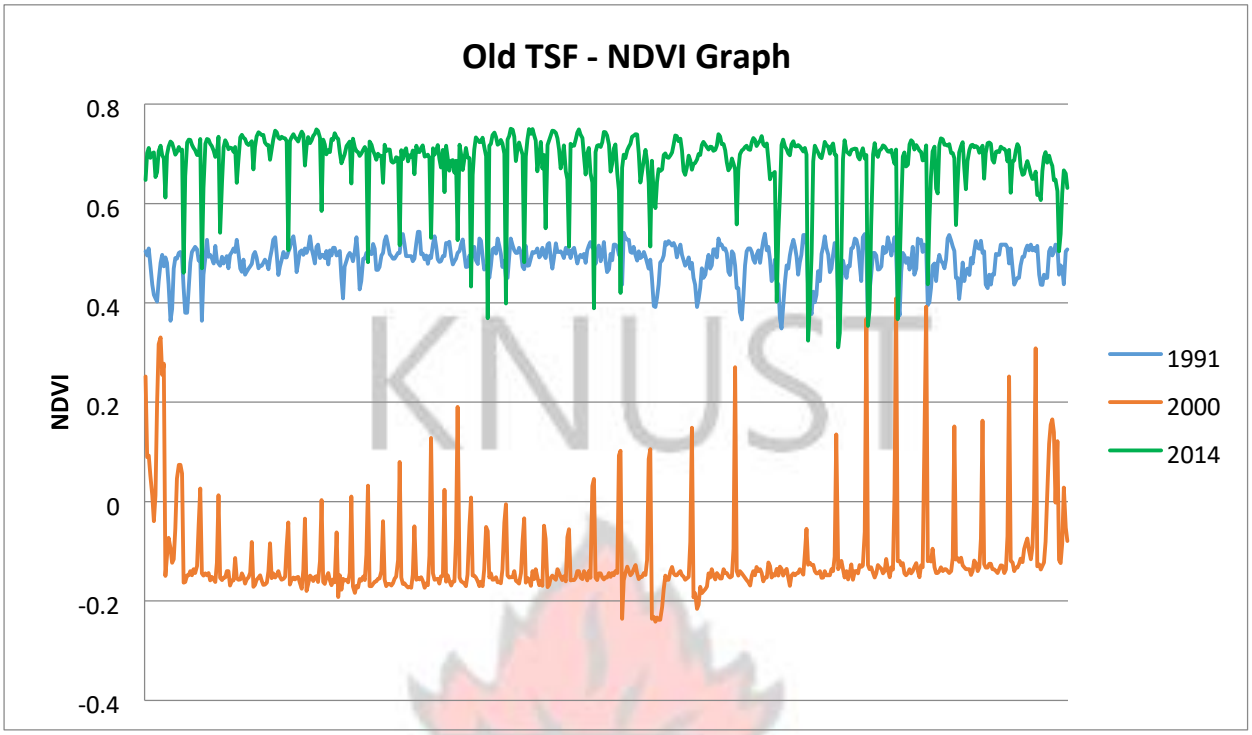

Figure 4. 4: Comparison of NDVI values for pre-mining (1991), after mining (2000) and after reclamation (2014) of Old TSF Rehabilitated site

Contrary to the decline of NDVI index for the study areas in the year 2000 as indicated in the above discussions an increase in NDVI was rather recorded for Neung Forest Reserve which shows that Mining activities has not impacted these areas. Comparative assessment of NDVI index for this undisturbed natural forest (Neung forest Reserve) revealed that average of 0.482 recorded in 1991 increased to 0.539 in 2000 and further increased to 0.617 in 2014 (Table 4.6 and Figure 4.5).

Table 4.6: Summary of NDVI values for undisturbed natural forest (Neung Forest) from 1991 - 2014

	N	Minimum	Maximum	Mean	Std. Deviation
1991.	8492	.4004	.5642	.481776	.0269111
2000.	8492	.4001	.6353	.539084	.0366727
2014.	8492	.4003	.7470	.617344	.0911890
Valid N (listwise)	8492				

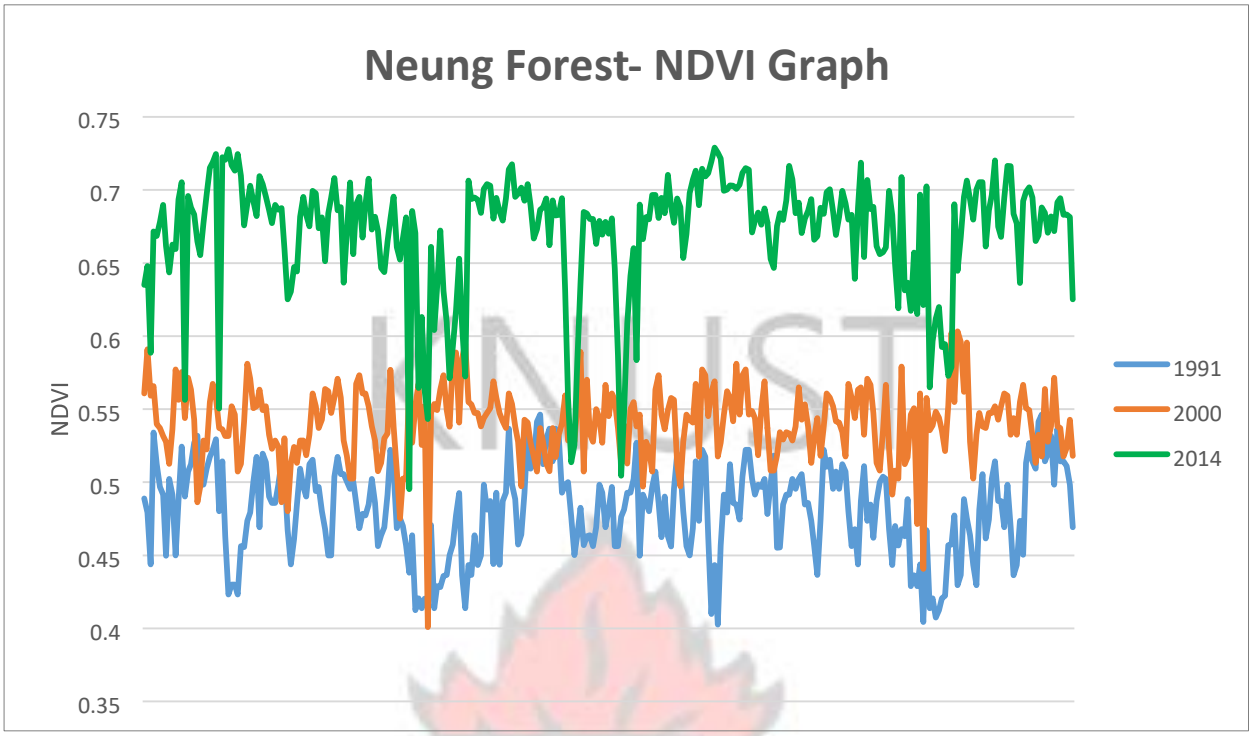

Figure 4. 5: Comparison of NDVI values for pre-mining (1991), after mining (2000) and after reclamation (2014) of Neung Forest Undisturbed site.

NDVI maps shows a visualization of spatial patterns of the study areas for the benchmark period 1991 – 2014 are presented in Figure 4.6 – 4.8

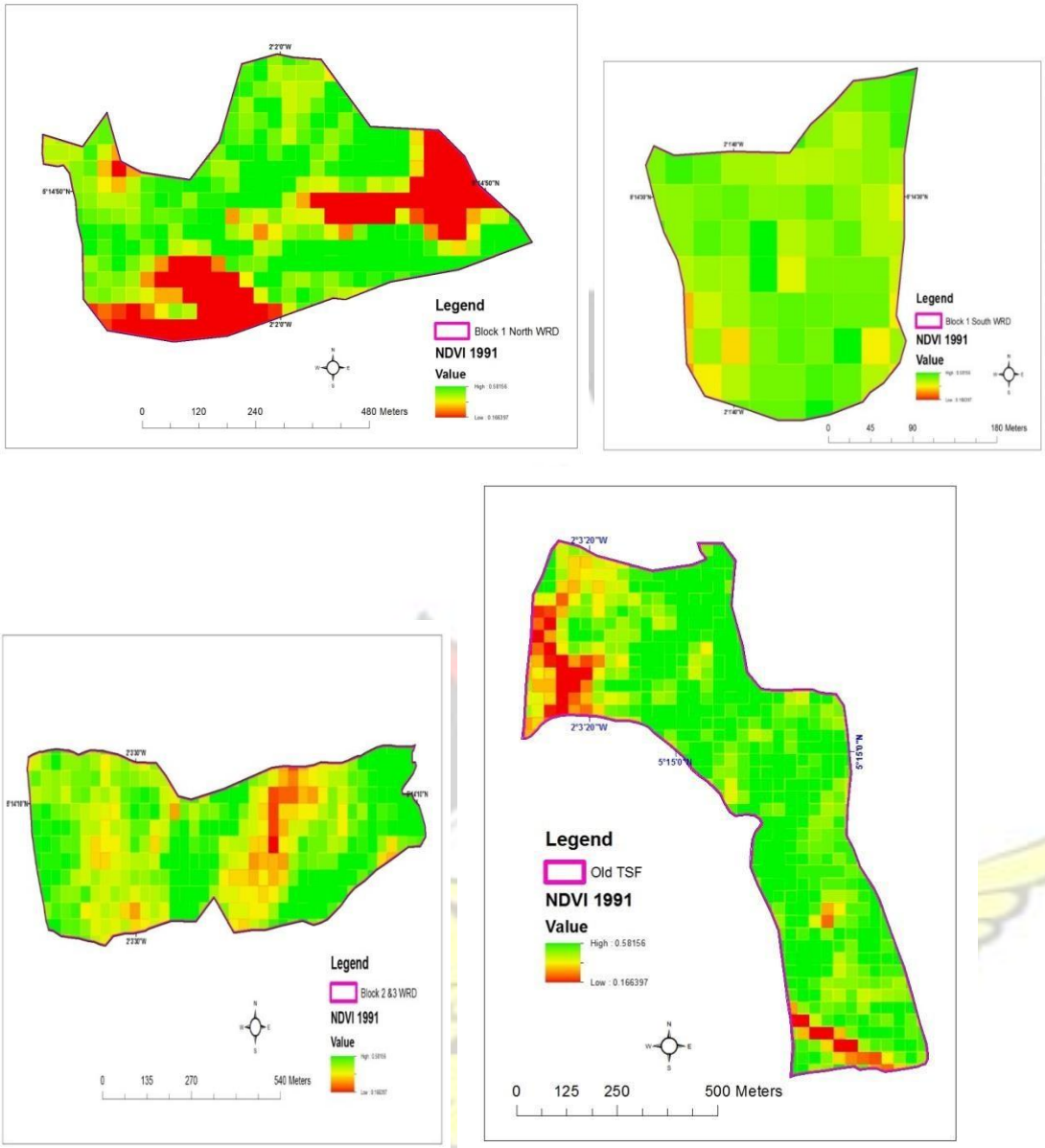

Figure 4. 6: Normalized Difference Vegetation index (NDVI) maps of the study areas for the year 1991

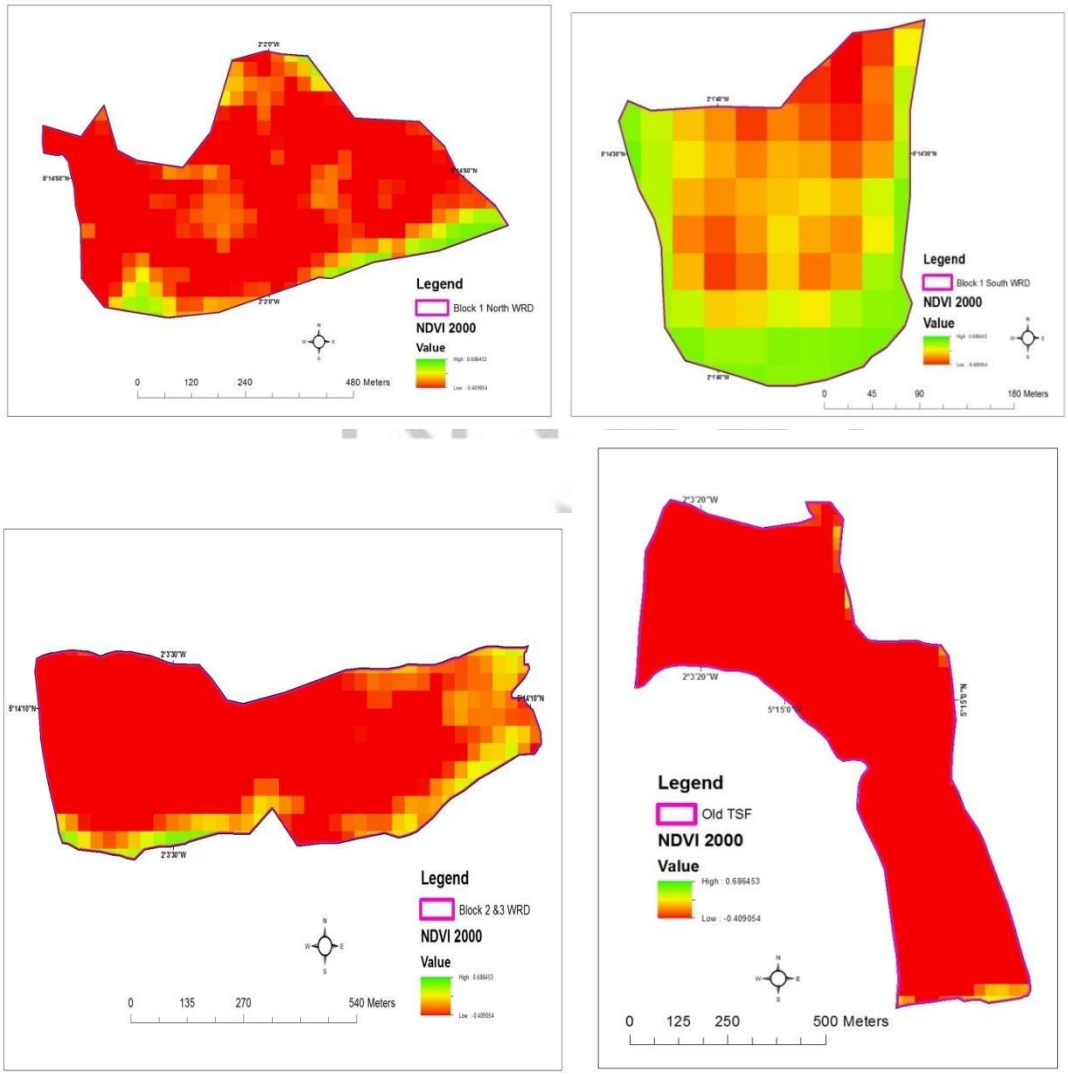

Figure 4. 7: Normalized Difference Vegetation index (NDVI) maps of the study areas for the year 2000

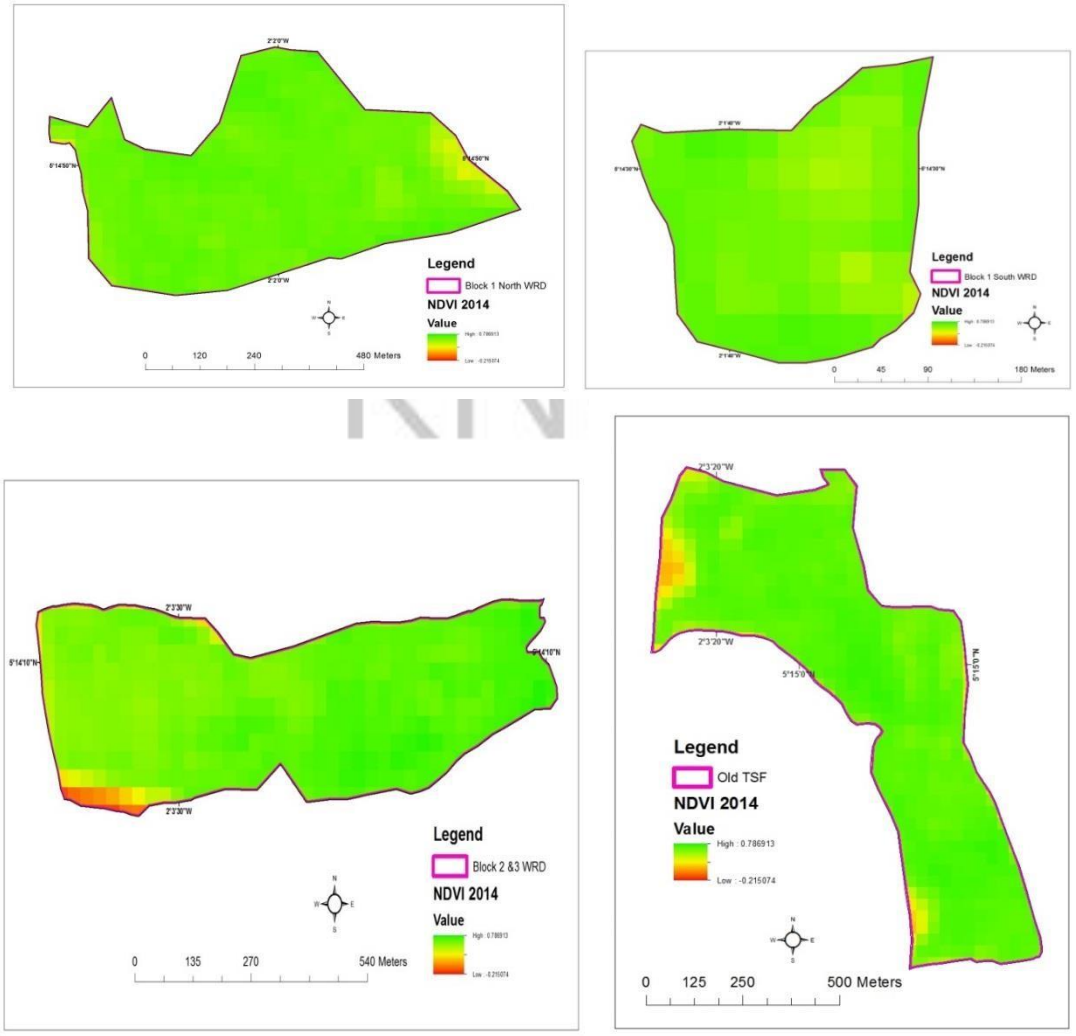

Figure 4. 8: Normalized Difference Vegetation index (NDVI) maps of the study areas for the year 2014

4.2 Spatiotemporal Change Assessment

The final maps derived from the land cover classification are presented in Figure 4.10 – 4.12 for Block 1 North, Figure 4.14 – 4.16 for Block 1 South, Figure 4.18 – 4.20 for Block 2 & 3 WRD and lastly Figure 4.22 – 4.24 for Old TSF Rehabilitated sites.

Temporal assessments of the study area for the benchmark period, indicated that at Block 1 North WRD; Forest/Vegetation reduced from 81% (of total land size) in 1991 to about 5 % in 2000, and then to 100% in 2014 (Figure 4.9). Relative change in terms of the land size which is the difference in area (ha) between 2014 (After reclamation) and 1991 (before mining) divided by 1991 area (ha) in percentage was 24% (Table 4.7) for Block 1 North which suggests that the land cover degradation recorded in 2000 due to intensive mining and dumping activities has been recovered.

Table 4.7: Summary of temporal changes from 1991 to 2014 for Block 1 North Rehabilitated site

Block 1 North WRD	1991		2000		2014		
LULC Category	Area total (ha)	% of land	Area total (ha)	% of land	Area total (ha)	% of land	Relative change 1991-2014 (%)
Bare earth	0.27	1%	25.65	81%	0	0%	-100%
Shrubs or grassland	5.85	18%	4.41	14%	0.00	0%	-100%
Forest\Vegetation	25.74	81%	1.89	5%	31.95	100%	24%
Total	**31.86**	**100 %**		**100 %**		**100 %**	
			31.95		**31.95**		

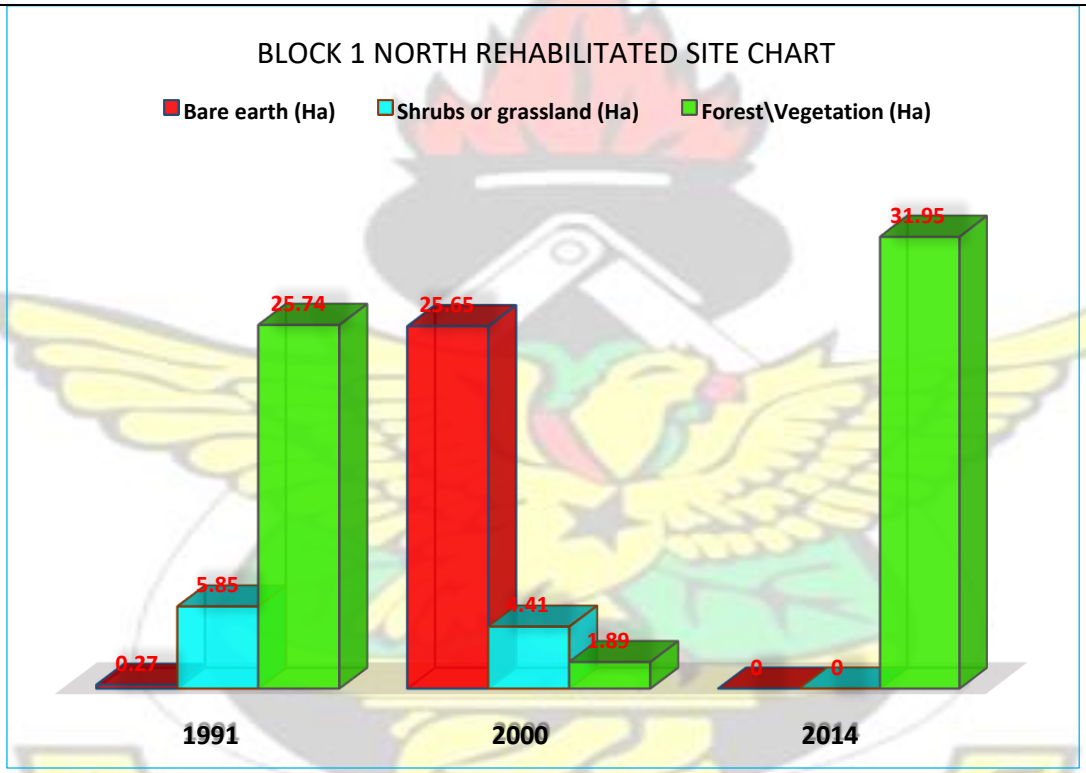

Figure 4. 9: Histogram Chart of Block 1 North Temporal changes for benchmark period 1991 - 2014

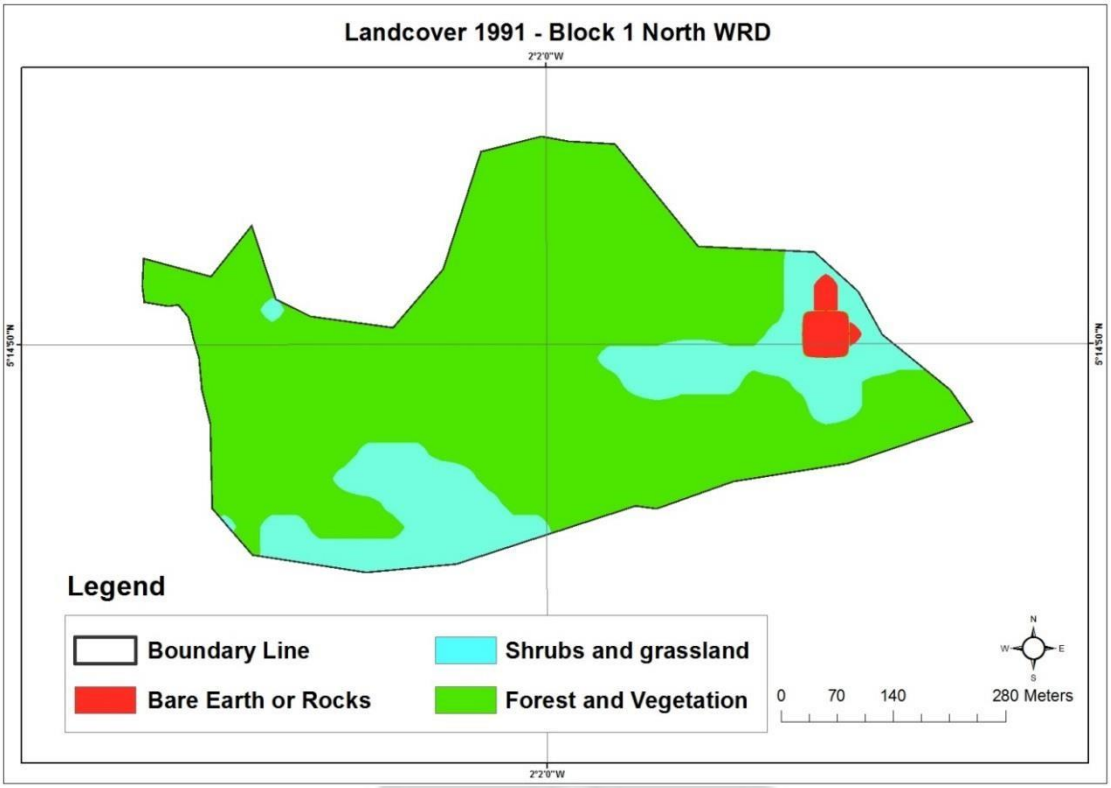

Figure 4. 10: Landuse Land cover (LULC) map of Block 1 North rehabilitated site for the year 1991

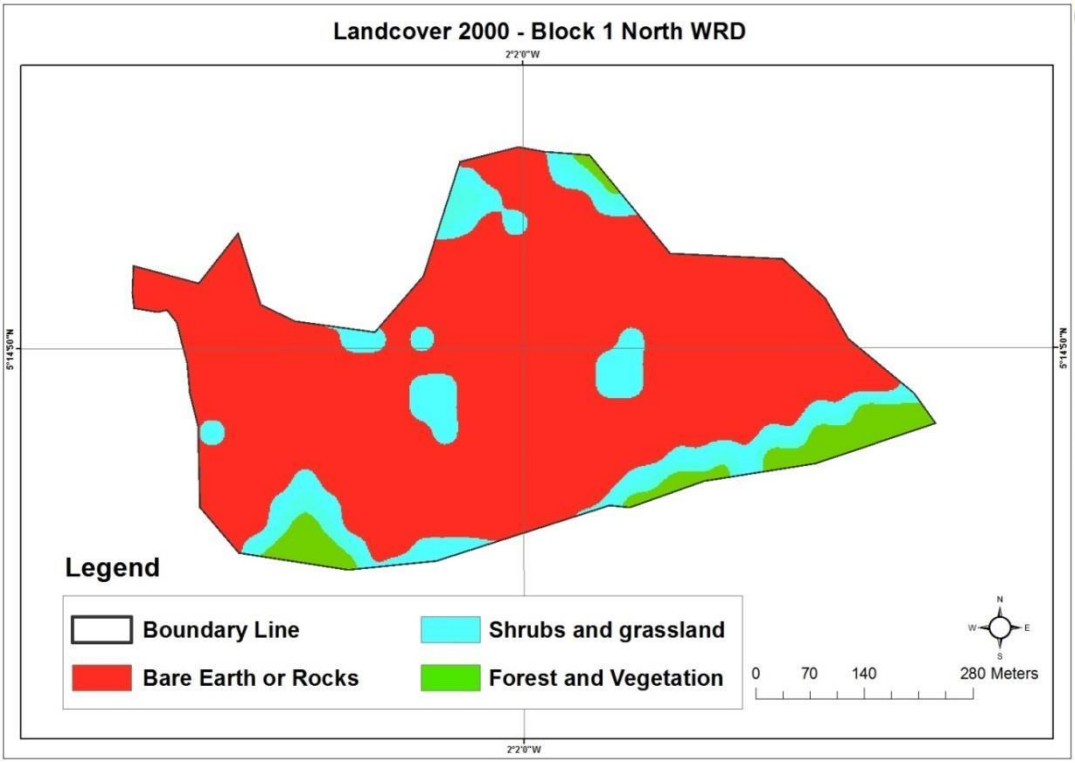

Figure 4. 11: Landuse Land cover (LULC) map of Block 1 North rehabilitated site for the year 2000

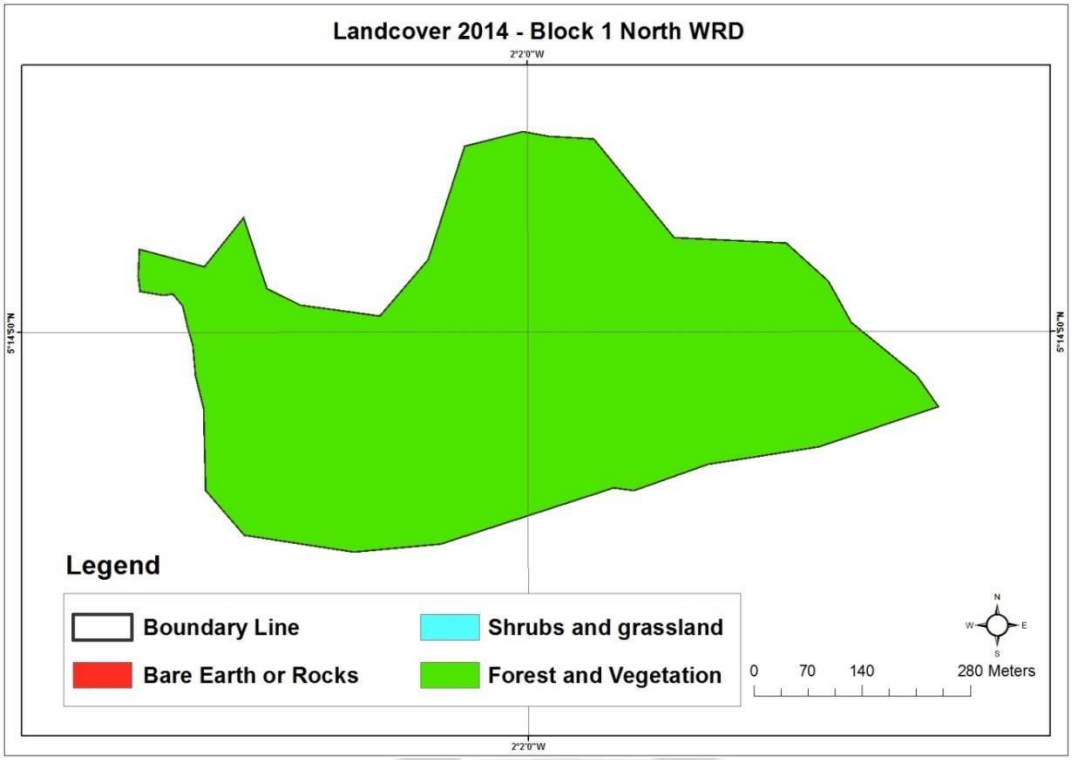

Figure 4. 12: Landuse Land cover (LULC) map of Block 1 North rehabilitated site for the year 2014

Furthermore the results recorded at Block 1 South WRD suggest that Forest / Vegetation in 1991 contracted from 100% of the total land size to 40% in 2000 (Figure 4.13) and then to 100% in 2014. Relative change between 1991 and 2014 was 0% (Table 4.8) an indication of full recovery of the pre-mining land cover of the study area.

Table 4.8: Summary of temporal changes from 1991 to 2014 for Block 1 South Rehabilitated site

Block 1 South WRD	**1991**		**2000**		**2014**		
	Area (ha)	**% of total land**	**Area (ha)**	**% of total land**	**Area change (ha) 1991**	**% of total land**	**Relative 2014 (%)**
LULC Category							∞
Bare earth	0	0%	0.99	15%	0	0%	

Shrubs or grassland	0	0%	2.97	45%	0.00	0%	∞
Forest\Vegetation	6.57	100%	2.61	40%	6.57	100%	0%
		100		**100**		**100**	
Total	**6.57**	**%**	**6.57**	**%**	**6.57**	**%**	

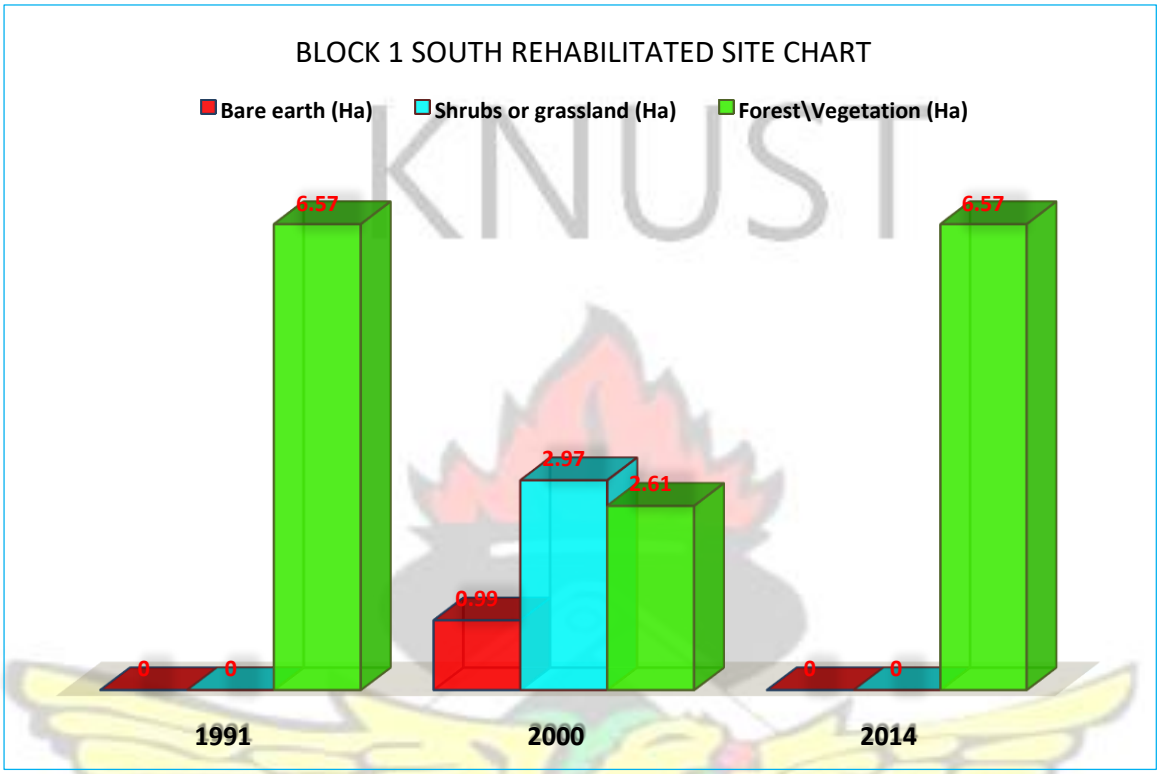

Figure 4. 13: Histogram Chart of Block 1 South Temporal changes for benchmark period 1991 - 2014

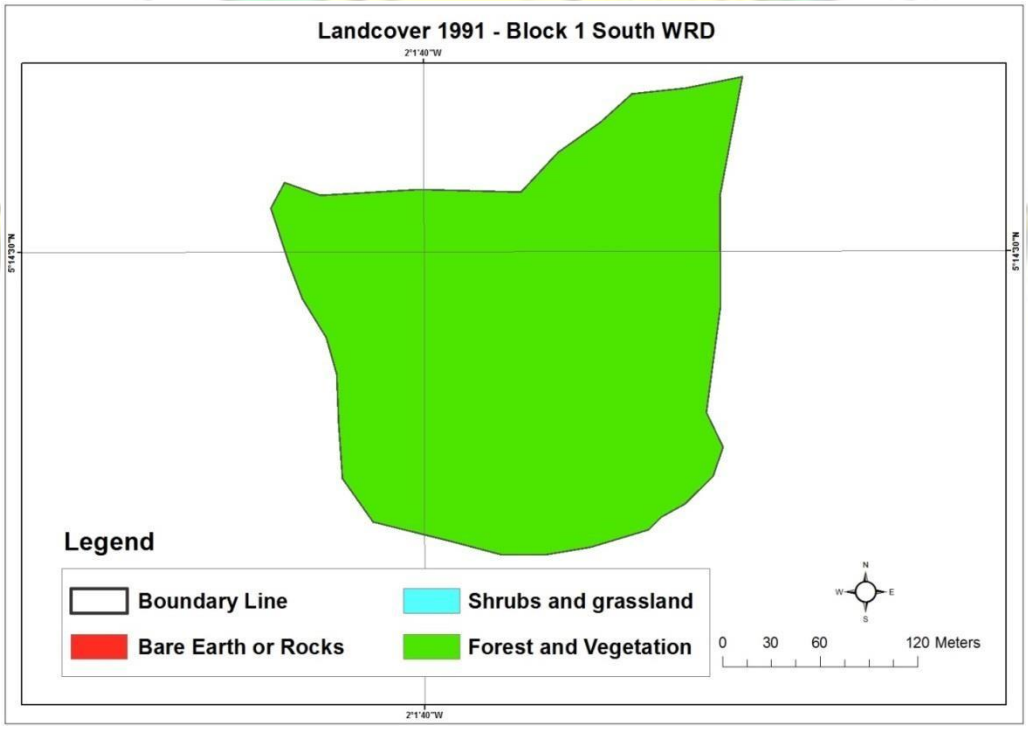

Figure 4. 14: Landuse Land cover (LULC) map of Block 1 South rehabilitated site for the year 1991

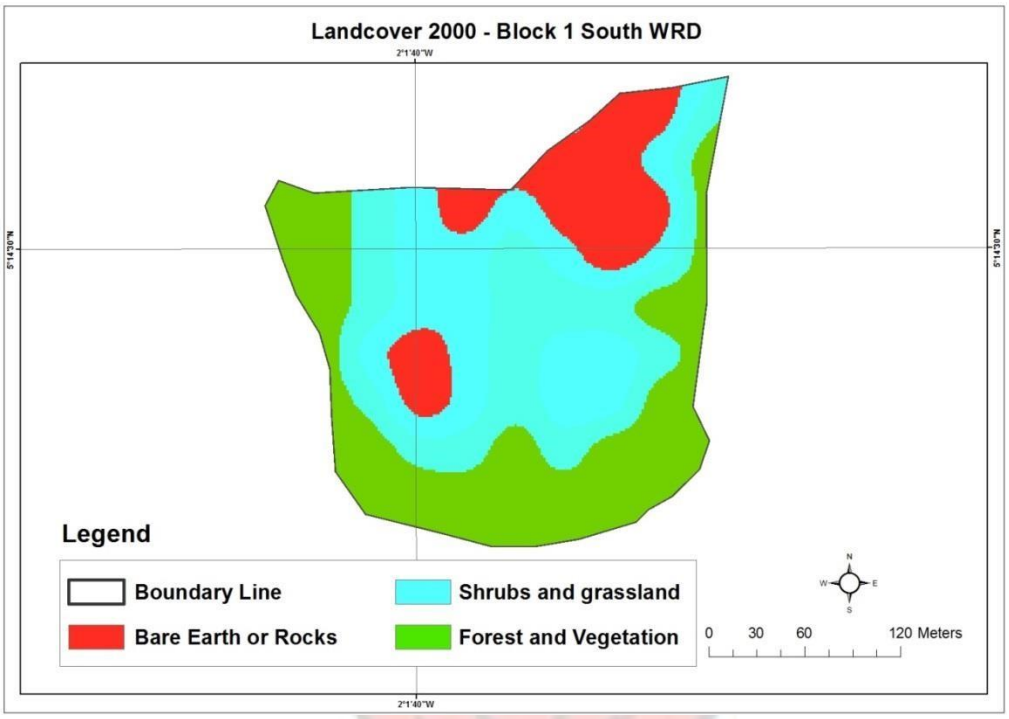

Figure 4. 15: Landuse Land cover (LULC) map of Block 1 South rehabilitated site for the year 2000

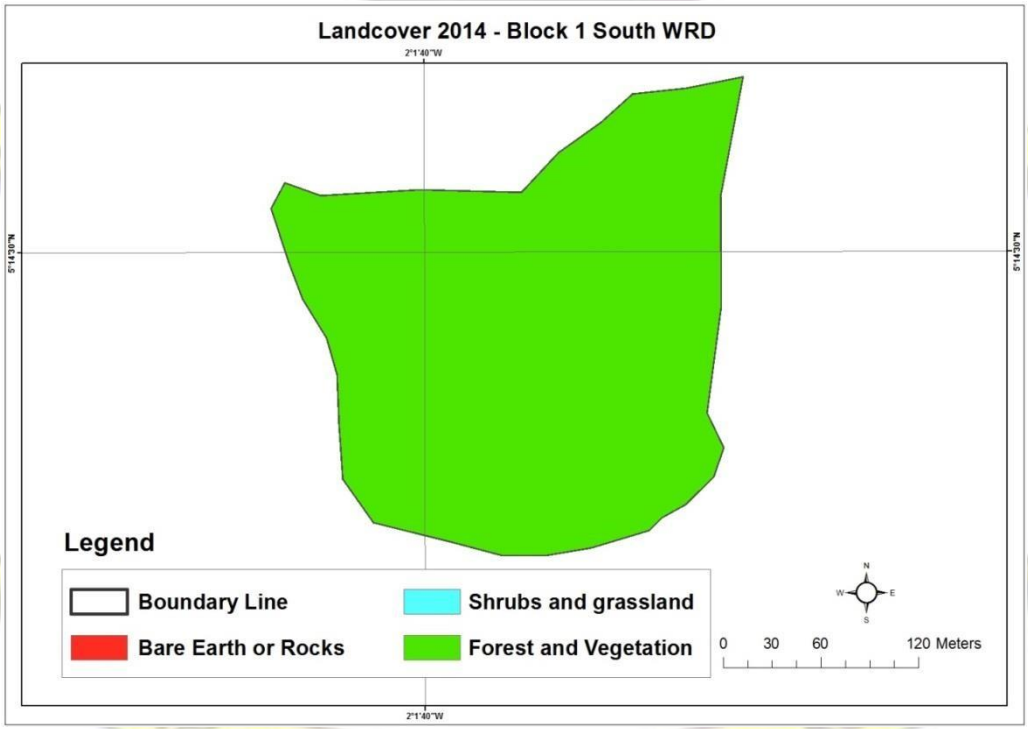

Figure 4. 16: Landuse Land cover (LULC) map of Block 1 South rehabilitated site for the year 2014

In addition to the above, results recorded from the spatio-temporal change analysis at Block 2 & 3 WRD was indifferent from that of Block 1 North and South WRD depicting a resemblance of full recovery of the Landcover type. From Table 4.9 and figure , 99% of the Lancover type (land size) represented Forest /Vegetation in 1991, this amount was degraded to bare earth and rocks as a result of mining activities, 1 %

Forest/Vegetation remained in 2000 which was consequently reclaimed to achieve 97% reclaimed status.

Table 4.9: Summary of temporal changes from 1991 to 2014 for Block 2 & 3 WRD Rehabilitated site

Block 2 & 3 WRD	**1991**		**2000**		**2014**		**Relative change 1991-2014 (%)**
LULC Category	**Area (ha)**	**% of total land**	**Area (ha)**	**% of total land**	**Area (ha)**	**% of total land**	
Bare earth	0	0%	25.47	79%	0.09	0%	∞
Shrubs or grassland	0.27	1%	5.4	17%	0.72	2%	167%
Forest\Vegetation **Total**	31.95	99%	1.35	4%	31.41	97%	-2%
	32.22	**100 %**	**32.22**	**100 %**	**32.22**	**100 %**	

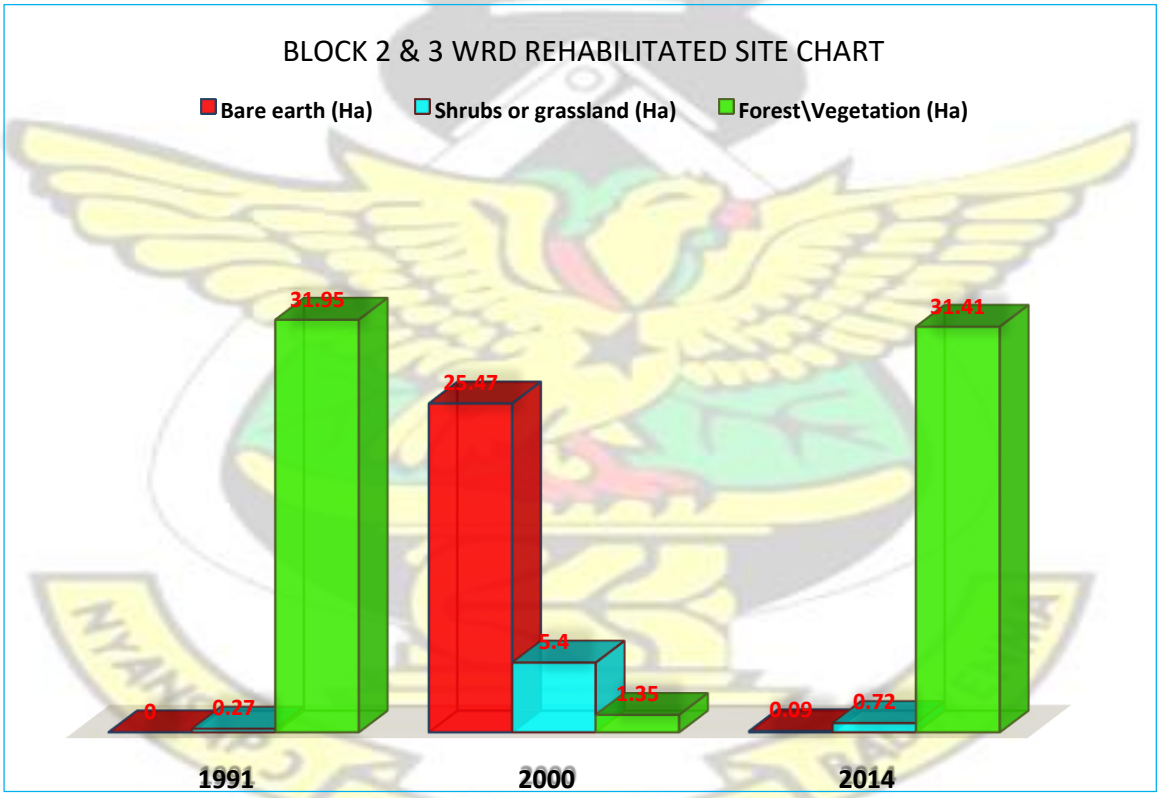

Figure 4. 17: Histogram Chart of Block 2 & 3 WRD Temporal changes for benchmark period 1991 - 2014

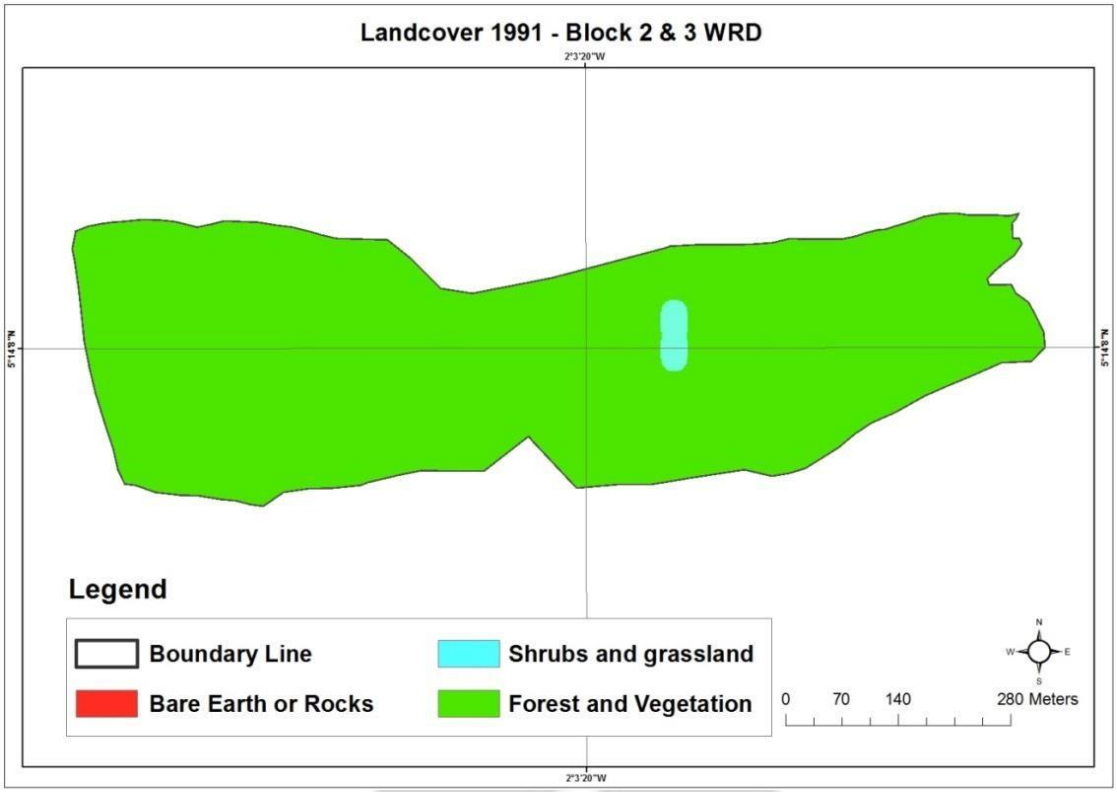

Figure 4. 18: Landuse Land cover (LULC) map of Block 2 & 3 WRD rehabilitated site for the year 1991

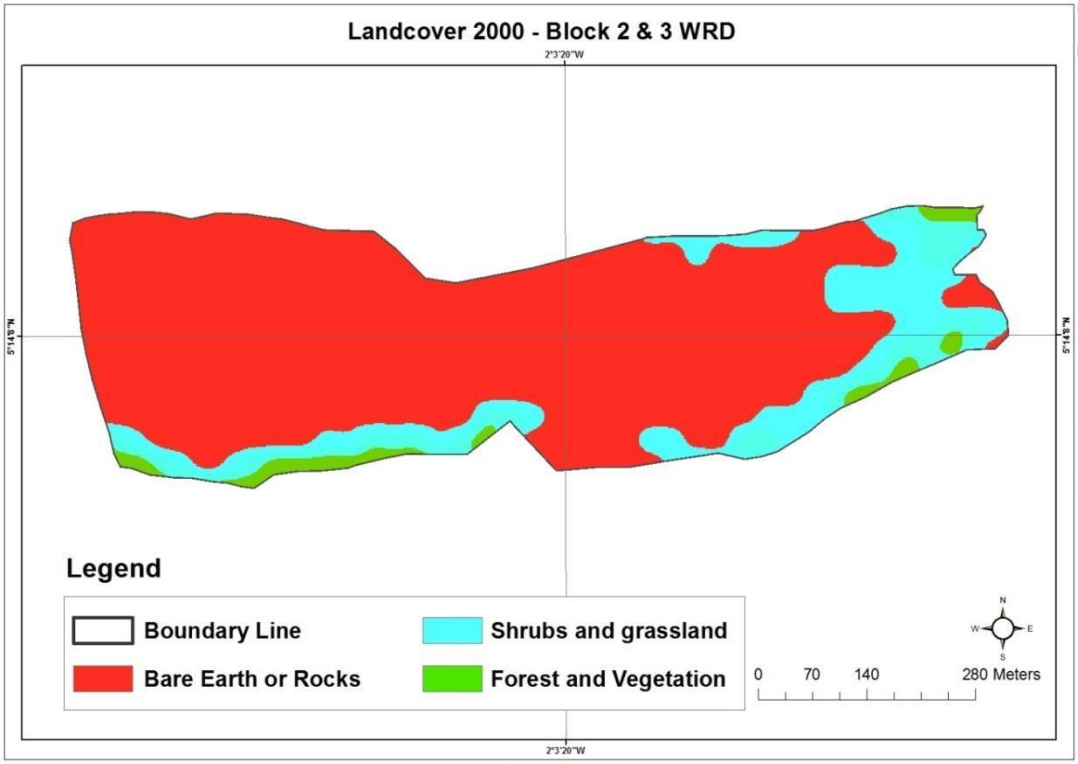

Figure 4. 19: Landuse Land cover (LULC) map of Block 2 & 3 WRD rehabilitated site for the year 2000

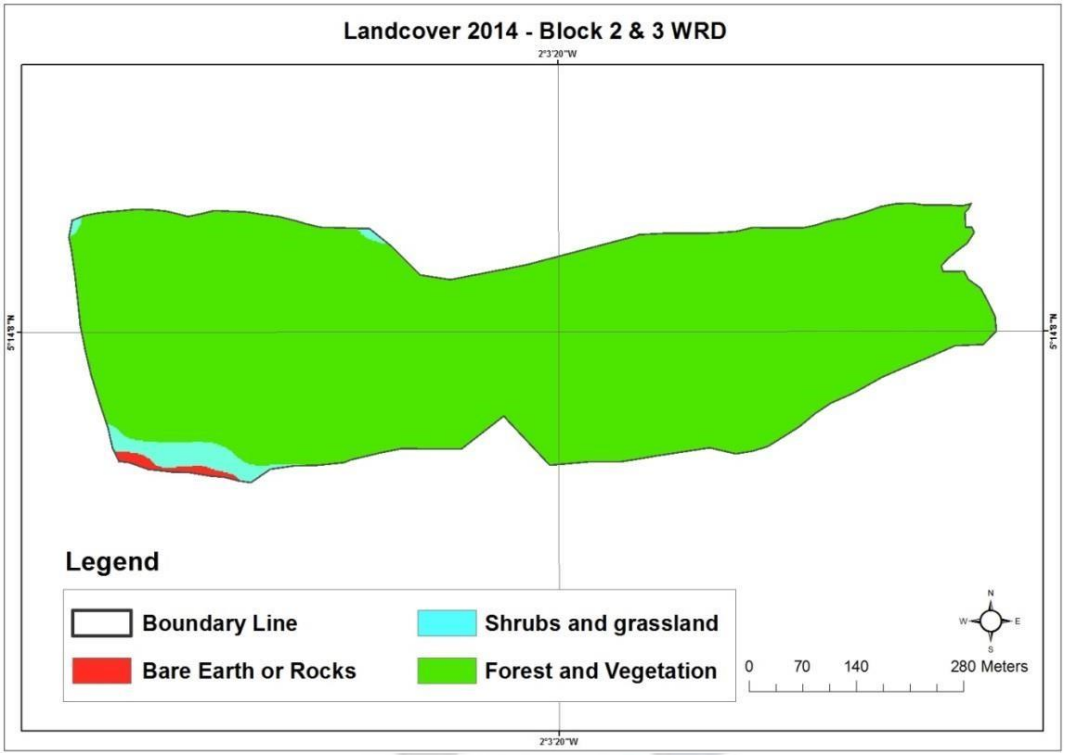

Figure 4. 20: Landuse Land cover (LULC) map of Block 2 & 3 WRD rehabilitated site for the year 2014

The result for Old Tailing Dam indicated that; Forest/Vegetation reduced from 96% (of total land size) in 1991 to about 1 % in 2000, and then to 98% in 2014 (Table 4.10). Relative change in terms of the land size was +2% for Old TSF which suggest that the landcover change recorded in 2000 due to tailing deposition activities has been recovered.

Table 4.10: Summary of temporal changes from 1991 to 2014 for Old TSF Rehabilitated site

Old TSF	**1991**		**2000**		**2014**		
	Area (ha)	**% of total land**	**Area (ha)**	**Area change (ha) 1991**	**% of total land**	**Area (ha)**	**% of total land**	**Relative 2014 (%)**
LULC Category								∞
Bare earth	0	0%	49.14	97%	0	0%		
Shrubs or grassland	1.8	4%	1.26	2%	0.81	2%	-55%	
Forest/Vegetation	48.96	96%	0.36	1%	49.95	98%	2%	
Total	**50.76**	**100 %**	**50.76**	**100 %**	**50.76**	**100 %**		

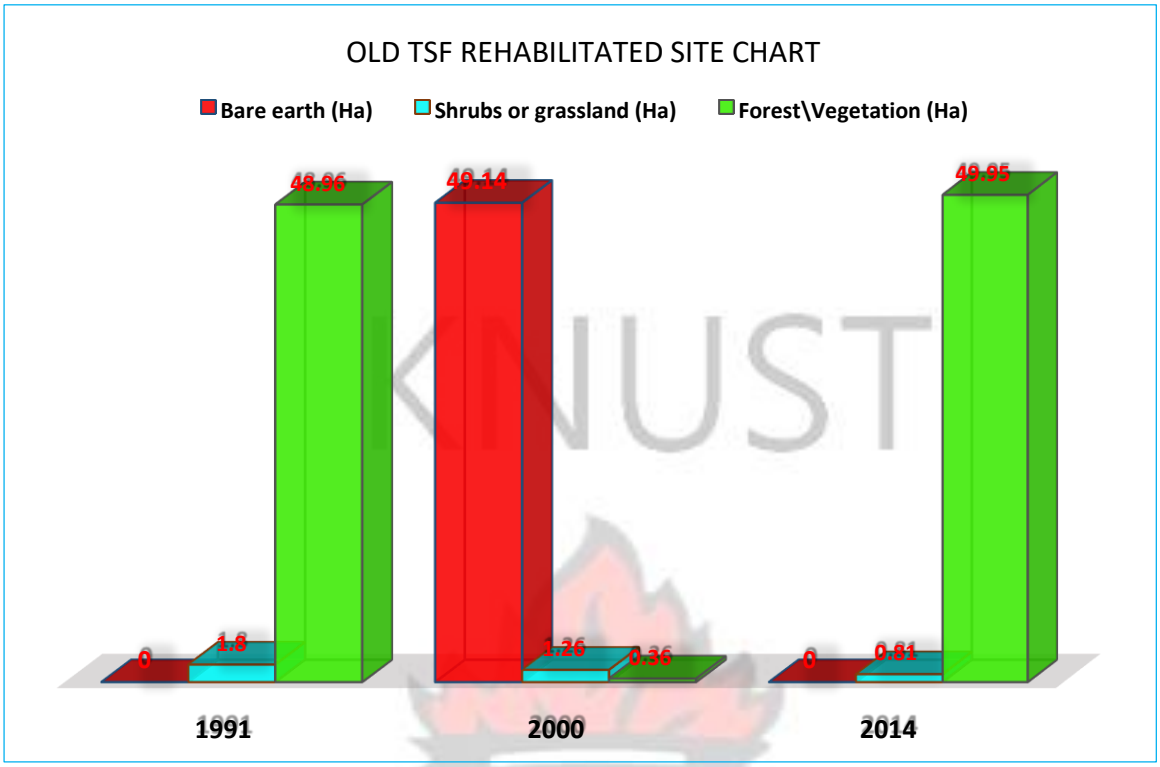

Figure 4. 21: Histogram Chart of Old TSF Temporal changes for benchmark period 1991 - 2014

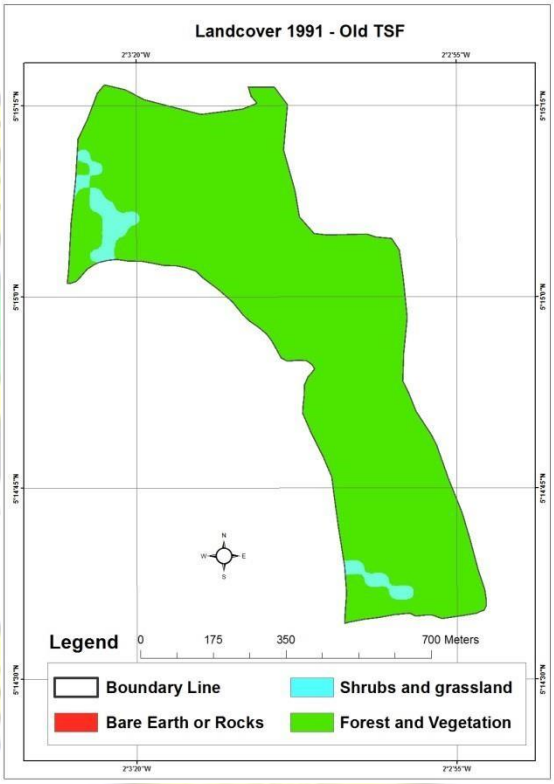

Figure 4. 22: Landuse Land cover (LULC) map of Old TSF rehabilitated site for the year 1991

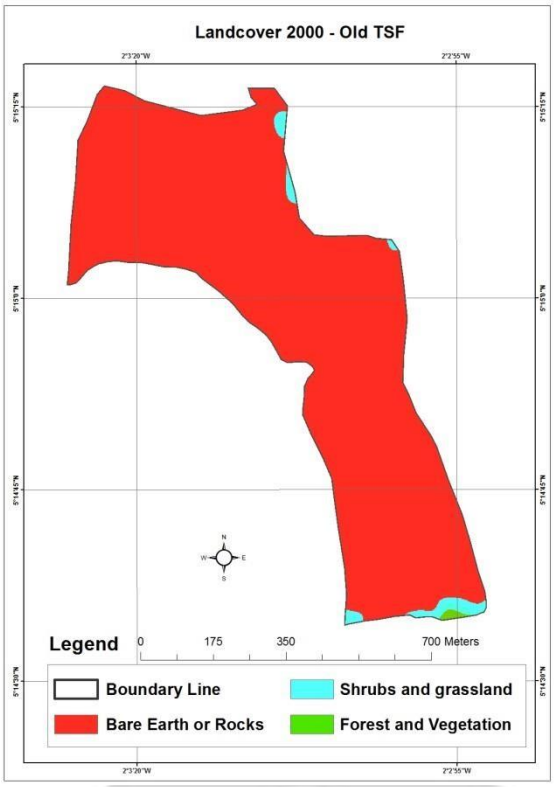

Figure 4. 23: Landuse Land cover (LULC) map of Old TSF rehabilitated site for the year 2000

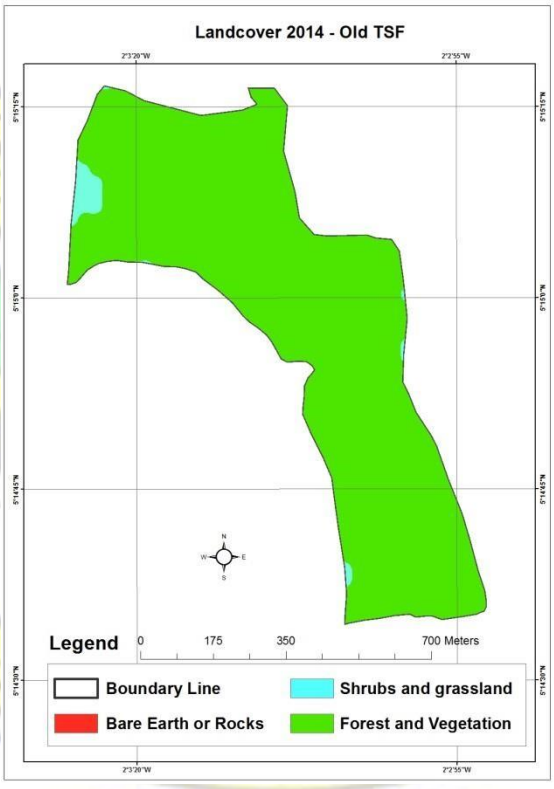

Figure 4. 24: Landuse Land cover (LULC) map of Old TSF rehabilitated site for the year 2014

Shrubs and grassland (SG) category for Block 1 North WRD decreased from 18% in 1991 to 14% in 2000, and then reclaimed to 0% in 2014.

At Block 1 South WRD SG increased from 0% in 1991 to 45% in 2000, and then reduced to 0% in 2014, Block 2 & 3 WRD also showed an increase in SG from 1% in 1991 to 17% in 2000, and then to 0% in 2014. Old TSF depicted in decreased from 4% in 1991 to 2% in 2000, and then maintained 2% in 2014

However, Bare Earth and Rocks (BER) categories show consistent trends; in the case of Block 1 North WRD, it increased from 1% in 1991 to 79% in 2000, and then decreased by 100% to 0% in 2014.

At Block 1 South WRD it increased from 0% to 15% before it was reduced to 0%. Similarly at Block 2 & 3 WRD Bare earth and rocks category increased from 0% to 79% and then to approximately 0%. On the other hand Old TSF recorded an increase in BER from 0% to 97% and subsequently reduced to 0% in 2014 due to extensive rehabilitation ensued within the benchmark period.

The result from the temporal assessment reveals in general that; the benchmark period of 23 years assessed (from 1991 to 2014), all types of LULC were found to have depicted a change in land cover types over the study areas.

4.3 Vegetation Structural attributes assessment using LiDAR

4.3.1 LiDAR Error Analysis

The LIDAR derived tree canopy height model from the study shows the heights interpolated for all points in the canopy as a 5 m pixel spaced grid size. Tree height is defined by (St-Onge, 2000) as the pixel having the highest value in a high valued pixel cluster that corresponds to a crown. With the Exception of large hardwood trees with the top pixel sometimes situated a few pixels away from the center but mostly at the center of individual tree crown are found the top pixel (St-Onge, 2000).

Statistical analysis (Linear regression) was performed between field measured heights and LiDAR CHM. The average of the two field height measured was regressed against the matching height read from the CHM for the 17 trees. The linear model yielded a strong correlation of R^2 of 0.931 (RMSE = 1.961, Figure 4.25 – 2.30)

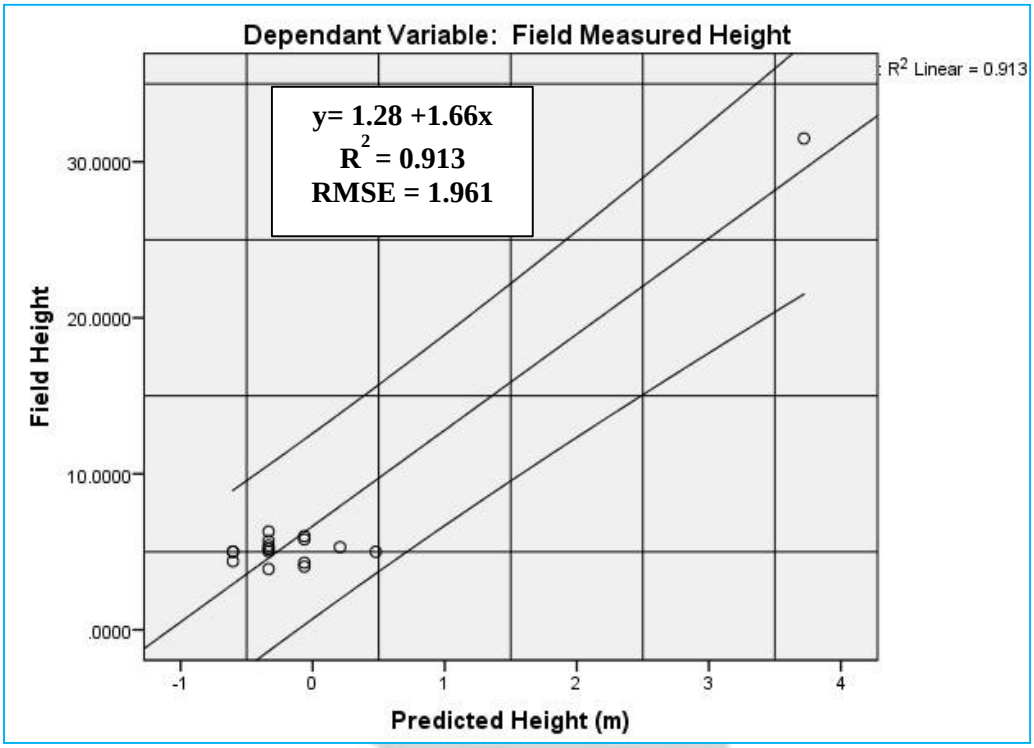

Figure 4. 25: Ground Thruthing and regression tree predicted top canopy height using LIDAR dataset. Field measured top canopy versus LIDAR estimate of the canopy height. The estimates of canopy height from LIDAR corresponds closely to the field estimate (RMSE = 1.96 m and R^2 = 0.913)

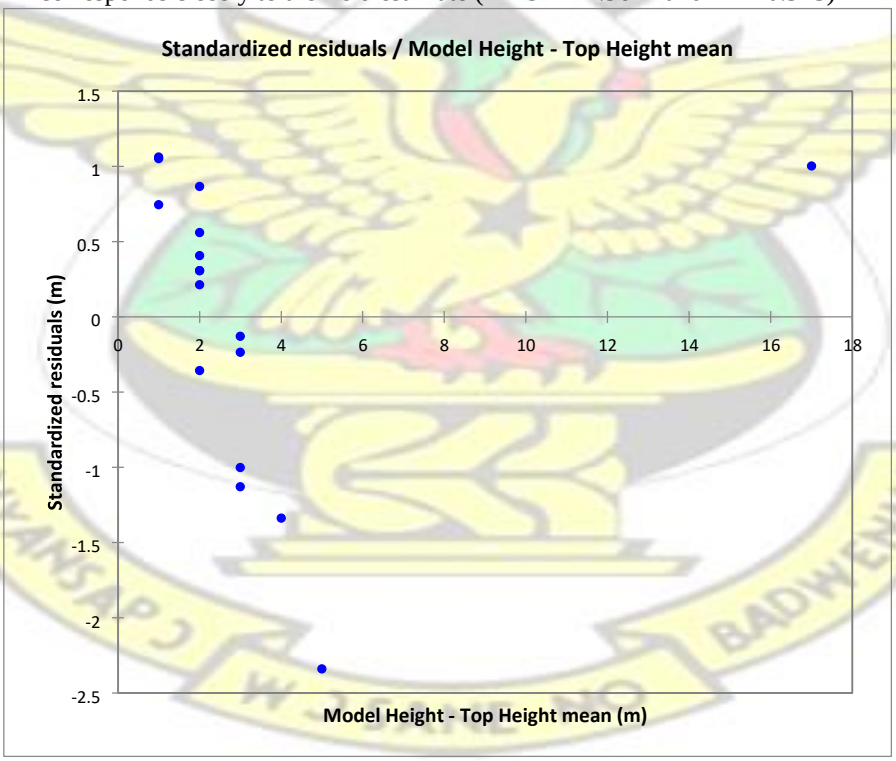

Figure 4. 26: Standardized Residual values of modelled height from LIDAR versus Modelled Height – Hop Height Mean

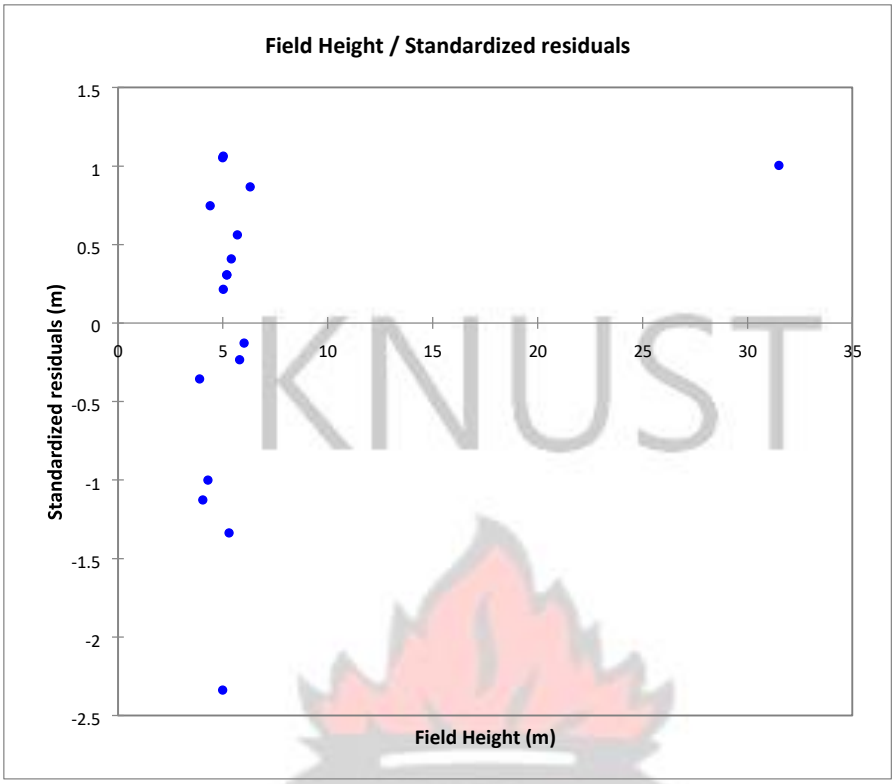

Figure 4. 27: Standardized residual values of field height versus Field measured height

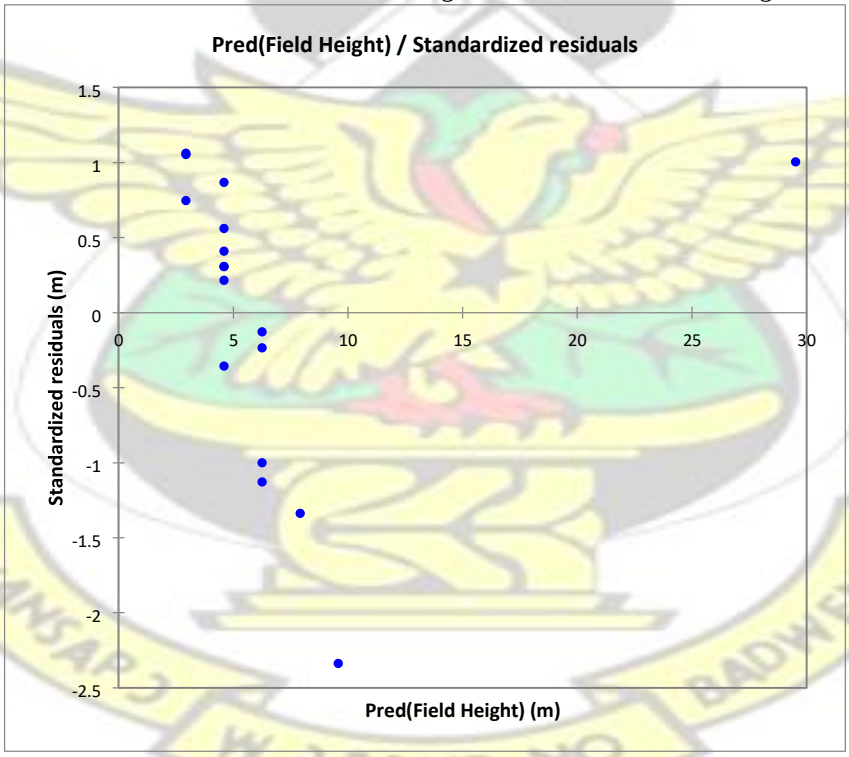

Figure 4. 28: Standardized residual values of predicted field height versus Regression tree predicted Field height

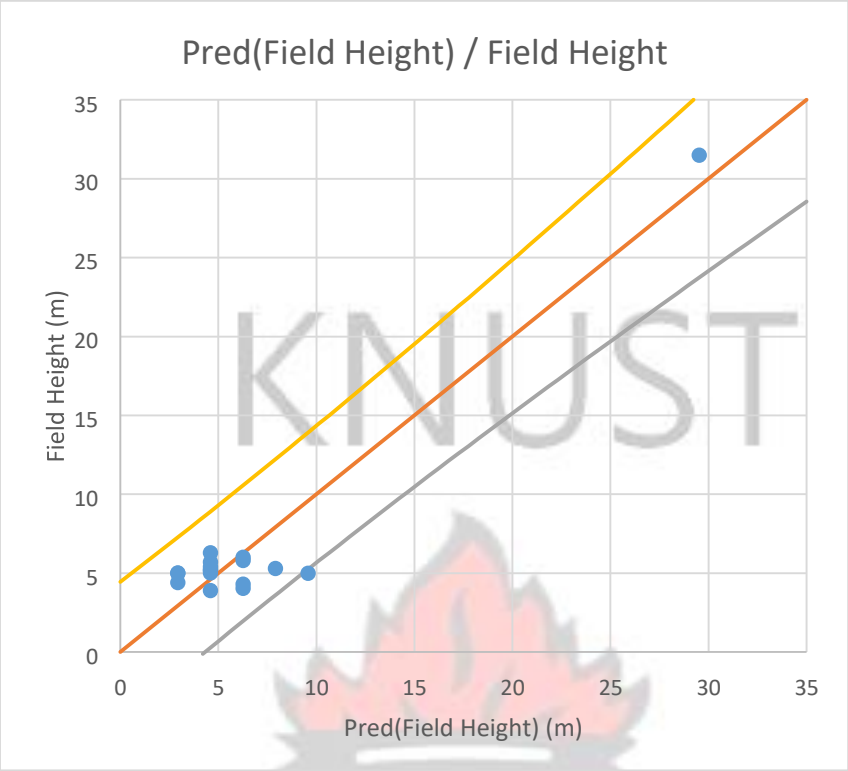

Figure 4. 29: Field Measured Canopy height versus Regression tree predicted top canopy height

Figure 4. 30: Field Observations versus standardized residuals of field observation height

4.3.2 Canopy Heights (CHM) at the Rehabilitated Sites

The definition of tree height adopted for the purpose of this study refers to the height of the tree apex (topmost point) above ground.

Summary of LIDAR grid metrics computations reveal a maximum average height of 17.3 m with an average canopy height of 11.59 m at block 2 & 3 waste rock dump rehabilitated site and a least maximum average height of 7.31 m with a mean height of 4.56m at Block 1 south waste rock dump rehabilitated site (Table 4.11 – 4.13).

Table 4.11: Summary of Average Gridmetrics output for the LIDAR data within the rehabilitated sites and the Control sites

Outlier: 2 : 60	**AVERAGE**				
Only first returns used for cover statistics	**Block 2/3**	**OTSF**	**Block 1 N**	**Block 1 S**	**Neung forest**

Density count total	111.43	69.03	67.75	46.85	92.81
Minimum height (m)	2.68	2.711	2.45	2.21	4.07
Maximum height (m)	17.30	10.99	10.45	7.31	26.45
Mean height (m)	11.59	7.35	6.58	4.56	17.88
Standard Deviation (m)	3.72	2.05	2.09	1.41	5.78
50^{th} height Percentile (m)	12.35	7.49	6.67	4.51	18.80
75^{th} height Percentile (m)	14.37	8.83	8.08	5.55	22.20
95^{th} height Percentile (m)	16.27	10.24	9.64	6.73	25.07
Coefficient of variations	0.32	0.28	0.32	0.30	0.34
Density (Cover above 3m height break %)	96.52	91.13	80.18	67.22	97.22
Age (years)	10	9	4	3	> 20

Table 4.12: Summary of Maximum Gridmetrics output for the LIDAR data within the rehabilitated sites and the Control

`Outlier: 2 : 60	**MAXIMUM**				
Only first returns used for cover statistics	**Block 2/3**	**OTSF**	**Block 1 N**	**Block 1 S**	**Neung forest**
Density count total	398	204	240	206	721
Minimum height	15.47	14.30	16.10	8.70	48.34
Maximum height	29.73	27.15	26.86	22.74	51.97
Mean height	21.91	19.77	20.24	16.66	49.67
Standard Deviation	9.08	9.99	8.48	6.31	24.07
50^{th} height Percentile	24.97	21.34	23.10	17.96	50.61
75^{th} height Percentile	26.94	33.14	24.13	20.04	51.61
95^{th} height Percentile	28.84	33.86	26.15	21.46	51.88
Coefficient of variations	0.89	1.037	1.19	0.81	1.91

Density (Cover above 3m height break)	100.00	100.00	100.00	100.00	100.00

Table 4.13: Summary of Minimum Height Gridmetrics output for the LIDAR data within the rehabilitated sites and the Control

Outlier: 2 : 60	**MINIMUM**				
Only first returns used for cover statistics	**Block 2/3**	**OTSF**	**Block 1 N**	**Block 1 S**	**Neung forest**
Density count total	4.00	4.00	4.00	4.00	4.00
Minimum height	2.00	2.00	2.00	2.00	2.00
Maximum height	2.90	2.11	2.32	2.16	2.06
Mean height	2.37	2.04	2.15	2.11	2.04
Standard Deviation	0.092	0.045	0.070	0.05	0.02
50^{th} height Percentile	2.22	2.03	2.09	2.04	2.02
75^{th} height Percentile	2.44	2.05	2.15	2.14	2.04
95^{th} height Percentile	2.71	2.10	2.31	2.15	2.06
Coefficient of variations	0.0114	0.015	0.013	0.023	0.0038
Density (Cover above 3m height break)	0.00	0.00	0.00	0.00	0.00

Generally low tree heights were recorded at Block 1 South rehabilitated site with 96 % of the tree heights below 9m (Figure 4.37 - 4.38) whilst high tree heights recorded at Block 2 & 3 especially towards the western portions of the site. Block 2 & 3 WRD is mainly dominated by Tree heights above 9 m, which represents about 80% of the total trees and below 9m representing 20% (Figure 4.31 - 4.32) compared with approximately 98% of total trees at Neung forest undisturbed site above 9m benchmark height (Figure 4.39 - 4.40)

The CHM derived reveals a similar patterns of tree height, from one CHM to another. A non-continuum spatial distribution of vegetation height is seen across the sites with clusters of high and low canopy heights at different vantage areas within the study sites.

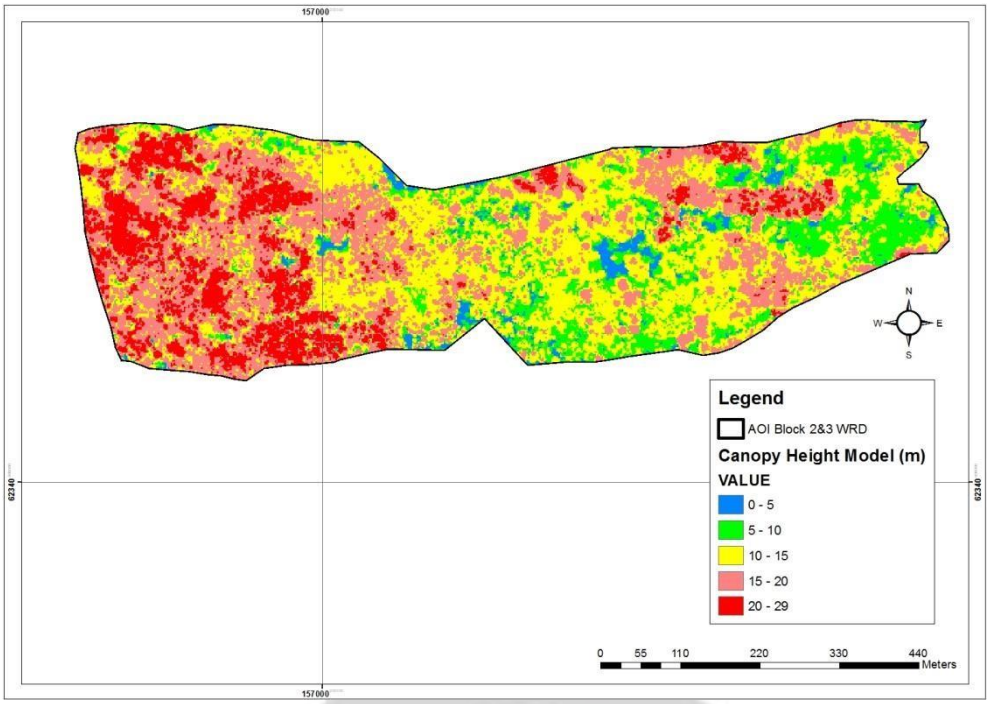

Figure 4. 31: Spatial Map of Tree Height estimated from LIDAR Dataset for Block 2&3 WRD Rehabilitated site

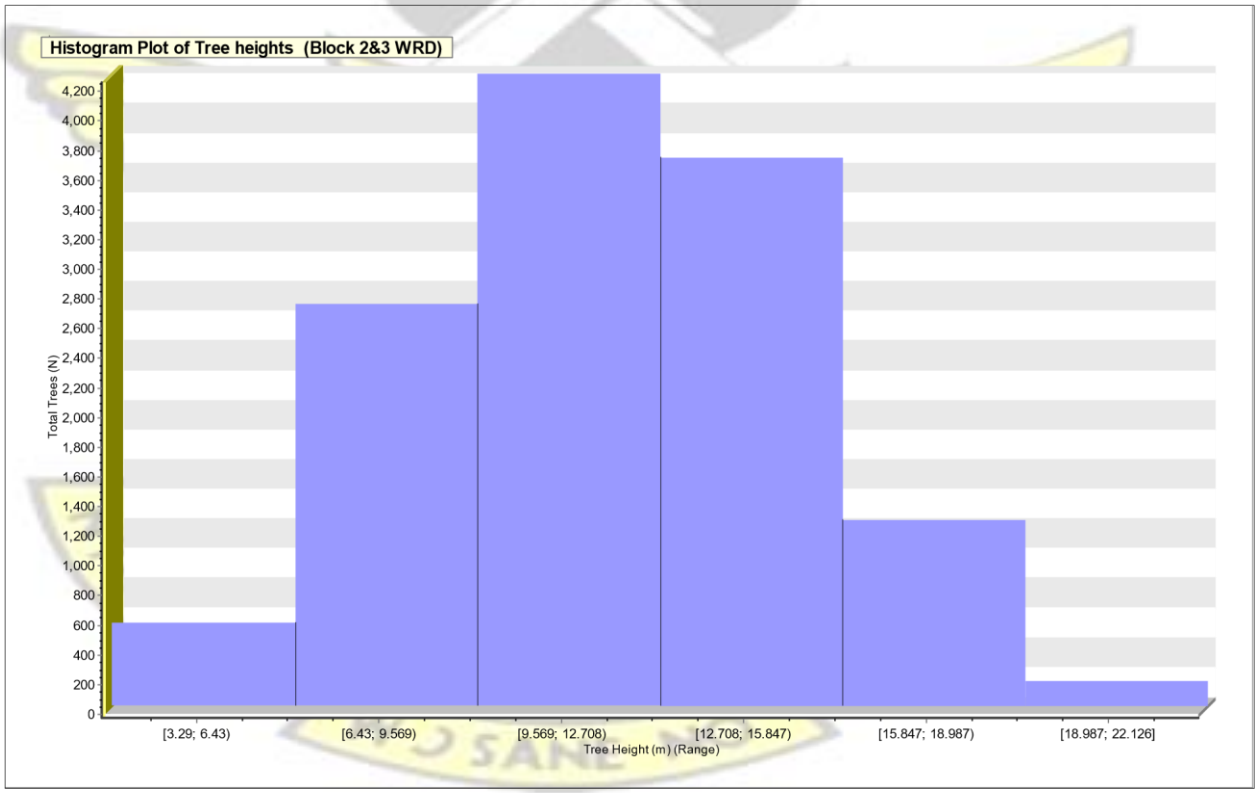

Figure 4.32: Histogram Plot showing Dominant Range of Tree Height and Total Number of Trees for a given Range at Block 2 & 3 WRD Rehabilitated Site

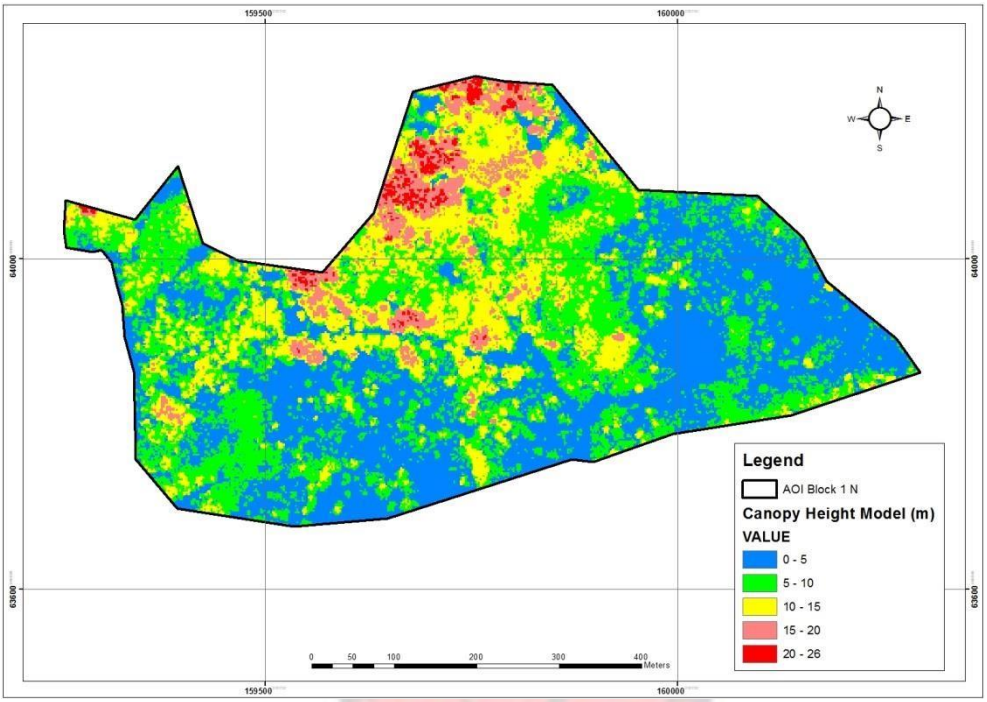

Figure 4.33: Spatial Map of Tree Height estimated from LIDAR Dataset for Block 1 North Rehabilitated site

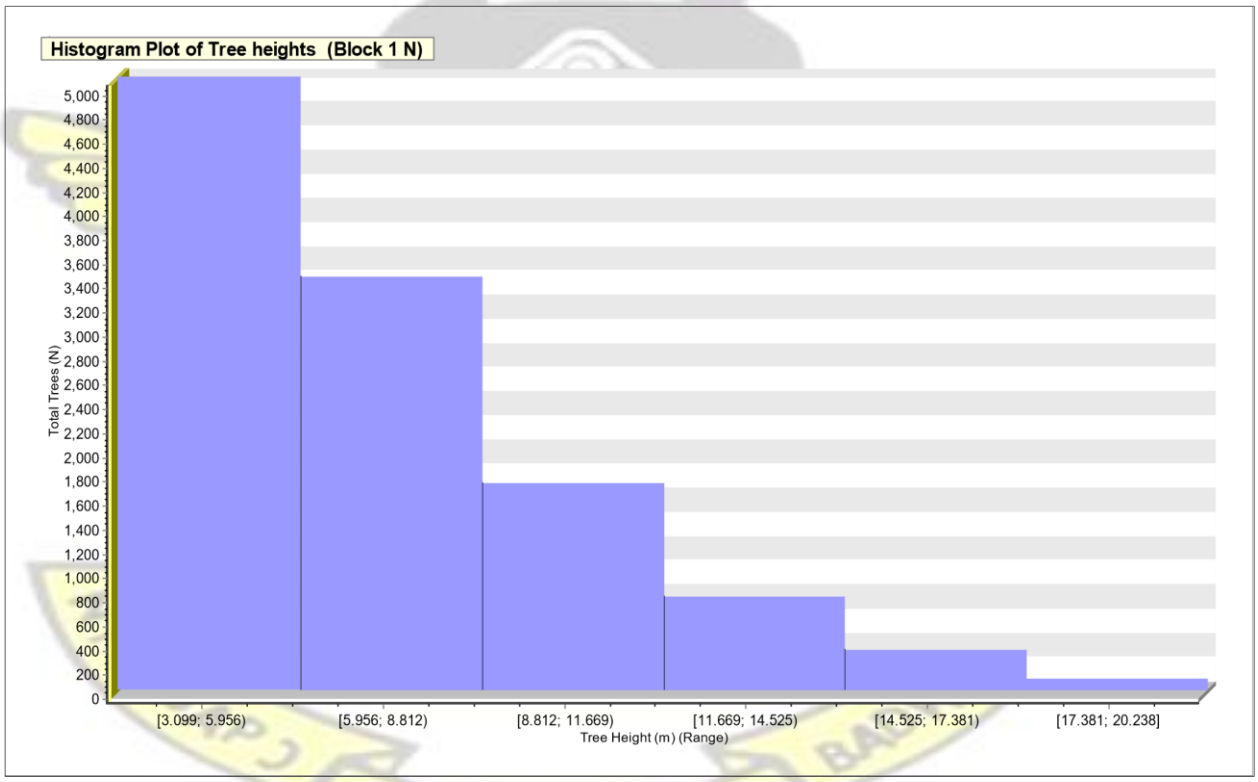

Figure 4.34: Histogram Plot showing Dominant Range of Tree Height and Total Number of Trees for a given Range at Block 1 North WRD

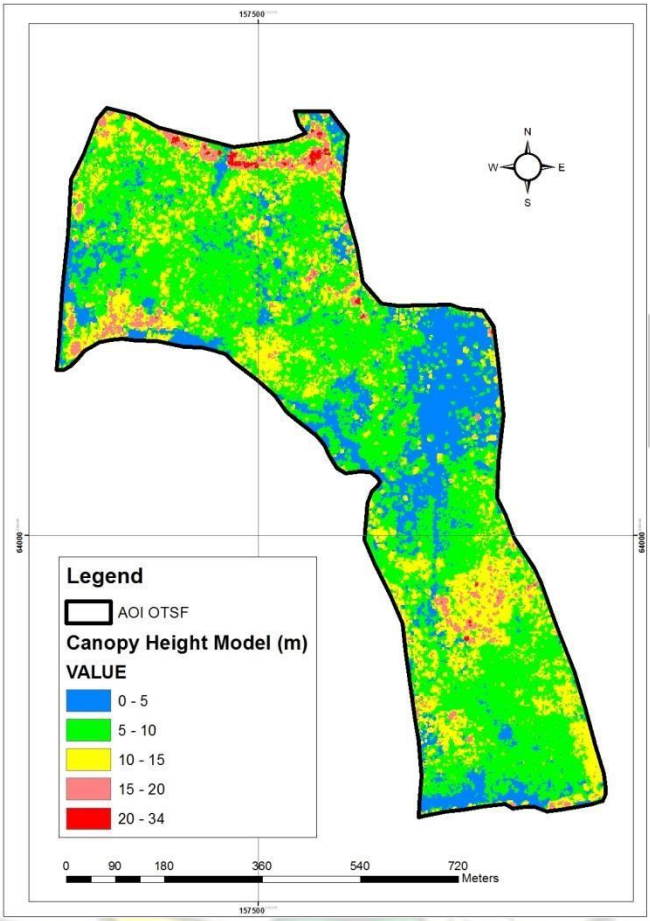

Figure 4.35: Spatial Map of Tree Height estimated from LIDAR Dataset for Old TSF Rehabilitated site

Analysis of tree heights at Old TSF rehabilitated site reveals that more than 60% of trees present are below 9m in height with majority of the trees falling between the ranges of 4m – 8 m, representing 50% (Figure 4.35 – 4.36)

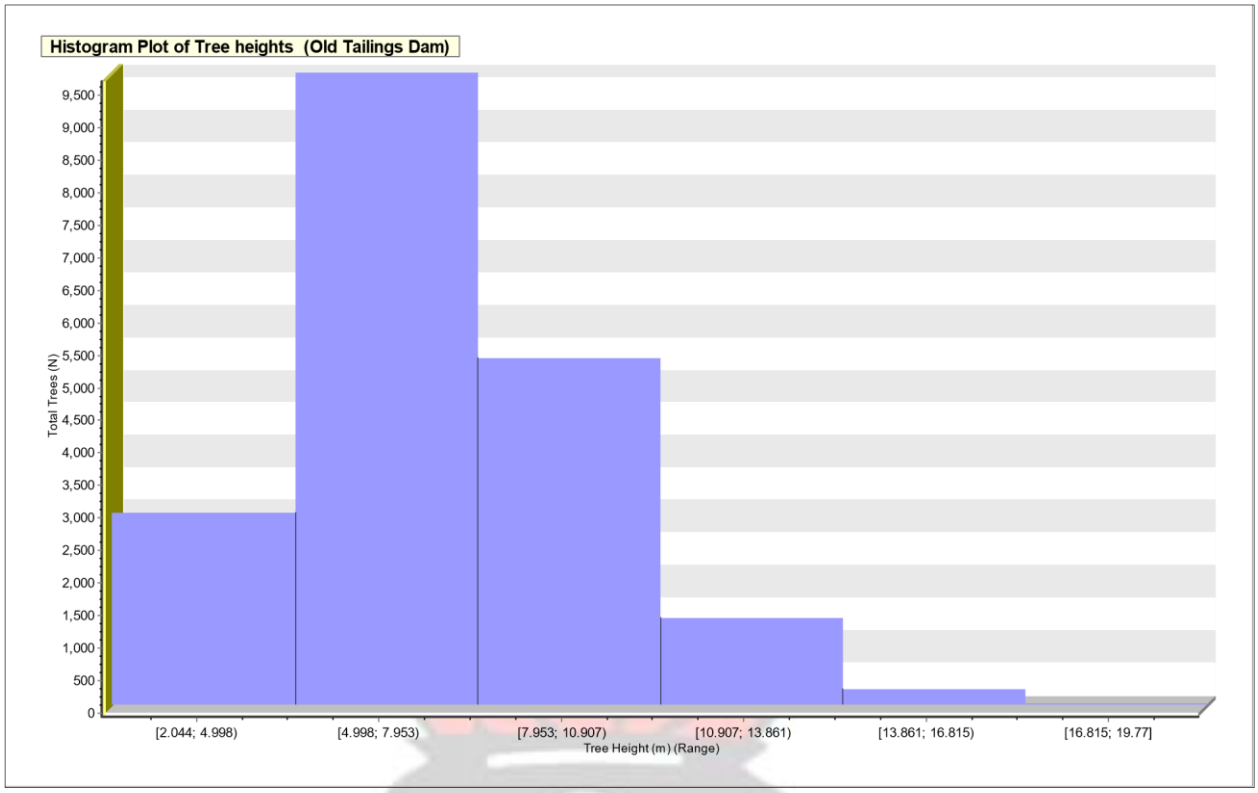

Figure 4. 36: Histogram Plot showing Dominant Range of Tree Height and Total Number of Trees for a given Range at Old TSF

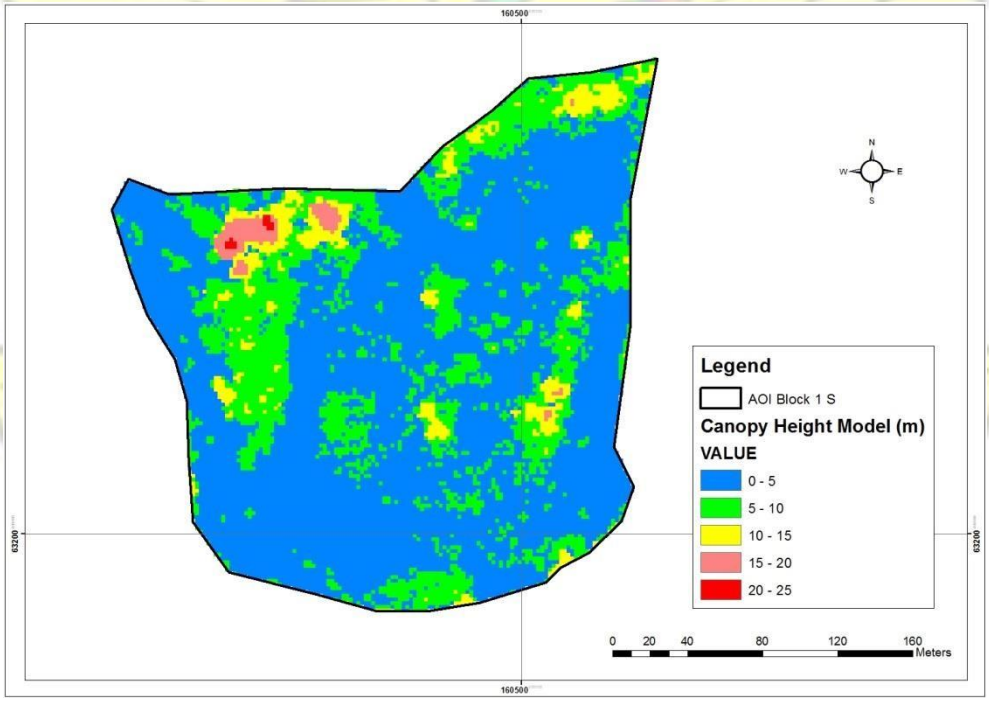

Figure 4.37: Spatial Map of Tree Height estimated from LIDAR Dataset for Block 1 South Rehabilitated site

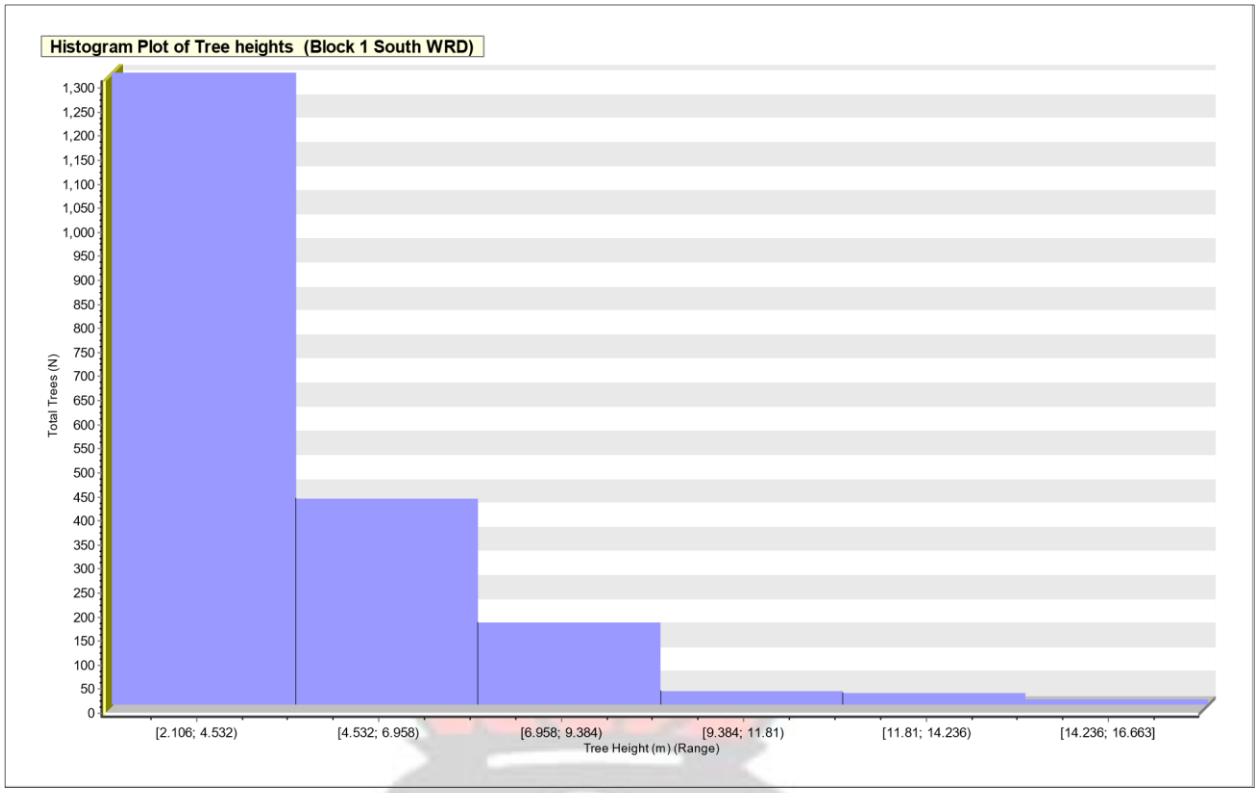

Figure 4.38: Histogram Plot showing Dominant Range of Tree Height and Total Number of Trees for a given Range at Block 1 South WRD

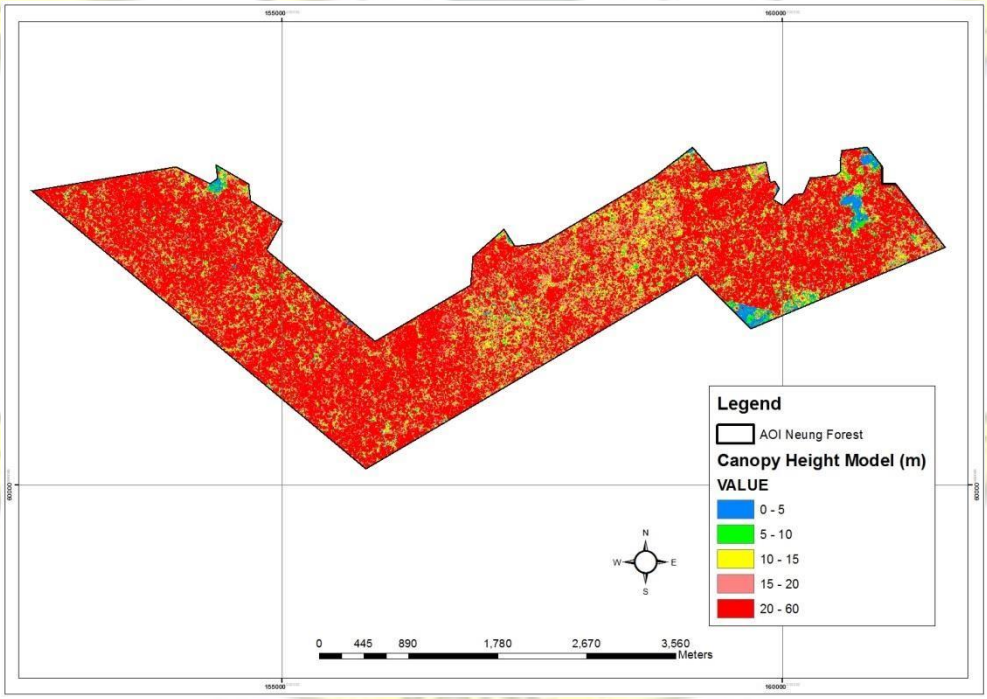

Figure 4.39: Spatial Map of Tree Height estimated from LIDAR Dataset for Control Undisturbed Neung Forest Reserve

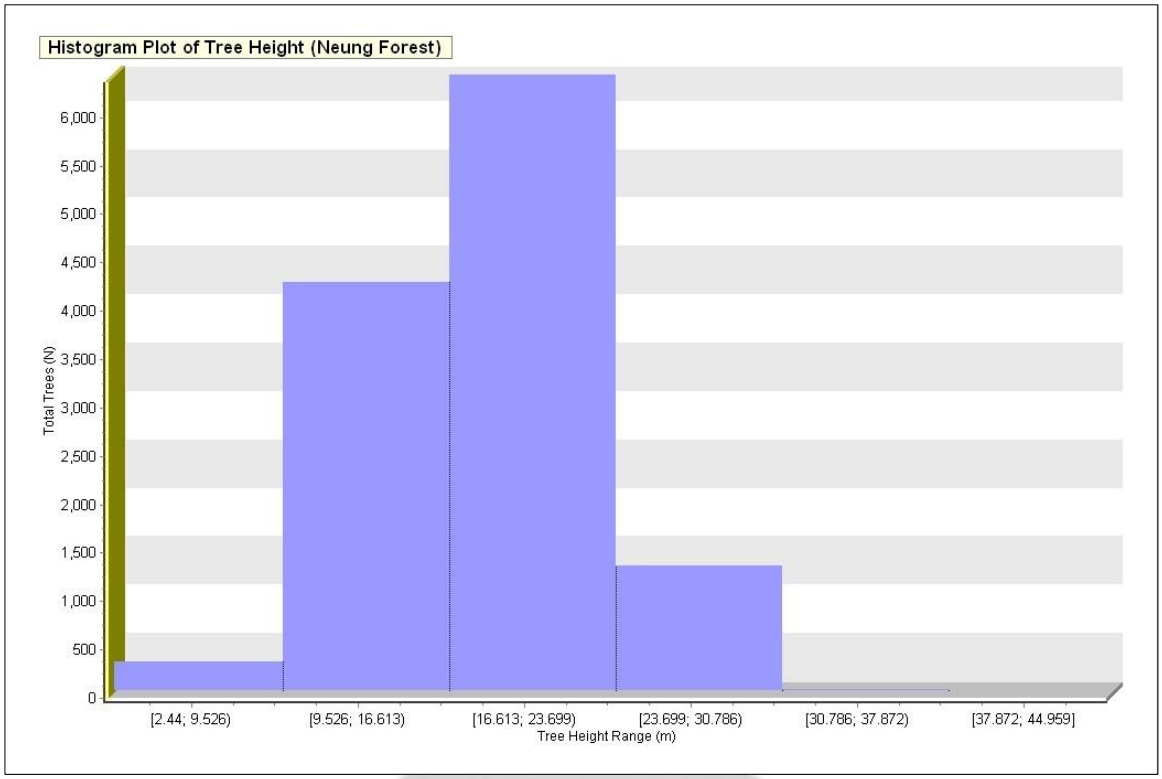

Figure 4. 40: Histogram Plot of Tree height at Neung Forest undisturbed site

4.3.3 Estimate of Canopy Closure of the Rehabilitated Sites

A 3m cover cutoff threshold was adopted for the study areas since they are dominated by relatively taller trees.

The density count total and standard deviations (Table 4.11) suggest a more vertical structure detected at Block 2 & 3 waste rock dump rehabilitated site as well as a denser canopy cover of 96.52% (Figure 4.41) than all the other rehabilitated sites and also comparable to the control site (Neung forest) with 97.22 (Figure 4.43).

Old tailing dam rehabilitated site depicted a dense canopy of 91.13% (Figure 4.43) slightly below that of block 2 & 3 rehabilitated site even though they are close in terms of age and this can be attributed to vegetation clearance for trial plot establishment at some portions of the study area. From the Canopy Cover Model derived from LIDAR, most of the areas particularly the Middle East portions that recorded between 0-20% cover was the trial plot mainly covered by cocoa and oil palm seedlings (Appendix 6).

Block 1 south waste rock dump showed a lower percentage canopy cover of 67.2 % (Figure 4.44) comparing with the other sites which can be explained by the age of the rehabilitation at the time of LIDAR survey. Rehabilitation of Block 1 south was preceded by that of Block 1 N and this explains why canopy cover 80.18% (Figure 4.42) recorded at the later site.

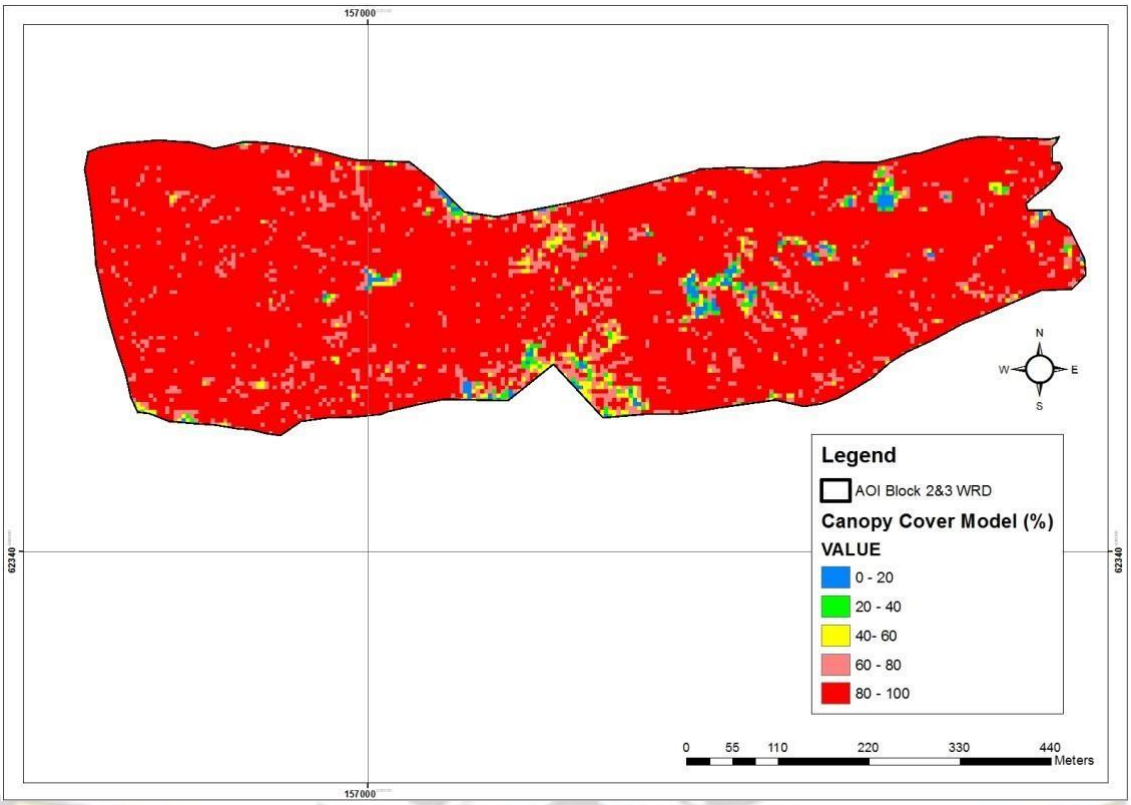

Figure 4.41: LIDAR Derived Percentage Canopy Cover Estimate for Block 2 & 3 Rehabilitated site

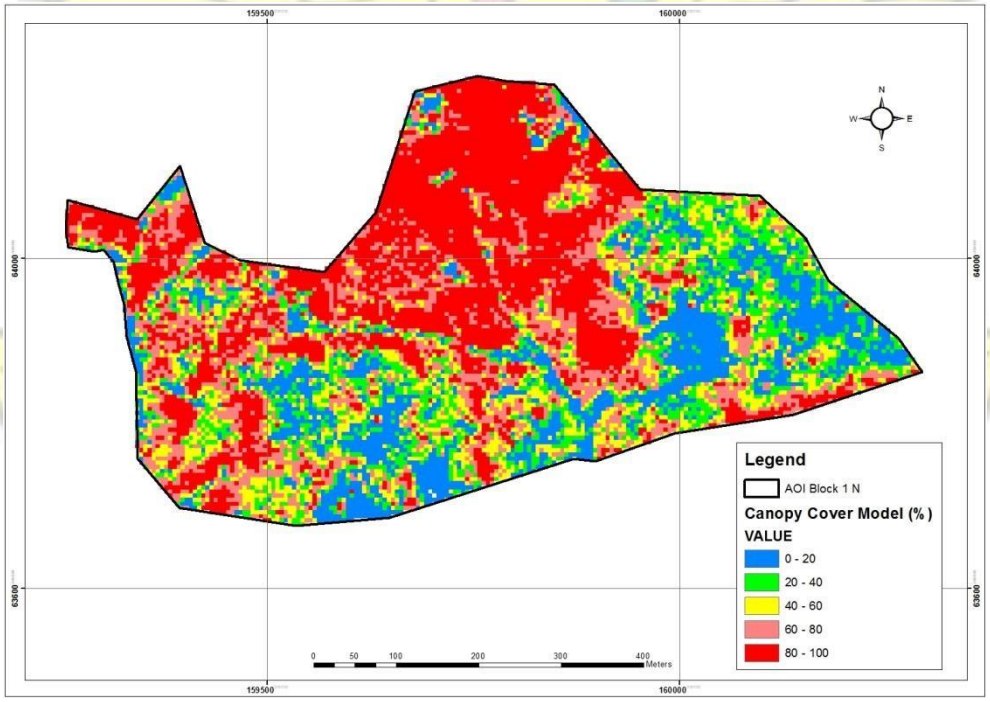

Figure 4.42: LIDAR Derived Percentage Canopy Cover Estimate for Block 1 North Rehabilitated site

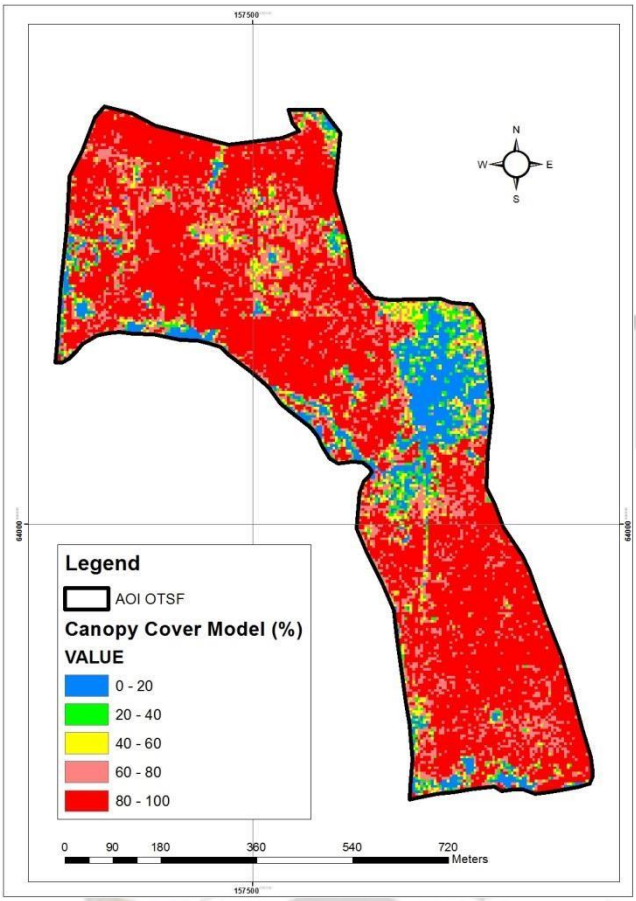

Figure 4. 43: LIDAR Derived Percentage Canopy Cover Estimate for Old TSF Rehabilitated site

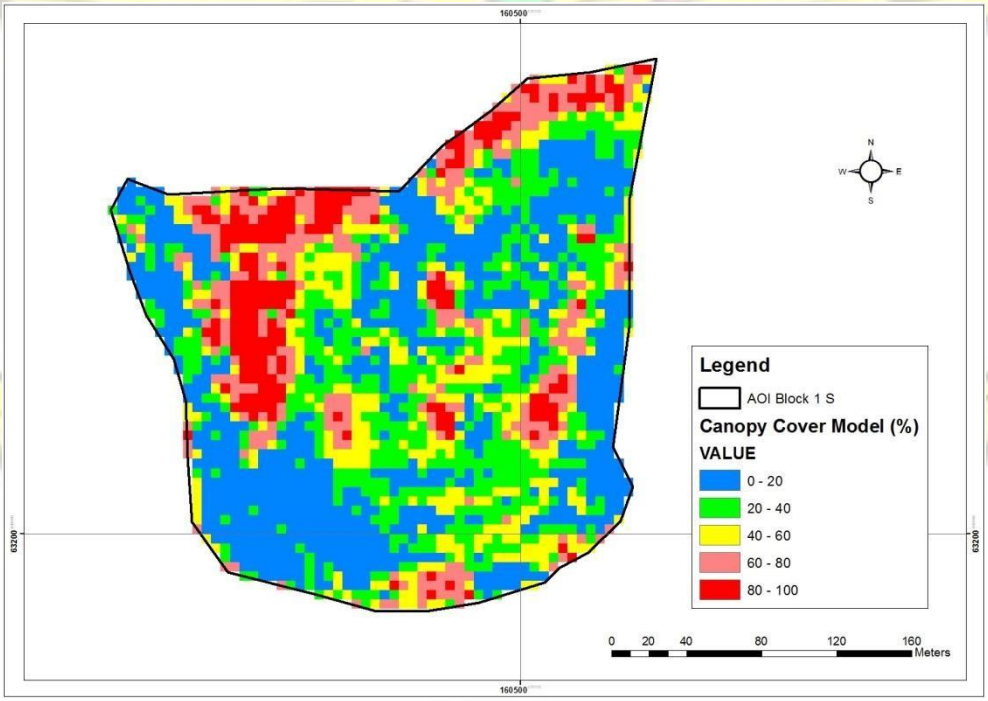

Figure 4. 44: LIDAR Derived Percentage Canopy Cover Estimate for Block 1 south Rehabilitated site

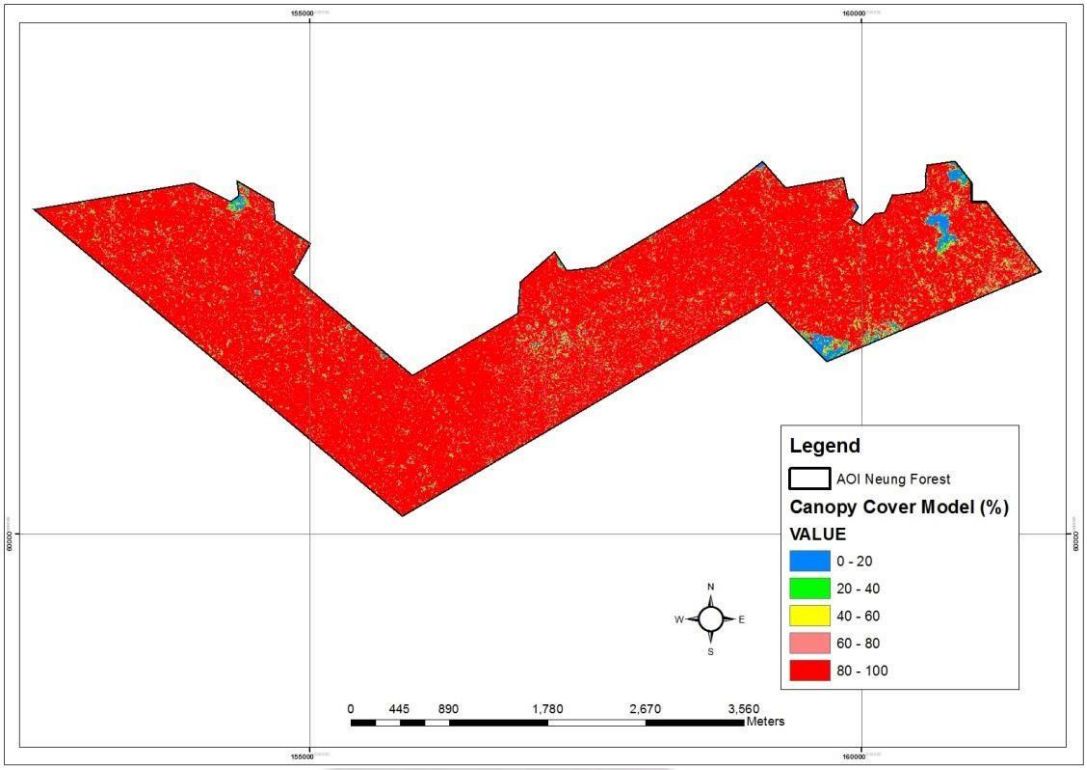

Figure 4.45: LIDAR Derived Percentage Canopy Cover Estimate for Control Undisturbed Neung Forest Reserve

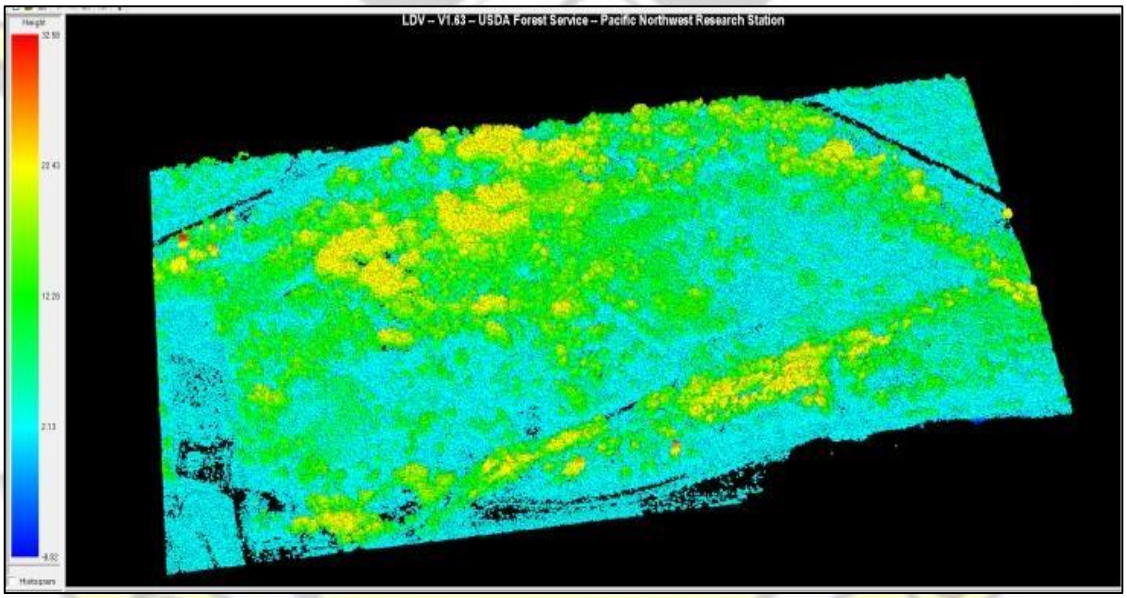

Figure 4.46: Block 1 North 3D Plotting of LIDAR point cloud data Normalized with ground returns to display canopy heights in LiDAR Data Viewer LDV in Fusion Software

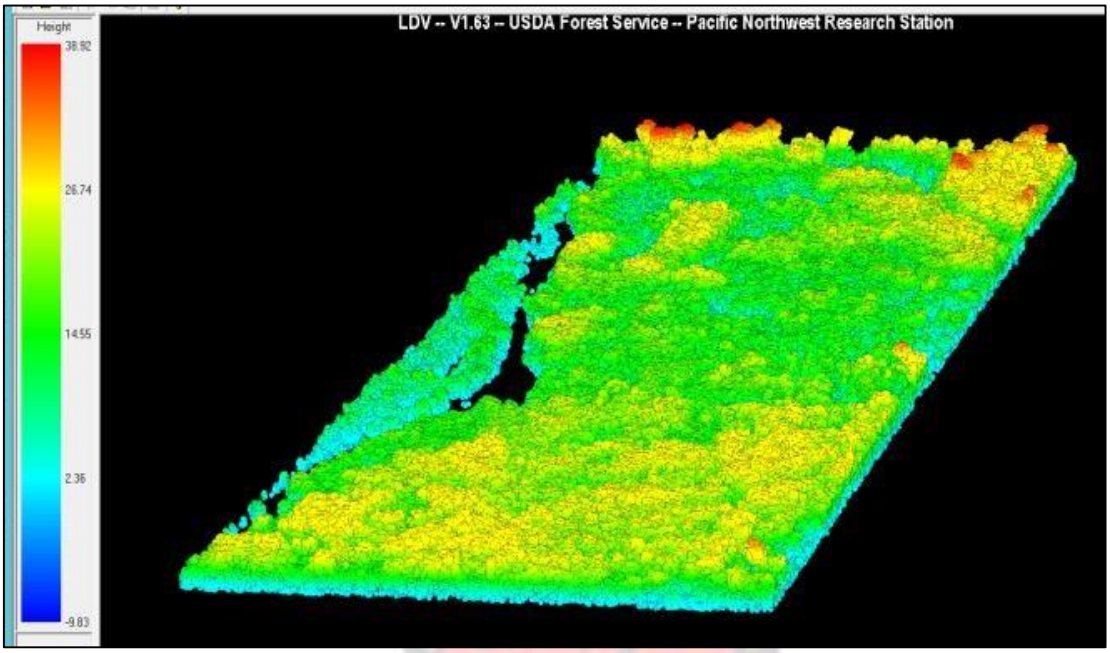

Figure 4.47: 3D Plotting of Block 2 & 3 LIDAR point cloud data Normalized with ground returns to display canopy heights in LiDAR Data Viewer (LDV) in Fusion Software

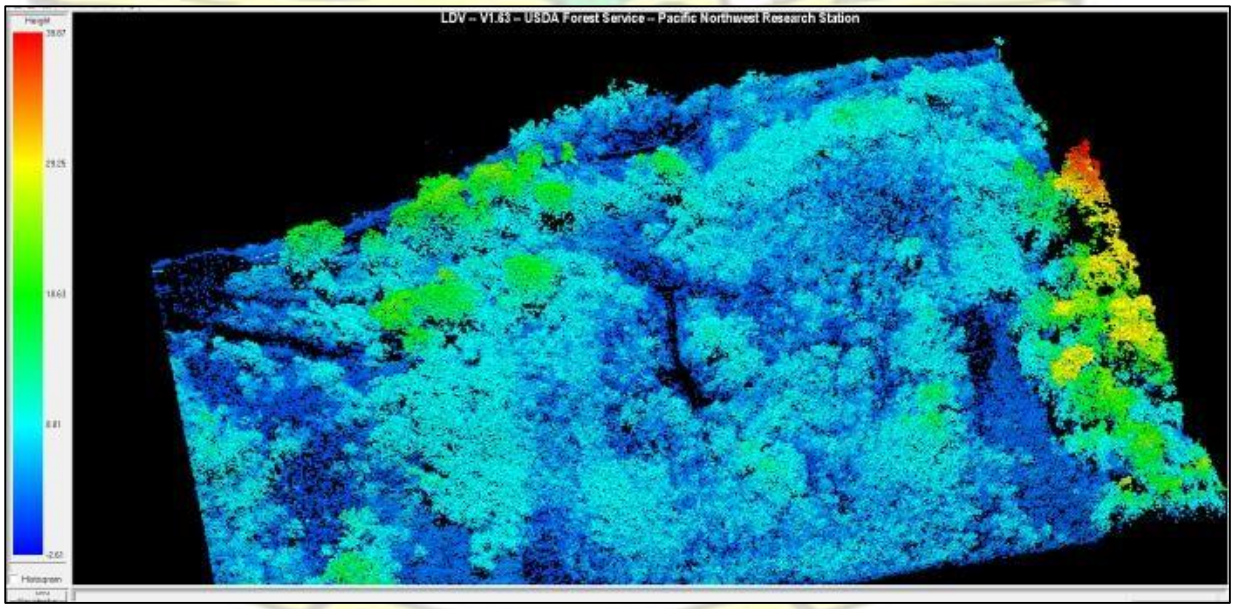

Figure 4.48: 3D Plotting of Block 1 South LIDAR point cloud data Normalized with ground returns to display canopy heights in LiDAR Data Viewer (LDV) in Fusion Software

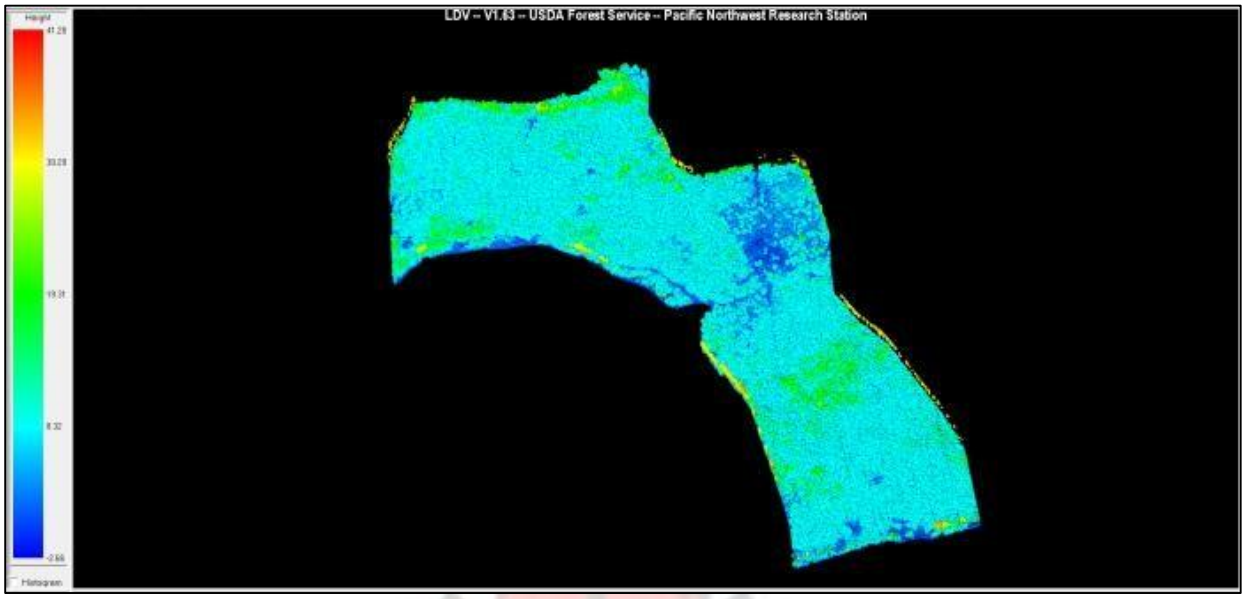

Figure 4.49: 3D Plotting of Old TSF LIDAR point cloud data Normalized with ground returns to display canopy heights in LiDAR Data Viewer (LDV) in Fusion Software

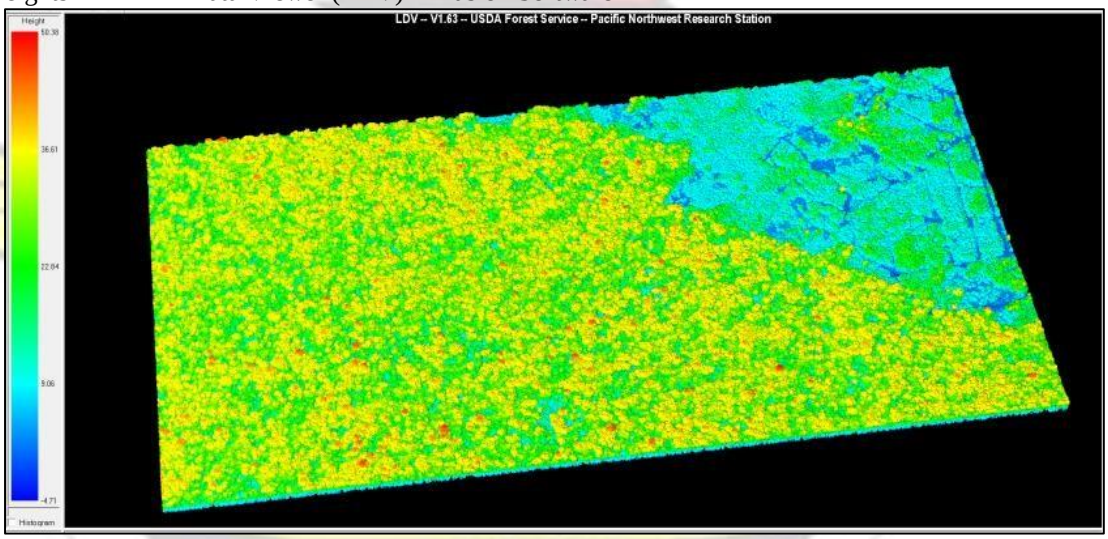

Figure 4.50: 3D Plotting of Neung Forest point cloud data Normalized with ground returns to display canopy heights in LiDAR Data Viewer (LDV) in Fusion Software

CHAPTER FIVE CONCLUSION AND RECOMMENDATION

5.1 Conclusions

Landsat Multi – spectral remote sensing data has been used to identify the pre-mining land cover of the study area and other land cover parameters measured and compared with after mining conditions of the land units, and finally a comparative assessments conducted with the conditions of the study area after reclamation has taken place in 2014. Results from the study in general reveals that the reclaimed sites have regained its initial land cover after significant impacts due to intensive mining activities in the year 2000 that affected the pre-mining land cover type.

The utility and effectiveness of LIDAR has been demonstrated in reclamation monitoring, the technology was applied in the assessment and monitoring of reclaimed disturbed mine-lands at the AngloGold Ashanti Iduapriem mine in the Tarkwa area of the Western Region of Ghana

Reclamation forest structural attributes such as tree canopy height and percentage cover of reclaimed disturbed lands within AngloGold Ashanti Iduapriem mine were estimated with dataset derived from Light detection and ranging (LIDAR) technology. Field tree measurement were undertaken to validate the LIDAR derived canopy heights. Stepwise regression analysis performed on field measured height and LIDAR derived height showed a strong correlation of $R^2 = 0.913$. The findings of this research thus support the research outcome of Wulder and Seeman (2003) that field measurements of tree height compares well with that obtained from LIDAR.

The research findings further support the fact that AAIL has made substantial progress in the implementation of concurrent reclamation projects within the catchment areas of the mine. However, it is hoped that the company will continue to adopt feasible strategies on sustainable environmental management practices towards improving the monitoring and management of reclaimed lands.

5.2 Recommendations

Further to the above, research to model other biophysical attributes of the reclaimed forest must be conducted to understand other forest variables such as Leave area index (LAI) (a key requirement in the reclamation security agreement between the mine and

EPA), Biomass, Gross stem volume, Basal area and the likes of the reclaimed mined out lands within the catchment areas of the mine.

Furthermore LiDAR heights derived for the study were generally low compared with field measured heights. St-Onge, 2000, studies revealed that height value of individual trees are generally lower in a LIDAR CHM than it is in actuality because the tree top, especially of a softwood tree, is quite narrow, and for this reason may be missed by LIDAR hits, and as a result truncating the tree top. It is therefore recommended in subsequent studies to develop and apply a correction equation for such phenomenon.

REFERENCES

Akabzaa, T., & Darimani, A. (2001). Impact of Mining Sector Investment in Ghana: A Study of the Tarkwa Mining Region", Draft Report Prepared for SAPRI.

Aryee, B.N.A., Ntibery, B.K. and Atorkui, E. (2003) ―Trends in the Small-scale Mining of precious minerals in Ghana: A perspective on its environmental impact‖. Journal of Cleaner production.

Balkau, F., (1993). Environmental Auditing at Mines. Technical paper, United Nations Environment Programme, Paris.

Barnhisel, R. I., Darmody, R. G., Daniels, W. L., Bartels, J., Hatfield, J. L., Volenec, J. G., & Dick, W. A. (2000). Reclamation of drastically disturbed lands. American Society of Agronomy.

Bradshaw A.D. (1996). Restoration of mined lands—using natural processes Department of Environmental and Evolutionary Biology, University of Liverpool

Bradshaw, A.D., (1992). The biology of land restoration. In: Jain, S.K., Botsford, L.W. (Eds.), Applied Population Biology. Kluwer, Dordrecht, pp. 25–44.

Chander, G., Markham, B.L. and Helder, D.L., 2009. Summary of current radiometric calibration coefficients for Landsat MSS, TM, ETM+, and EO-1 ALI sensors. Remote sensing of environment, 113(5), pp.893-903.

Chen, L., Chiang, T. and Teo, T., 2005, November. Fusion of LIDAR data and high resolution images for forest canopy modelling. In Proc. 26th Asian Conf. on Remote Sensing.

DeFries, R. and Townshend, J. 1994. NDVI-derived land cover classifications at a global scale. International Journal of Remote Sensing, 15(17), 3567-3586.

Deyong, Y., Hongbo, S., Peijun, S., Wenquan, Z., Yaozhong, P. 2009. How does the conversion of land cover to urban use affect net primary productivity? A case study in Shenzhen city, China. Agricultural and Forest Meteorology, 149: 2054–2060.

Diouf, A. and Lambin, E. 2001. Monitoring land-cover changes in semi-arid regions: remote sensing data and field observations in the Ferlo, Senegal. Journal of Arid Environments, 48(2), 129- 148

Friedl, M. A., et al. 2002. Global land cover mapping from MODIS: algorithms and early results. Remote Sensing of Environment, 83(1), 287-302.

Goodwin, N., N.C. Coops and D.S. Culvenor. (2006). Assessment of forest structure with airborne LIDAR and the effects of platform altitude. Remote Sensing of Environment 103: 140–152

Gordon, S., 2010. LIDAR Analysis in ArcGIS® 9.3.1 for Forestry Applications, Esri Australia Pty. Ltd., Adelaide, South Australia

Guyot, G.. and Gu X., 1994, Effect of radiometric corrections on NDVI-determined from SPOT-HRV and LandsatTM data. Remote Sensing of Environment, 49, 169-180.

Gyimah B. (2004). Resolution of economic controversy in mining (2-6 July Edition of Daily Graphic).

Hansa Luftbild Group, 2011. Laser Scanning Solutions for Planning and Terrain Management, Hansa Lufbild German Air Surveys

Hansen, M., et al. 2000. Global land cover classification at 1 km spatial resolution using a classification tree approach. International Journal of Remote Sensing, 21(6-7), 1331-1364

Hemery G. (2011), "How to calculate tree height using a smartphone", https://gabrielhemery.com/2011/05/15/how-to-calculate-tree-height-using-asmartphone/, Accessed: May 15, 2011.

Horion, S., *et al.* 2014. Using earth observation-based dry season NDVI trends for assessment of changes in tree cover in the Sahel. *International Journal of Remote Sensing*, 35(7), 2493-2515.

Huete, A.R., 1988. A soil-adjusted vegetation index (SAVI). Remote sensing of environment, 25(3), pp.295-309.

Jacquin, A., Sheeren, D. and Lacombe, J.-P. 2010. Vegetation cover degradation assessment in Madagascar savanna based on trend analysis of MODIS NDVI time series. International Journal of Applied Earth Observation and Geoinformation, 12, S3-S10.

Jensen, J., 2007. Remote Sensing of the Environment. Pearson Prentice Hall

Laes, D., S. Reutebuch, B. McGaughey, P. Maus, T. Mellin, C. Wilcox, J. Anhold, M. Finco, and K. Brewer, 2008. Practical Lidar Acquisition Considerations for Forestry Applications, RSAC-0111-BRIEF1, Salt Lake City, Utah, U.S. Department of Agriculture, Forest Service, Remote Sensing Applications Center, 7 p.

Lambin, E. F. and Ehrlich, D. 1997. Land-cover changes in sub-Saharan Africa (1982–1991): Application of a change index based on remotely sensed surface temperature and vegetation indices at a continental scale. Remote Sensing of Environment, 61(2), 181-200.

Lewis, P. and Hancock, S., 2007. LiDAR for vegetation applications. UCL, Gower St, London, UK.

Liang, S., 2005. Quantitative remote sensing of land surfaces. John Wiley & Sons

Lillesand, T. M., Kiefer, R. W. and Chipman, J. W. (2004, 5th ed.) Remote Sensing and Image Interpretation, John Wiley, New York

Lunetta, R. S., Knighta, J. F., Ediriwickremab, J., Lyonc, J.G., and Worthy, L. D.. 2006. Land-cover change detection using multi-temporal MODIS NDVI data. Remote Sensing of Environment, 105(2): 142-154

Magnussen S. and P. Boudewyn. 1998. Derivations of stand heights from airborne laser scanner data with canopy-based quantile estimators. Canadian Journal of Forest Research. 28: 1016–1031.

Magnussen, S., P. Eggermont and V.N. LaRiccia. (1999). Recovering tree heights from airborne laser scanner data. Forest Science 45: 407–422.

Manandhar, R., Odeh, I.O. and Ancev, T., 2009. Improving the accuracy of land use and land cover classification of Landsat data using post-classification enhancement. *Remote Sensing*, *1*(3).

Markus, J. J. (1997). Mining Environmental Handbook: Effects of Mining on the Environment and American Environmental Controls on Mining. Imperial Collage Press.

Martínez B. and Gilabert M. A. 2009. Vegetation dynamics from NDVI time series analysis using the wavelet transform. Remote Sensing of Environment, 113: 1823–1842.

Mas, J.-F. 1999. Monitoring land-cover changes: a comparison of change detection techniques. International Journal of Remote Sensing, 20(1), 139-152.

Mborah, C., Bansah, K. J., & Boateng, M. K. (2015). Evaluating Alternate PostMining Land-Uses: A Review. Environment and Pollution, 5(1), 14.

McCallum K., Beaty M. & Mitchell B. (2014), First Order LIDAR Metrics: A supporting document for LIDAR deliverables, RedCastle Resources Inc., Remote Sensing Applications Center (RSAC), Salt Lake City, Utah.

McGaughey, R. 2013. FUSION/LDV: software for LIDAR data analysis and visualization. Version 3.41. Seattle, WA: U.S. Department of Agriculture, Forest Service, Pacific Northwest Research Station [online]. Available http://forsys.cfr.washington.edu/fusion/fusionlatest.html.

Miller, G.C., Lyons, W.B and Davis, A. (1996). Understanding of water quality of pit lakes. Environmental Science Technical Paper, 30: 105-125 A.

Montrie Chad (2003). To Save the Land and People: A History of Opposition to Surface Coal Mining in Appalachia. United States: The University of North Carolina Press. pp. 17.).

Mustapha, A. (2013). Assessment of Rehabilitated Surface Mine Lands In AngloGold Ashanti, Obuasi, Kwame Nkrumah University of Science and Technology, Kumasi, Ghana

Obiri, S., Dodoo, D.K, Okai-Sam, F, Essumang, DK and Adjorlolo-Gasokpoh, A. (2006). Cancer and non-cancer health risk from eating cassava grown in some mining communities in Ghana. Environ Monit Assess 118: 37-49.

Pettorelli, N., Vik, J. O. , Mysterud, A., Gaillard, J., Tucker, C. J. , and Stenseth, N. 2005. Using the satellite-derived NDVI to assess ecological responses to environmental change. TRENDS in Ecology and Evolution.

Pichtel, J. R., Dick, W. A., & Sutton, P. (1994). Comparison of amendments and management practices for long-term reclamation of abandoned mine lands. Journal of Environmental Quality, 23(4), 766-772.

Rosette J., Suárez J., Nelson R., Los S., Cook B. and North P (2012). LIDAR Remote Sensing for Biomass Assessment, Remote Sensing of Biomass - Principles and Applications, Dr. Lola Fatoyinbo (Ed.), ISBN: 978-953-51-0313-4, InTech,

Available from: http://www.intechopen.com/books/remotesensing-ofbiomass-principles-and-applications/LIDAR-remote-sensing-for-biomassassessment

Shalaby, A. and Tateishi, R. 2007. Remote sensing and GIS for mapping and monitoring land cover and land-use changes in the Northwestern coastal zone of Egypt. *Applied Geography*, 27(1), 28-41.

Sheoran, V., Sheoran, A. S., & Poonia, P. (2010). Soil reclamation of abandoned mine land by revegetation: a review. International Journal of Soil, Sediment and Water, 3(2), 13.

Sopper, W. E. (1992). Reclamation of mine land using municipal sludge. InSoil Restoration (pp. 351-431). Springer New York.

St-Onge, B., & Achaichia, N. (2000). Measuring Forest Canopy Height Using a Combination of LiDAR and Aerial Photography Data. Department of Geography, Université du Québec à Montréal, Canada.

Stow, D. A., et al. 2004. Remote sensing of vegetation and land-cover change in Arctic Tundra Ecosystems. Remote Sensing of Environment, 89(3), 281-308.

Tetteh, E.N. (2010). Evaluation of land Reclamation practices at AngloGold Ashanti; Iduapriem Mines Ltd, Tarkwa. MSc Thesis. Kwame Nkrumah University of Science and Technology, Kumasi. P 19-44, 78-84,

Tsou, Ming-Hsiang, and Ken Yanow. "Enhancing general education with geographic information science and spatial literacy." URISA Journal 22.2 (2010): 45.

Turner, B. L. and Meyer, W. B. 1994. Global land-use and land-cover change: an overview. Changes in land use and land cover: a global perspective, 4(3).

Veldkamp, A. and Lambin, E. F. 2001. Predicting land-use change. Agriculture, Ecosystems & Environment, 85(1), 1-6.

Wang, J, Price, K.P. and Rich, P.M. 2001. Spatial patterns of NDVI in response to precipitation and temperature in the central Great Plains. Int. J. Remote Sensing, 22(18): 3827–3844.

Wes B., and. Leslie B., (2006). Geospatial Technology Tools for Wildlife Management, Volume 6, Issue 4

Woodcock, C. E., Allen, A. A., Anderson, M., Belward, A. S., Bindschadler, R., Cohen, W. B., Gao, F., Goward, S. N., Helder, D., Helmer, E., Nemani, R., Oreapoulos, L., Schott, J., Thenkabail, P. S., Vermote, E. F., Vogelmann, J.,Wulder,M. A., &Wynne, R. (2008). Free access to Landsat imagery. Science, 320, 1011.

Wulder M. A., Christopher W. B., Coops N. C., Hilker T. & White J. C., (2012) The role of LIDAR in sustainable forest management, Canadian Forest Service (Pacific Forestry Centre), Department of Forest Resources Management

Wulder, M.A. and D. Seemann. (2003). Forest inventory height update through the integration of LIDAR data with segmented Landsat imagery. Canadian Journal of Remote Sensing 29: 536–543.

Xu, D. and Guo, X., 2014. Compare NDVI extracted from Landsat 8 imagery with that from Landsat 7 imagery. American Journal of Remote Sensing,2(2), pp.10-14.

Yengoh, G.T., Dent, D., Olsson, L., Tengberg, A. and Tucker, C., 2014. The use of the Normalized Difference Vegetation Index (NDVI) to assess land degradation at multiple scales: a review of the current status, future trends and practical considerations. Lund University Center for Sustainability Studies (LUCSUS), and the Scientific and Technical Advisory Panel of the Global Environment Facility (STAP/GEF).

Yirenkyire, S. (2008), surface mining and its socio-economic impacts and challenges gold fields Ghana ltd., Tarkwa, Ghana.

Yuan, D. and Elvidge, C. 1998. NALC land cover change detection pilot study: Washington DC area experiments. Remote Sensing of Environment, 66(2), 166-178.

Zhang C. and Qiu F. (2011), Mapping Individual Tree Species in an Urban Forest Using Airborne LIDAR Data and Hyperspectral Imagery, AAG Remote Sensing Specialty Group 2011 Award Winner.

Zimble DA, Evans DL, Carlson GC, Parker RC, Grado SC, Gerard PD. 2003. Characterising vertical forest structure using small-footprint airborne LiDAR. Remote sensing of environment, v87, p171.

APPENDICES

Appendix 1: Typical Waste Rock dump Construction at AAIL

Appendix 2: Spreading of Topsoil to 500mm as per Reclamation Security Agreement

Appendix 3: Rehabilitated Waste Rock Dump (Primary Completion)

Appendix 4: Rehabilitated Awunabeng Waste rock dump in 2010 Vegetation gradually taking cover

Appendix 5: Old TSF Pre -Reclamation stage in later 90's

Appendix 6: Reclaimed Old TSF in 2006 – Reclamation stage

Appendix 7: Establishment of Cocoa farm Demonstration plot on Old TSF Rehabilitated site in 2016

Appendix 8: Old TSF portions fully vegetated with mixed species

Appendix 9: Decommissioning Earthworks at Block 1 North Rehabilitated site in 2006

Appendix 10: Vegetation stand at Block 1 North rehabilitated site (2016)

Appendix 11: Status of Block 3 & 3 WRD Rehabilitated site in 2016

Appendix 12: Snapshot of Block 1 South Rehabilitated site in 2016